vgbe Technical-Scientific Report

Strain induced corrosion cracking in fossil-fired power plants

State of knowledge, operating experience, testing and integrity concepts for findings

VGBE-TW-532 (2024)

www.vgbe.energy

vgbe Technical-Scientific Report

Strain induced corrosion cracking in fossil-fired power plants

State of knowledge, operating experience, testing and integrity concepts for findings

VGBE-TW-532e

Publisher:
vgbe energy e.V.

Publishing house:
vgbe energy service GmbH
Verlag technisch-wissenschaftlicher Schriften
Deilbachtal 173 | 45257 Essen | Germany

Phone: +49 201 8128-200
E-mail: sales-media@vgbe.energy

ISBN 978-3-96284-366-3 (print, English)
ISBN 978-3-96284-367-0 (e-book, English)
ISBN 978-3-96284-364-9 (print, German)
ISBN 978-3-96284-365-6 (e-book, German)

www.vgbe.energy | www.vgbe.services

The German-language version of this vgbe report is the authoritative reference edition for translations.

Note on the treatment of proposed amendments

Suggestions can be sent to the e-mail address vgbe-standard@vgbe.energy.
The subject line should contain the short name of the document in question so that the content can be clearly assigned.

Notes on the translation

In English-language texts, the “dot” is generally used as the decimal separator with the “comma” as the thousands separator. In graphics originating from the German speaking world, the “comma” character may be used as the decimal separator with the “dot” as the thousands separator.

American English is the main language used in this vgbe publication.

Foreword

The design of components in the water-steam cycle of conventionally fired power plants is carried out according to the principles of strength theory, considering the specifications for the operation of plants. This considers the loads caused by mechanical stresses. As repeated cases of damage have shown, the interaction of liquid medium, material and alternating mechanical stress must be considered. In the case of pronounced operational stress or strain changes, unexpected damage has repeatedly occurred despite formal compliance with the permissible stresses, which in recent decades and to this day has repeatedly led to serious damage with high downtime and replacement costs in fossil fuel power plants and, until the 1990s, also repeatedly in nuclear power plants. One of the reasons for this is that mechanical nominal stresses can still be determined relatively easily with knowledge of the geometry and load. The determination or measurement devices for recording of strain rates in systems and components is much more demanding and is generally not part of the usual scope of operational monitoring. Non-destructive testing to determine damage caused by these mechanisms is challenging, too.

This shows that the damage mechanisms, which in the Anglo-American language area are recorded under the generic term of environmentally assisted cracking, were detected comparatively late on the real component. The three leading damage phenomena in the water-steam cycle are strain induced corrosion cracking (SICC), stress corrosion cracking (SCC) and corrosion fatigue (CF), more recently designated as environmentally assisted fatigue (EAF).

This technical-scientific report focuses on strain induced corrosion cracking (SICC). This mechanism forms the transitional area between stress corrosion cracking and corrosion fatigue cracking. A distinction is important to be able to define effective monitoring and remedial measures.

The authors would like to enable the reader to build up a basic understanding of the following points, based on information on the development of technical knowledge on SICC:

- current knowledge of the damage mechanism
- damaging influencing factors
- possible consequences of damage in the components
- possibilities for non-destructive testing
- remedial measures
- detection options to ensure temporary continued operation
  in the event of findings

Essen, July 2024
vgbe energy e.V.

Authors

The following authors of this technical-scientific report are warmly thanked by the vgbe energy office:

Dr. Mirko Bader	Uniper Kraftwerke GmbH
Steffen Bergholz	Framatome GmbH
Jens Ganswind-Eyberg	vgbe energy e.V.
Thomas Hansen	BASF SE
Thomas Hauke	Lausitz Energie Kraftwerke AG
Patrick Kozlowski	Lausitz Energie Kraftwerke AG
Stefan Medenbach	MuM Müller und Medenbach GmbH
Ralf Nothdurft	EnBW Energie Baden-Württemberg AG
Armin Roth	Framatome GmbH
Dr. Jürgen Rudolph	Framatome GmbH
Dr. Johanna Steinbock	TÜV SÜD Industrie Service GmbH
Kim Christens Thielsen	Ørsted Thermal Power
Dr. Annett Udoh	MPA Stuttgart
Dr. Martin Widera	formerly RWE Power AG

Table of contents

1 Introduction

Due to their typical stresses, power plant components are subject to typical damage mechanisms which – if properly understood – can be avoided or at least suitably monitored to prevent unacceptable damage consequences.

One of these damage mechanisms is strain induced corrosion cracking (SICC), with its variant of hydrogen-assisted strain induced corrosion cracking (H-SICC) reported in conventional power plant technology. Strain induced corrosion cracking can occur under unfavorable design and operational conditions in the water phase of the water-steam cycle on the inside of the pressure-bearing wall of pipes, tanks, apparatus, and fittings made of unalloyed and low-alloy steels. Due to the formation of cracks on the inside, this mechanism poses a potential risk to the integrity of the pressure-retaining wall, which must be adequately controlled during operation.

Since the beginning of the 21st century, conventional power plants have been operated more and more cyclically. This means that there are more and more short shutdowns, low-load periods, and peak-load periods. As a result of this change in operation, damage caused by SICC/H-SICC is occurring more frequently. This now also affects plant components that were previously considered to be at low risk, such as discharge lines.

Based on an orderly technical-scientific summary of the current state of knowledge, this paper is intended to provide practitioners with a good basis for technical decisions on appropriate ageing management for potentially affected components of conventional power plants.

1.1 Changed operating modes

The role of coal-fired conventional power plants has changed significantly because of the energy transition. On the one hand, they are increasingly only playing a marginal role in the base load when there is wind and sunshine, but on the other hand they must reliably supply electricity and keep the grid stable when renewables are unable to supply sufficient power during calm wind and darkness.

This means that there are four different key operating modes that increasingly need to be considered:

- Short-term standstill / long-term standstill
- Cyclical operation (recurring transients)
- Low-load operation (minimum load over a longer period)
- Peak load (short-term or longer period)

The technical report VGB TW-530e “Recommendations for the operation and monitoring of boiler circulation pumps” [1-1] is the first to deal in depth with the consequences of these new operating modes. It describes particularly clearly that the boiler circulation pumps can hardly be operated differently due to process engineering constraints. This means that the damage mechanism of the SICC/H-SICC in the pressure-bearing wall can become active.

2 State of knowledge of strain induced crack corrosion (SICC)

2.1 Definition of strain-induced crack corrosion

Systematic investigations of the corrosion systems relevant to the application, consisting of material, medium and mechanical load, have shown that medium-supported cracking only occurs for certain materials in specific strain rate ranges. This means that no cracking can be detected above or below this strain range. This form of damage is referred to as strain induced cracking corrosion (SICC) or “strain corrosion cracking”. This distinguishes it from other mechanisms of crack corrosion such as stress corrosion cracking (SCC) and corrosion fatigue (CF). It should be noted that the more correct term is “strain-rate-induced” crack corrosion, as the change in strain at the critical strain rate is the relevant influencing factor. First time the term “Strain-induced corrosion cracking” (SICC) was used by Hickling and Lenz in the 1980s, see e.g. [2-8].
The terms for the various forms of corrosion with cracking are described in the relevant standards (e. g. formerly in DIN 50900, now in DIN EN ISO 8044, as well as internationally, e. g. in ASTM G15-97a). Nevertheless, the classification, description and definition are not yet uniform and clear. This applies to both national and international publications.

Various approaches are available for differentiating the types of crack corrosion: The MPA Stuttgart classifies analytically using mathematical formulations (Tab. 2-1, [2-1]) and the Paul Scherrer Institute (PSI) uses application-related delimitations [2-1].

Tab. 2-1: Overview of the types of crack corrosion according to the MPA Stuttgart approach and their criteria for the strain rate at the crack tip (dε/dt)CT [2-1]

Designation	Type of mechanical stress
Stress corrosion cracking (SCC)	**static** with $(d\varepsilon/dt)_{CT} = 0$ (up to crack initiation)
Strain induced crack corrosion (SICC)	**static** with $(d\varepsilon/dt)_{CT} > 0$ (limited in time)
	static or **slowly rising** with $(d\varepsilon/dt)_{CT} > 0$ (permanent)
Corrosion fatigue (CF)	**cyclic** with high or low frequency with $(d\varepsilon/dt)_{CT} > 0$

2.2 Mechanism of the SICC and the H-SICC variant[1]

Strain induced crack corrosion (SICC)

Strain-induced crack corrosion is based on repeated cracking of the magnetite layer because of localized plastic deformation of the steel with subsequent electrochemical dissolution of the locally exposed metal surface. The dissolution continues until repassivation of this area has occurred. The magnetite layer is a non-metallic oxide layer. The tearing and complete rupture of the magnetite layer down to the base metal depends on the thickness and structure of the magnetite layer. It can generally be assumed that failure of the magnetite layer only occurs above the elastic yield point, i.e. when the steel plastically deforms.

As an engineering rule of thumb, it can be said that stresses are required for crack initiation that lead to significant plastic deformation of the steel, i.e. typically stresses at the level of the yield or elongation limit.

After failure of the magnetite layer, a localized corrosion element forms. The dynamics and mode of action of the corrosion cell depend on the composition of the medium (e. g. oxygen content, chloride, and sulfate content) and the temperature. The effect of certain proportions can already be relevant in the range of a few “parts per billion” (ppb).

SICC is possible in certain media if the mechanical stresses acting at the location of crack initiation (material surface) or crack growth (crack tip) maintain continuous plastic deformation of the material at a low strain rate. Usually, this process is generated by an externally applied stress or strain that increases continuously over time, e.g. in tensile tests with a slow strain rate (constant extension rate tensile test CERT, also called slow strain rate test SSRT) or in practice, e.g. during the start-up of thermal power plants. The processes on the specimen during CERT or SSRT tests basically include both the crack initiation starting from the surface and the subsequent crack growth up to mechanical failure. Depending on whether these tests – as is generally the case – are carried out until the specimen breaks or are interrupted earlier, the behaviour of the crack initiation can be either timely limited or the crack growth can be estimated from the respective results.

From a mechanistic point of view, the processes that lead to crack nucleation at the surface and crack growth at the crack tip are basically the same for all types of crack corrosion. According to the generally recognized “film rupture” mechanism and the very similar “slip-step dissolution” mechanism, the oxidic surface layer formed during operation in hot pressurized water (T > 100 °C), which in itself protects against further corrosion, is repeatedly ruptured under the applied stress and the locally exposed bare metal areas are subsequently dissolved anodically until repassivation occurs.

[1] Hydrogen-supported strain induced crack corrosion

- In the film rupture mechanism, the local rupture of the oxide top layer is caused solely by the elongation of the metallic substrate, as the elongation at break of the oxide is significantly lower than the elongation at break of the metal;
- In the slip-step dissolution mechanism, the cracking of the oxide surface layer occurs at slip steps, provided these are greater than the thickness of the oxide.

The kinetics of crack nucleation and crack growth depend on which of the steps dominates in the repeated interplay.

With regard to the influence of strain rate on the values of the relative fracture elongation or the reduction of area measured in tensile tests with a slow strain rate as a function of the strain rate, two variants of the behaviour of materials in the medium that differ in detail are shown here, which are labeled alloy “A” and alloy “B” in Fig. 2-1. Alloy “A” refers to the behaviour of metals or alloys that are susceptible to stress corrosion cracking in the medium under consideration. With decreasing (imposed) strain rate, alloys of this type show an increasing effect of surface cracks initiated by crack corrosion, which becomes maximum under static stress.

This contrasts with the alloy “B” variant, in which the values of the relative deformation parameters increase again at very low strain rates (see Fig. 2-1, alloy “B” curve). This means that there is no susceptibility to crack corrosion at very low strain rates. This behaviour is a typical feature of purely strain induced cracking corrosion (SICC), which is only triggered by externally acting strain rates. This phenomenon can be explained based on the slip-step dissolution mechanism. In the interaction of the competing processes in the corrosion system under consideration, repassivation is dominant over surface layer damage. This means that no continuous crack growth is maintained.

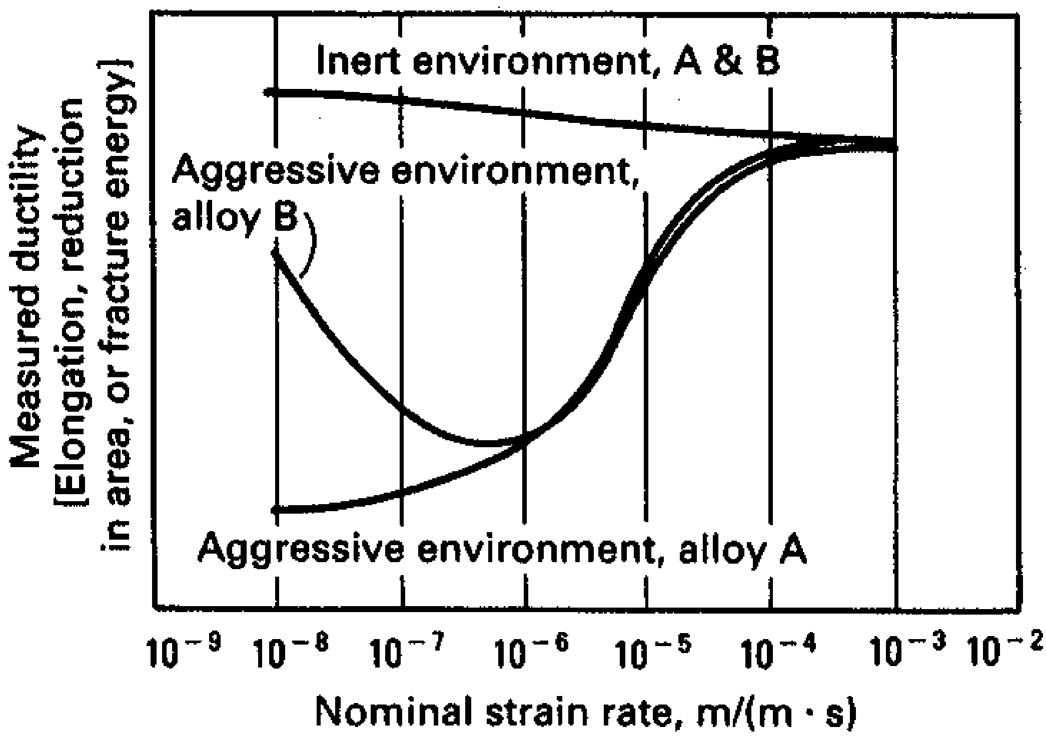

Fig. 2-1: Schematic diagram of deformation parameters of the tensile test (elongation at break, reduction of area at fracture) as a function of the strain rate in SSRT tests in an inert atmosphere and in the medium [2-3].

The quantitative, theoretical description of the kinetics of crack corrosion was presented by Ford & Andresen, [2-4], [2-5]. They theoretically modeled the crack growth according to the so-called “slip-step dissolution” mechanism and finally adapted it to existing measured values by parameter fitting. In a deterministic approach, basic principles of local plastic deformation under external load (crack tip strain rate as a function of the stress intensity factor) and electrochemistry (kinetics of repassivation and FARADAY's law) were used for modeling. The result of the modeling leads to two limiting cases, the so-called “low-sulfur line” and the so-called “high-sulfur line” (see Fig. 2-2) [2-6].

- “High-Sulfur Line” according to Ford & Andresen (1991):
  $da/dt = 9.6 \times 10^{-8}\ K^{1.4}$ mm/s, $[K] = MPa\sqrt{m}$

- “Low-Sulfur Line” according to Ford & Andresen (1991):
  $da/dt = 3.29 \times 10^{-14}\ K^{4}$ mm/s, $[K] = MPa\sqrt{m}$

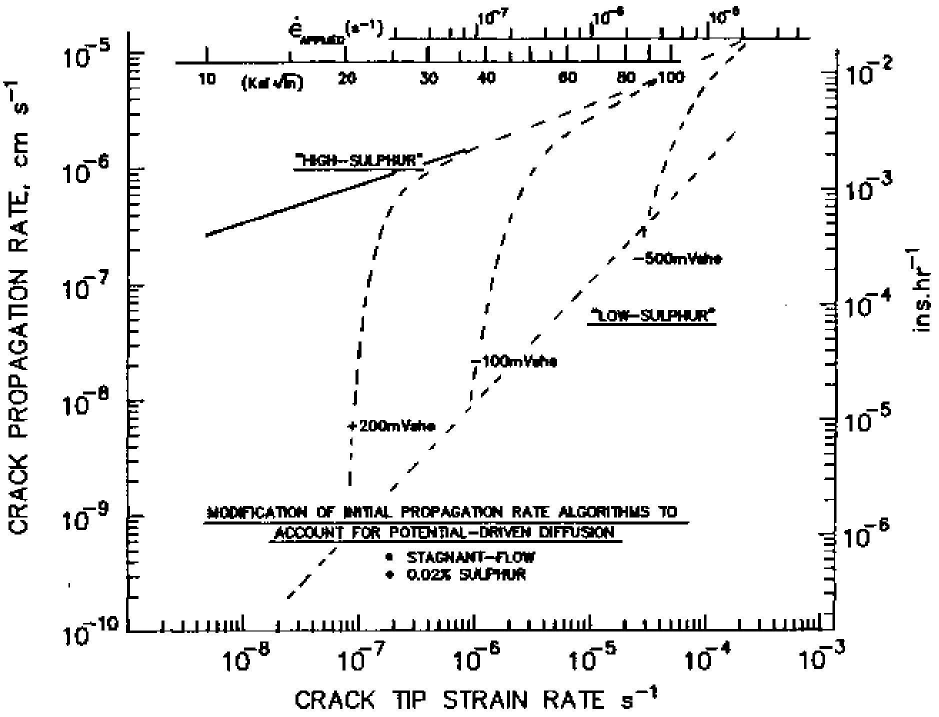

a) Crack growth rate as a function of the crack tip strain rate according to Ford et al. (1991) [2-7]

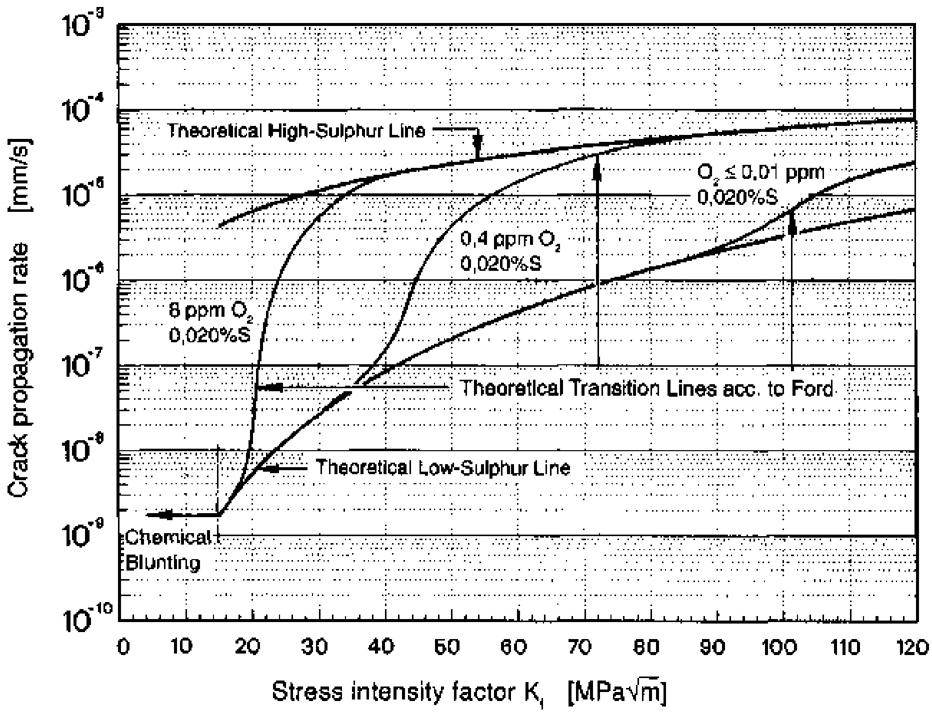

b) Crack growth rate as a function of the stress intensity factor according to Kußmaul et al. (1997) [2-1]

Fig. 2-2: Graphical representation of the crack growth limit curves "low-sulfur line" and "high-sulfur line" based on the "film rupture" and "slip-step dissolution" model from Ford & Andresen [2-4] [2-5].

These theoretical limit curves are based on the knowledge that a minimum concentration of sulfur-containing anions (sulfate or sulfide) is required in the crack to maintain crack growth (low sulfur line). This is provided either by a correspondingly contaminated medium or by the progression of the crack itself, which leads to the continuous supply of sulfur-containing anions in steels with manganese sulfide precipitations. On the other hand, the possible crack growth rate is limited upwards by a corresponding maximum concentration, above which no further acceleration is possible (high sulfur line).

Hydrogen-assisted strain induced crack corrosion (H-SICC)

The mechanism of strain induced crack corrosion is a damage mechanism that has been observed for a very long time in conventional power plant technology in the water-steam cycle area exposed to water, see Chapter 3.3.1, Fig. 2-3. A relevant step in the technical interpretation of this mechanism was the publication by Lenz et al. [2-8]. A key point of this paper is the finding that a reduction in ductility occurs in all the materials investigated under medium and very slow strain rates.

This embrittlement effect can be attributed to hydrogen [2-12]. It is important to note that the influence of sulfur as an alloy impurity is not required for the damage mechanism. A change in the crack propagation rate can thus be derived on the one hand from the different sensitivity of the materials to hydrogen and on the other hand from the supply of hydrogen through the electrochemical reaction in the crack.

The effect of an electrochemical reaction in the crack area is easy to understand. The electrolyte is water. The electrochemical reaction is the formation of a magnetite layer on the still free surface, parallel to the surfaces already covered with magnetite.

In order to draw a clear distinction from the theory discussed in the previous subchapter, the mechanism thus understood is called “hydrogen-assisted strain induced cracking corrosion” (H-SICC).

Current investigations into the damage mechanism on T24 (7CrMoVTiB10-10) describe this relationship.

H-SICC is characterized by the non-negligible influence of local electrochemical processes, because of which material embrittlement occurs before the crack tip due to local hydrogen ingress. In general, it must be assumed that H-SICC is always present in high-temperature water and that the embrittling effect of hydrogen takes place before the crack tip. Quantitative statements regarding the effect on crack propagation are not yet possible due to the large number of influencing parameters.

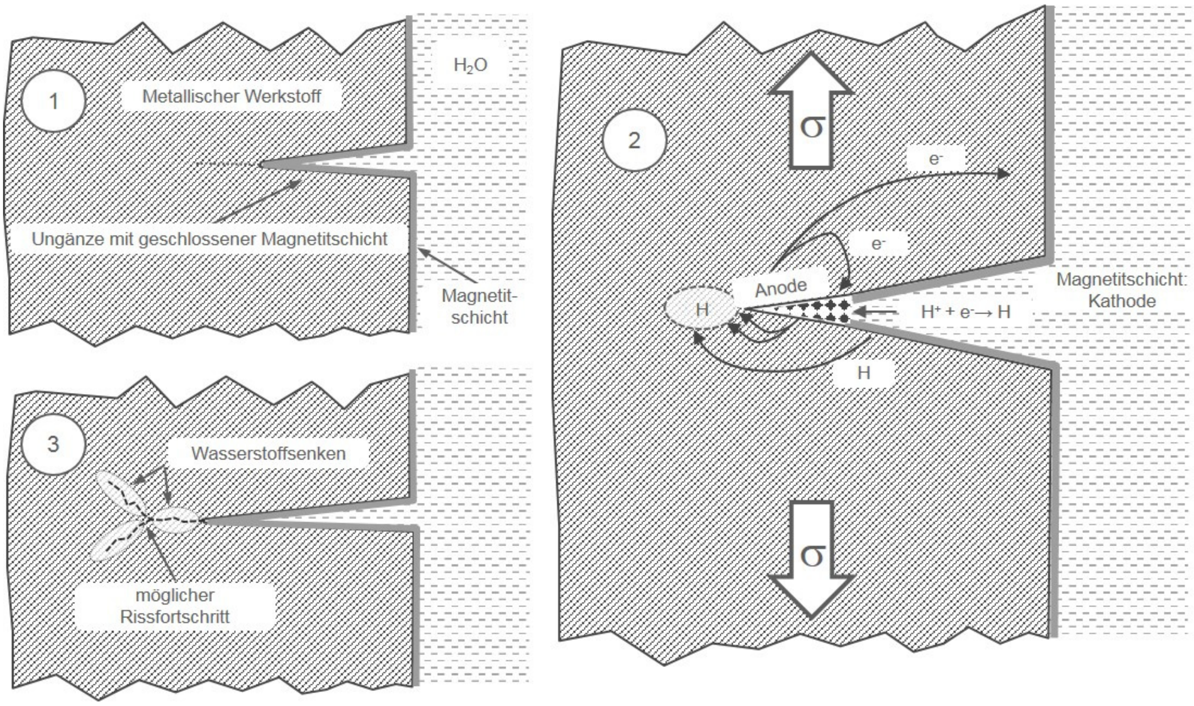

Fig. 2-3: Schematic of the H-SICC

Fig. 2-3/1: The initial state is generally a surface imperfection, which develops into a crack with oxidized flanks. In the water-steam cycle, this oxide is generally magnetite, which acts as a protective layer of the metallic surface against the medium (high-temperature water).

Fig. 2-3/2: If the crack or the discontinuity is opened further, the surface near the crack tip is initially bare metal and electrochemical reactions for magnetite formation occur (Schikorr-Reaction). The metallic base material always acts as the anode due to the release of electrons. Atomic hydrogen is released [2-13]. This subsequently penetrates the metallic material and diffuses preferentially into areas with increased tensile stresses. Within the material, it orients itself in front of the crack tip, favored by local strains [2-14].

Fig. 2-3/3: The hydrogen atoms lead to local embrittlement of the material and facilitate crack propagation. Subsequent cracks are usually oriented as quasi-collinear crack propagation or at an angle of approx. 45° in the locally embrittled zone. Recombination of the hydrogen atoms in the material can be largely ruled out with these materials and temperatures, as the material cohesion works against the pressure build-up and prevents gas phase formation.

Translation	
German	**English**
Metallischer Werkstoff	Metallic material
Ungänze mit geschlossener Magnetitschicht	Discontinuity with closed magnetite layer
Wasserstoffsenken	Hydrogen sinks
Möglicher Rissfortschritt	Possible crack propagation
Kathode	Cathode

Lenz et al. [2-8] already described indications that crack growth in HT water is favored by hydrogen from the anodic corrosion process, whereby this effect increases with increasing strength of the material. Thus, SICC and H-SICC are not fundamentally different mechanisms but are to be regarded as related variants in a common physical spectrum, in which the material and the corrosion system influence whether hydrogen becomes rate-determining for crack growth (H-SICC) or not (SICC).

In addition to the mechanical strain rate, the H-SICC can therefore be described with three additional boundary conditions:

- local supply of hydrogen in the crack tip area as a result of the local electrolytic reaction (medium, new free metal surface, temperature);
- local material embrittlement in the crack tip area because of the aforementioned local hydrogen absorption;
- imposed mechanical strain rate.

It can be seen that the time factor is essential for the mechanism in an interaction with an electrochemical reaction. This means that the chemical reaction requires time to produce sufficient hydrogen. The produced atomic hydrogen must enter the metal lattice via the medium/metal phase boundary and then diffuse to the crack tip in the area of the expanded lattice, in particular the plastic zone. Therefore, as the strain rate decreases, the influence of the hydrogen becomes increasingly effective. There are numerous studies and observations on the influence of the strain rate on the reduction of elongation at break and embrittlement [2-9] [2-10]. For ferritic materials, i.e. typical materials for stressing in the water vapor cycle at 200 °C to 300 °C, this influence reaches a maximum value in the range of 10^{-6} s^{-1} to 10^{-7} s^{-1}. A relationship to the diffusion rate of hydrogen in the metal lattice of approx. 10^{-5} m^2s^{-1} [2-11] is consistent. Since the absorption of hydrogen and its effect is linked to the lattice expansion, no further significant reduction in ductility is to be expected below a lower limit value of the strain rate. This is because as soon as the plastic zone in front of the crack tip is saturated with hydrogen, only a very limited hydrogen absorption of the areas behind it is possible. In laboratory tests with a constant supply of hydrogen, no further significant decrease in ductility can be determined. Under practical conditions, the tendency to embrittlement can apparently decrease, as the hydrogen supply is reduced by boundary layer changes, for example, and the amount of hydrogen in the microstructure can be reduced by continuous removal.

Lower strain rates do not lead to a further intensification of the damage process.

2.3 General parameters influencing the SICC

At the typical operating temperatures of thermal power plants with a water-steam cycle, a protective oxide coating forms on unalloyed and low-alloy steels in oxygen-containing high-temperature water (HT water) from approx. 20 ppb to 50 ppb dissolved oxygen at temperatures above approx. 150 °C, a protective oxide coating is formed which provides sufficient protection against attack by uniform surface corrosion (i.e. without additional mechanical stress) and also against erosion by flow-assisted corrosion (FAC, also known as erosion corrosion EC).

In order to trigger crack corrosion, critical values of specific parameters of the corrosion system must be present at the same time, which is determined by the combination of

- material or material condition,
- medium and
- mechanical stress.

A prerequisite for the existence of susceptibility is the simultaneous exceeding of critical threshold values for material, medium and mechanical stress.

The main influencing or effect parameters for the various types of crack corrosion are shown in Tab. 2-2.

Tab. 2-2: Crack corrosion relevant parameters for low-alloy steels in HT water

Material	***Medium***	***Mechanical Stress***
• S dose or form, size, density, homogeneity, orientation of the MnS precipitates • Strength • Sensitivity to Dynamic Strain Ageing (DSA), especially with weld metal	• Temperature • Concentration of dissolved oxygen (or corrosion potential) • Electrical conductivity and concentration of impurities such as sulfate and chloride • Flow velocity	• Tension and stretching • Stress state • Residual stresses • Notch effect (for crack initiation) • Stress intensity factor (for crack growth) • Type of stress (“active” or “passive”, i.e. force-controlled or displacement-controlled) • Tensile force-time curve (constant load, cyclical load, load transients) • Relaxation • Crack closure effects

Detailed information on the influence of the individual parameters has been presented elsewhere (e.g. [2-15][2-16][2-17]). The following is therefore only a summary of the key aspects.

2.3.1 Mechanical stress

First of all, some general findings on the influence of mechanical stress on the initiation and growth of cracks due to types of crack corrosion should be pointed out.

Stress and strain

From the point of view of mechanical stress, the driving force is the globally acting mechanical stress, which can cause plastic deformation with a low strain rate locally on smooth surfaces or at crack tips. Crack corrosion is only possible if tensile stresses are present in the component at the metal/medium phase boundary.

Stress state and notch effect

Regarding the occurrence of crack initiation on smooth sample and component surfaces, the level of stresses resulting from the superposition of any residual stresses present and the operating stress is decisive. With technically smooth surfaces, roughness, or small, production-related notches, e. g. as a result of welding, are nevertheless to be expected. This may result in a multi-axial stress state and a stress-increasing notch effect.

Stress intensity factor

In the case of cracked surfaces, e. g. fracture mechanics specimens with fatigue cracks or postulated cracks in components, crack growth may be determined by the stress intensity factor, which describes the stress level at the crack tip.

Type of stress (“active” or “passive”)

As already mentioned, in the corrosion system of unalloyed and low-alloy steels in high-temperature water under consideration, the way in which the force is applied is decisive. In plant operation, “active” stress corresponds in particular to stresses generated by pressure differences, e. g. internal pressure (“primary stress”). Stresses that are generated by temperature differences, e. g. deflections caused by thermal expansion or impeded thermal expansion (“secondary stresses”), correspond to “passive” stresses in a stationary state.

Force-time curve (constant load, cyclic load, load transients)

In a given corrosion system, the initiation of cracks and their growth through types of crack corrosion depends decisively on the type and level of mechanical stress. In principle, as the level and variation of the mechanical stress increases, e. g. high static load values or cyclic load, critical parameters of the medium recede into the background as criteria, and vice versa.

Residual stresses

Production-related residual stresses, e. g. resulting from welding-related shrinkage processes, cold forming, or surface treatment, contribute to the overall stress level of a component subsequently subjected to operational stresses by superposition of operational stresses with residual stresses. The magnitude, sign and direction of residual stresses determine whether the susceptibility to crack corrosion is either increased or decreased under the relevant operating conditions, i.e. whether the stresses are (undesirable) tensile or (desirable) compressive stresses, and whether the residual stress contribution has a significant value. Residual stresses must therefore always be included in the evaluation of the operational behaviour of parts and components regarding crack formation and crack growth.

Crack closure effects

Crack closure effects are the effect that occurs when the two opposing surfaces of a crack can no longer fully contact each other as a result of changes in the crack due to decreasing mechanical stress, i.e. the crack is no longer fully closed. This effect is caused, for example, by increased surface roughness or as a result of the formation of thick oxide deposits, as can be the case in crack gaps in HT water. The plasticization of the crack tip can also prevent the crack from closing if the plastically deformed zone in front of the crack prevents it from closing completely when the load is removed. As a rule, crack closure effects lead to a significant reduction in the stress intensity factor acting locally on the crack and are therefore to be considered fundamentally favorable for the reduction of crack corrosion sensitivity. They are sometimes held responsible for the fact that unexpected crack arrest is repeatedly observed in laboratory tests.

2.3.2 Strain rate

From the perspective of practical engineering terminology, the SICC is understood here as a mechanism that is generated by a strain rate imposed on the material due to system conditions. This includes in particular the strain rates generated by changes in pressure or temperature in the system under consideration.

Local strain rates, which can also occur with correspondingly high static loads and which are subject to the same basic laws, are not considered here.

Friedrich et al. [2-18] were not only able to confirm the known dependency at strain rates down to approx. 10^{-7} s^{-1} (Fig. 2-4), but also showed in particular that the sensitivity for SICC decreases again with further decreasing strain rates below a certain value, which is reflected in the increase in the relative fracture constriction. This leads to the conclusion that at the very low local strain rates that can occur locally under constant static loading, there is no longer any sensitivity to SICC. This conclusion is clearly supported by the tests under constant load, which under these circumstances show practically no sensitivity to cracking in the medium.

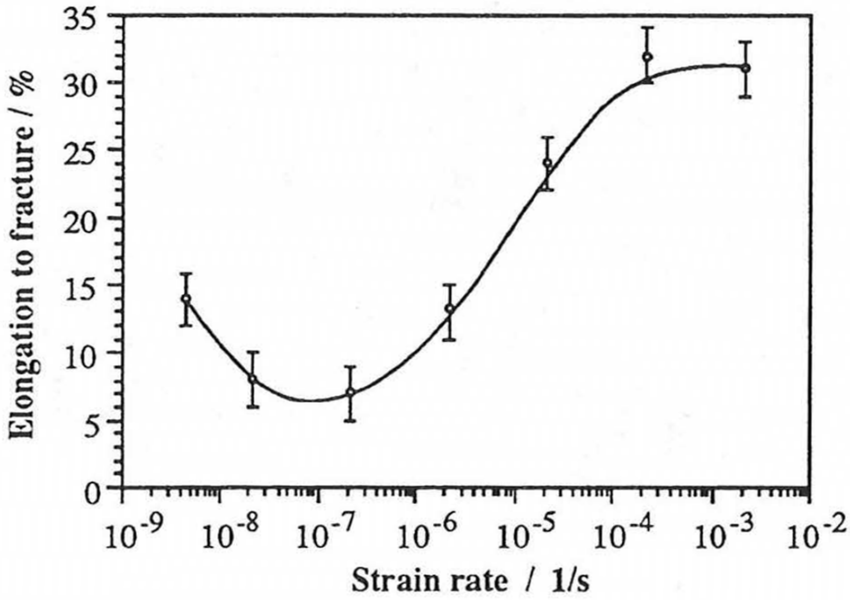

Fig. 2-4: Dependence of the elongation at fracture of a low-alloy reactor pressure vessel steel on the strain rate in SSRT tests in HT water [2-18]

In addition, the work of Rippstein et al. [2-19] has shown that crack initiation in SSRT/CERT tests with a low-alloy fine-grained structural steel in HT water only occurs close to the tensile strength (approx. 95 % Rm) and the correspondingly high strains. A control experiment with an initially faster strain rate showed that the observed crack depths do not depend on the total test duration, but on the time from the onset of crack initiation, Fig. 2-5.

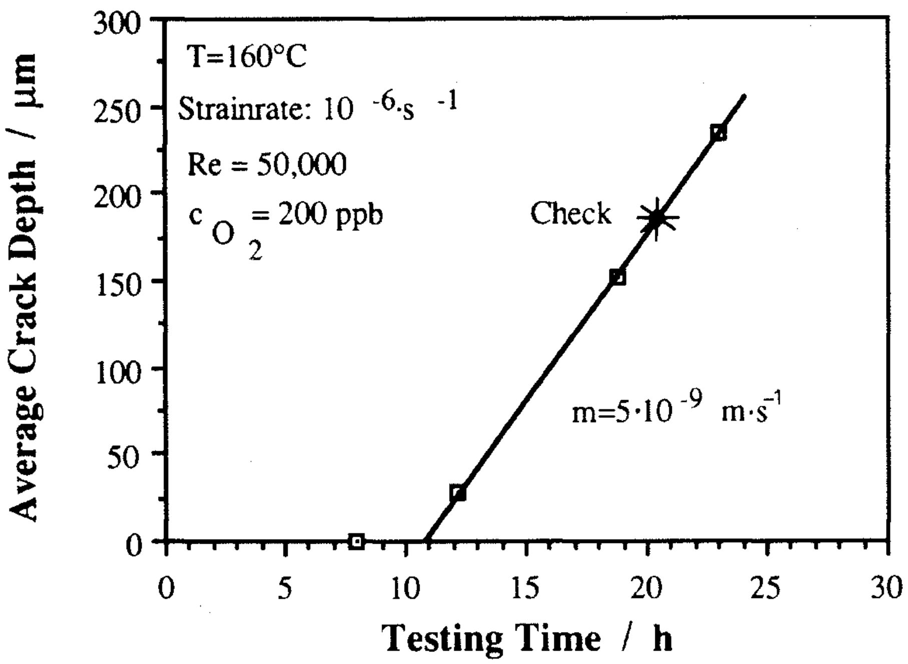

*Fig. 2-5: Crack depth in tensile specimens from SSRT tests of a low-alloy steel in HT water as a function of the test time; the control specimen marked with * was elongated at a faster elongation rate with a significantly shorter test time up to the suspected crack initiation point and then elongated further at a correspondingly slower rate [2-19]*

Note on Fig. 2-5:
In the "Check" test, the time axis with slow elongation only begins at 11 h. Prior to this, an elongation corresponding to the elongation of the other tests at 11 h was generated with a significantly faster elongation rate in a correspondingly shorter time.

For practical evaluations, SICC can also be regarded as a limiting case of CF under LCF conditions at very low frequencies ("very Low Cycle Fatigue" – vLCF), in which extreme mechanical stresses due to plastic deformation with low strain rates in combination with the medium ensure crack initiation and growth in every load increase phase.

2.3.3 Material

Sulfur content or size, density, shape, distribution, orientation of the MnS precipitates

Laboratory tests to investigate crack corrosion have shown that the S content of the medium is a significant influencing factor for crack initiation and growth (see [2-15] [2-16]). This is also reflected in the theoretical considerations and the resulting quantitative calculation model for crack growth rates developed by Ford & Andresen (see e. g. [2-4] [2-5]). The content of sulfur-containing anions, which, depending on the corrosion potential, are present as sulfide or sulfate ions at the site of crack nucleation or at the tip of a growing crack, is therefore decisive for the speed of the reaction that takes place. It is fundamentally irrelevant whether these sulfur-containing anions are produced by chemical or electrochemical dissolution of the MnS precipitates contained in the steel or are supplied via corresponding impurities in the medium. If the steel itself is the source of the sulfur, its effect depends decisively on how quickly manganese sulfide precipitates are released in the microstructure by a growing crack (e. g. in [2-20] [2-21] [2-22]) and thus on how these are originally distributed in the microstructure of the steel. Rippstein et al. [2-19] have shown that in slow tensile tests in HT water with samples from a very impure, high-sulfur, inhomogeneous test melt in oxygen-containing HT water, crack initiation occurs preferentially at MnS inclusions, which are located on the polished sample surface.

Accordingly, for the same sulfur content, the susceptibility in materials with coarse, inhomogeneously distributed MnS inclusions is significantly higher than in batches with a very fine and homogeneous distribution of precipitates. This applies in particular if the crack plane lies in a plane of MnS lines.

<u>Strength</u>

The dependence on strength is of marginal importance for plant operation as long as the hardness does not exceed a value of 350 HV10 or the yield strength a value of at least approx. 900 MPa (cf. [2-23]).

<u>Sensitivity to dynamic strain ageing (DSA)</u>

The sensitivity of materials to dynamic strain ageing is a key influencing parameter ([2-24] [2-25] [2-26] [2-27]). In principle, the susceptibility to Environmentally Assisted Cracking (EAC) in oxygen-containing high-temperature water increases with increasing sensitivity to DSA, which is due to the greater tendency to local deformation and thus to the formation of higher slip levels.

<u>Influence of DSA on crack corrosion</u>

Since the mechanism of crack corrosion of low-alloy steels in oxygen-containing high-temperature water is essentially determined by the local plastic deformation behaviour, e. g. at the tip of growing cracks, an influence of dynamic strain aging on the speed of the processes occurring during crack corrosion can also be assumed.

Detailed investigations of the surface of samples from SSRT tests under simulated medium conditions in oxygen-containing high-temperature water [2-28] show that the appearance of crack initiation clearly depends on the degree of sensitivity to DSA. The materials with low susceptibility to DSA typically show clusters with the initiation of many cracks (Fig. 2-6), whereas with high susceptibility to DSA the initiation of single cracks dominates (Fig. 2-7).

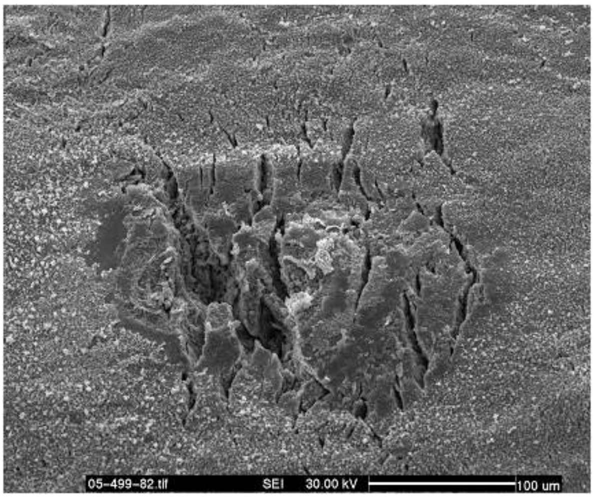

Fig. 2-6: Initiation of multiple cracks in a low-alloy steel with low DSA susceptibility [2-28]

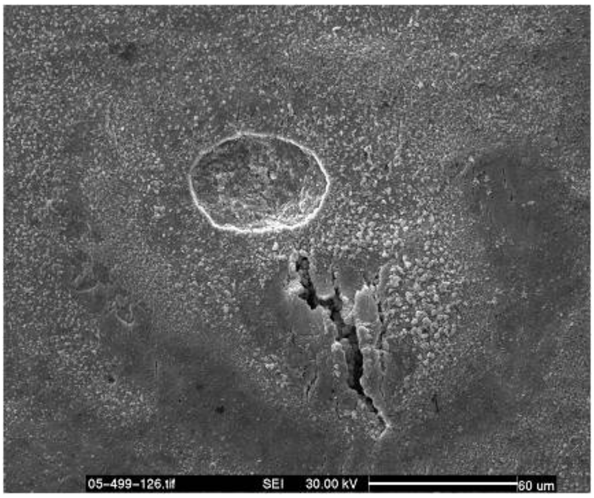

Fig. 2-7: Initiation of single cracks in a low-alloy steel with high DSA susceptibility [2-28]

It was shown that the formation of individual cracks occurs particularly in areas with coarse slip (Fig. 2-8) or intersecting slip bands (Fig. 2-9).

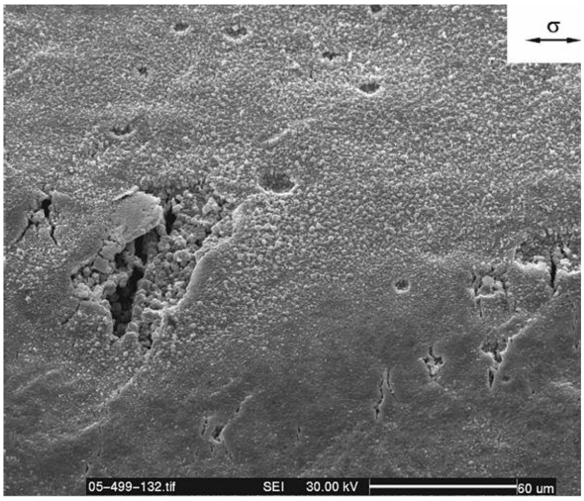

Fig. 2-8: Local crack initiation by SICC on a coarse sliding strip in a low-alloy steel with high DSA sensitivity [2-28]

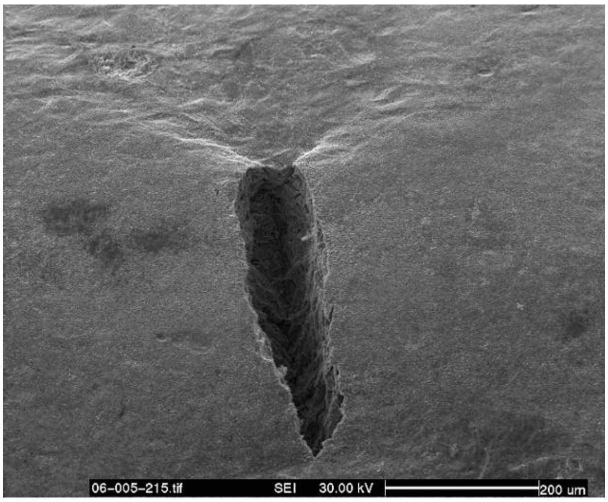

Fig. 2-9: Local crack initiation by SICC at an intersection of slip bands in a low-alloy steel with high DSA sensitivity [2-28]

The susceptibility to DSA on the one hand and the susceptibility to crack corrosion on the other can be regarded as experimentally proven. Increasing susceptibility to DSA leads to an increase in susceptibility to crack corrosion.

2.3.4 Temperature

The temperature of the medium has a significant influence on the speed of the processes that take place during crack corrosion (see Fig. 2-10, Fig. 2-11). This occurs on the one hand via the temperature dependence of the electrochemical reactions themselves, and on the other hand via the temperature dependence of other influencing factors such as mass transport, conductivity, pH value, solubility of oxides and yield strength of the material.

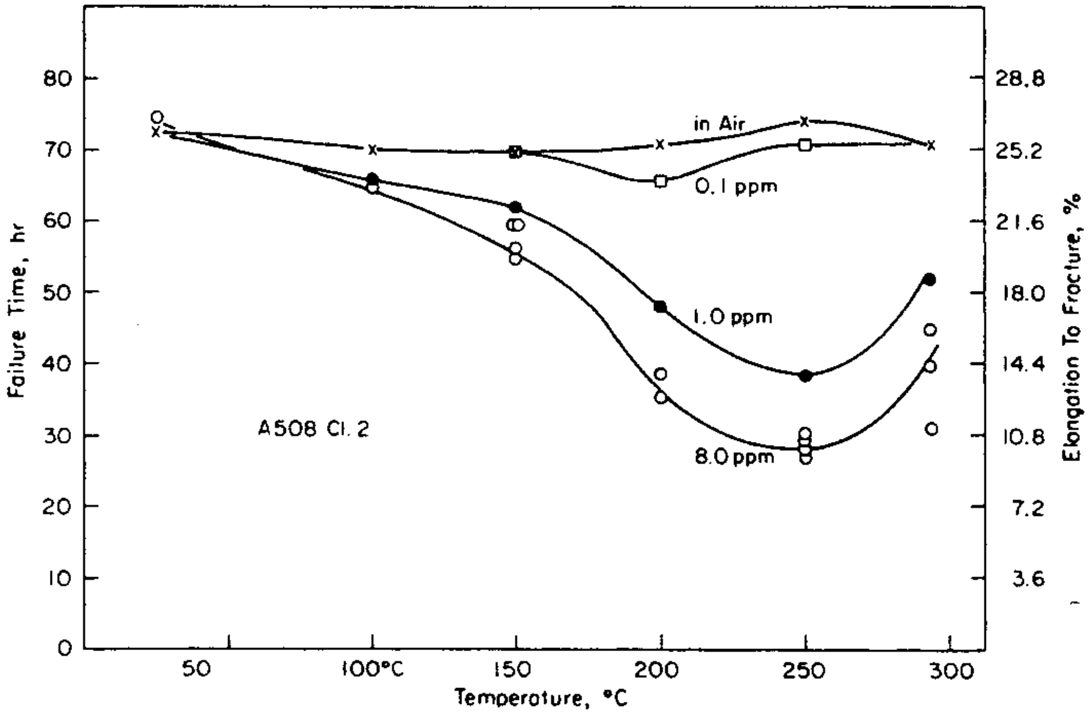

Fig. 2-10: Dependence of time to fracture (corresponding to elongation at fracture) on temperature in SSRT tests with a low-alloy steel in HT water, as a function of oxygen content up to saturation content in ppm [2-29]

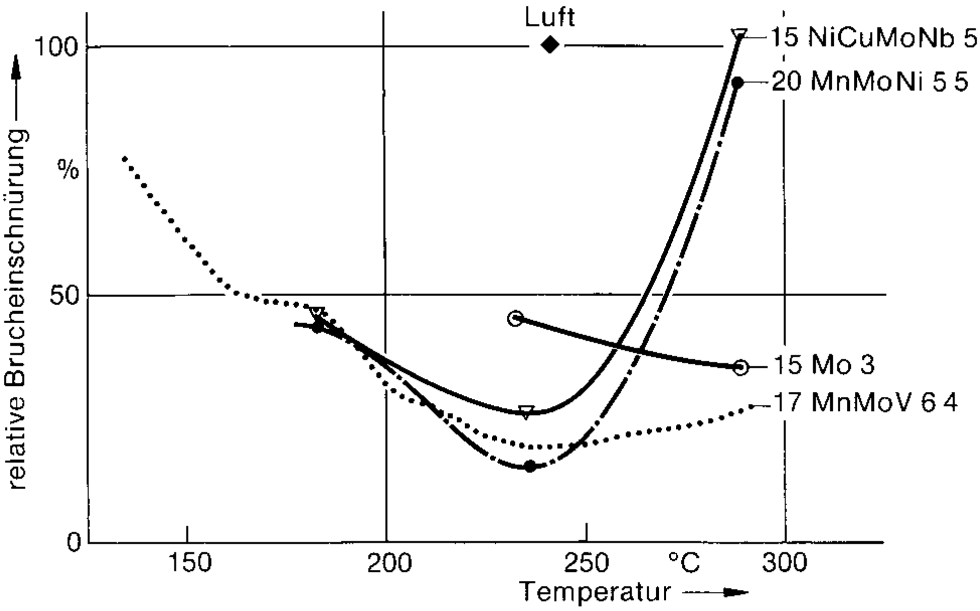

Fig. 2-11: Progression of the relative fracture necking of low-alloy steels as a function of temperature in SSRT tests in HT water [2-8]

Translation	
German	**English**
Relative Brucheinschnürung	Relative reduction of area at fracture
Luft	Air
Temperatur	Temperature

2.3.5 Medium

Concentration of dissolved oxygen (or corrosion potential)

Dissolved oxygen, temperature and local flow conditions of the medium are the parameters that directly and primarily influence the electrochemical corrosion potential of steels in HT water (Fig. 2-12).

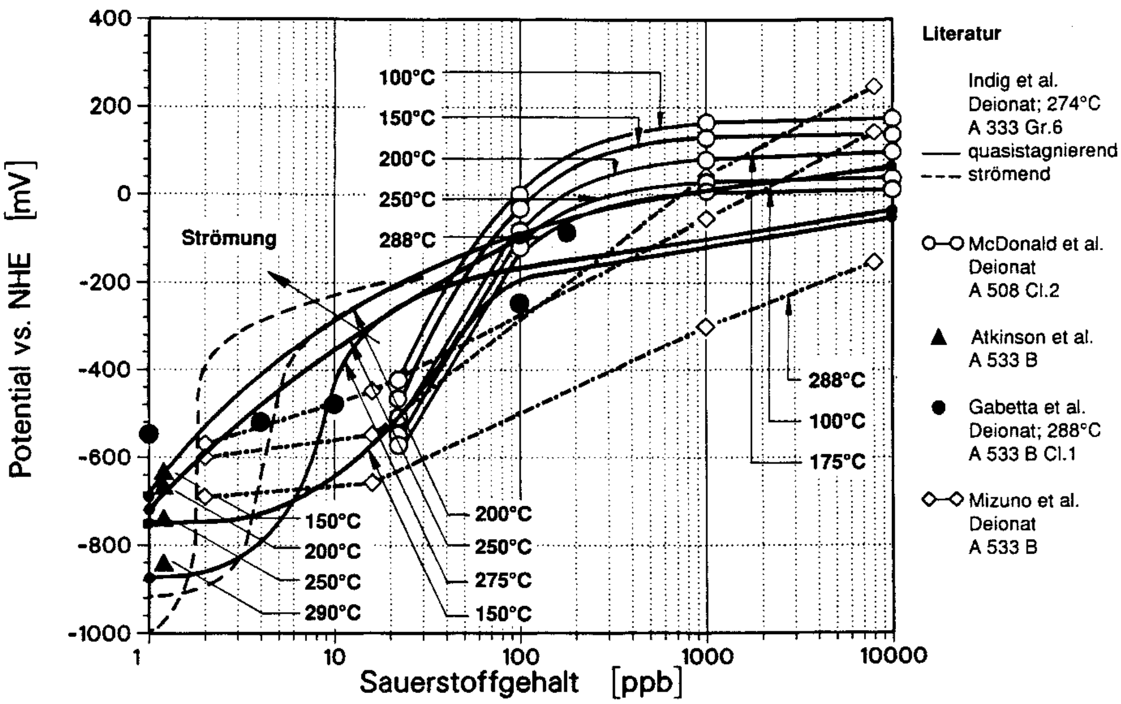

Fig. 2-12: Summarized presentation of literature data on the dependence of the corrosion potential of steels in HT water on dissolved oxygen content, temperature and flow velocity, according to [2-30]

Translation	
German	**English**
Sauerstoffgehalt	Oxygen content
Strömung	Flow
Literatur	Literature
quasistagnierend	practically stagnating
strömend	Flowing

As the mechanism of crack corrosion is based on electrochemical reactions, a direct dependence of the kinetics on the corrosion potential is to be expected. This results, among other things, in indirect dependencies on dissolved oxygen, temperature and local flow velocity. The transition from low to high potential values takes place over a few hundred millivolts within a limited range of oxygen content. This transition essentially depends on temperature, flow velocity and the composition of the medium.

<u>Electrical conductivity or concentration of ionic impurities</u>

Under free corrosion conditions, the sum of anodic and cathodic partial currents must compensate each other in order to maintain the principle of electroneutrality. This means that the value of the respective partial current sums also depends in particular on the respective sizes of the anodically and cathodically active surfaces on which

these occur (“surface rule of corrosion”). Therefore, an influence of the electrical conductivity, regardless of its cause (ionic impurities or temperature effects on the self-dissociation), on the corrosion rate is generally to be expected.
Ionic impurities can affect the kinetics of crevice corrosion in three different ways. Firstly, ionic impurities can have a conductivity-increasing effect, i.e. they accelerate the corrosion reaction, which results in an increase in the cathodically effective surface area. Secondly, depending on their nature, ionic impurities can act as additional oxidizing or reducing agents, which may have an additional influence on the corrosion potential alongside oxygen. Thirdly, ionic impurities can also intervene directly in the kinetics of anodic and cathodic partial reactions through chemical interactions. On the one hand, this is possible by changing the composition of the oxide, which can influence the kinetics of the cathodic partial reaction. On the other hand, they can have an influence on the stability of the oxide (e. g. due to chloride) or its repassivation rate (e. g. due to sulfate).

Flow

The kinetics of the corrosion reactions that take place depend on the local composition of the medium, which determines both its oxidizing effect and the stability of the oxide. In addition to diffusion, migration and convection, the local concentration of the medium is influenced by the flow of the medium. The geometric condition of the surface is also a decisive influencing factor. Cracks and geometrically similar crevice-like defects, e. g. design- or production-related crevices, notches, or folds, represent flow dead zones in which the chemical composition of the medium can change locally, depending on the geometry, largely independently of the composition of the so-called “bulk volume”. Enrichment and depletion processes are therefore determined by the local flow conditions. A significant influence of the flow is therefore generally to be expected if the corrosion sensitivity is determined either by the transport-controlled delivery of the oxidizing agent or by the local change in ionic concentrations. It therefore depends on both the flow velocity and the flow direction whether and to what extent the kinetics of the crack corrosion are influenced. In principle, corrosion is accelerated if corrosion-causing species, e. g. oxidizing agents such as dissolved oxygen, are transported faster due to a favourable flow direction and/or higher flow velocity. In this case, there is also a flow-induced shift in the corrosion potential. However, this effect applies more to corrosion systems with a low oxygen content, e. g. when conventional fossil-fired thermal power plants are operated accordingly. Conversely, the corrosion rate is slowed down or completely suppressed if the flow direction and speed accelerate the removal of corrosion-causing species, e. g. sulfate/sulfide anions, from cracks or other geometric surface defects, thus reducing existing local accumulations of ions or preventing their formation in the first place.

2.4 General assessment of the characteristic dependencies of the SICC

Critical values for the key parameters for SICC in laboratory tests were derived from the test results presented. The prerequisite or favourable conditions for crack initiation of unalloyed and low-alloy steels by SICC on smooth sample surfaces in HT water determined based on laboratory tests (CERT/SSRT tests) are

- Temperature 150 °C < T < 250 °C
- Dissolved oxygen content (O_2)
  (above 30 ppb – 80 ppb, depending on the flow velocity)
- Strain rate dε/dt = 10^{-3} s^{-1} ... 10^{-7} s^{-1} in the plastic range.

The susceptibility area of parts and components for SICC can be represented graphically in a three-dimensional diagram as a function of the primary parameters strain rate, oxygen content and temperature (Fig. 2-13).

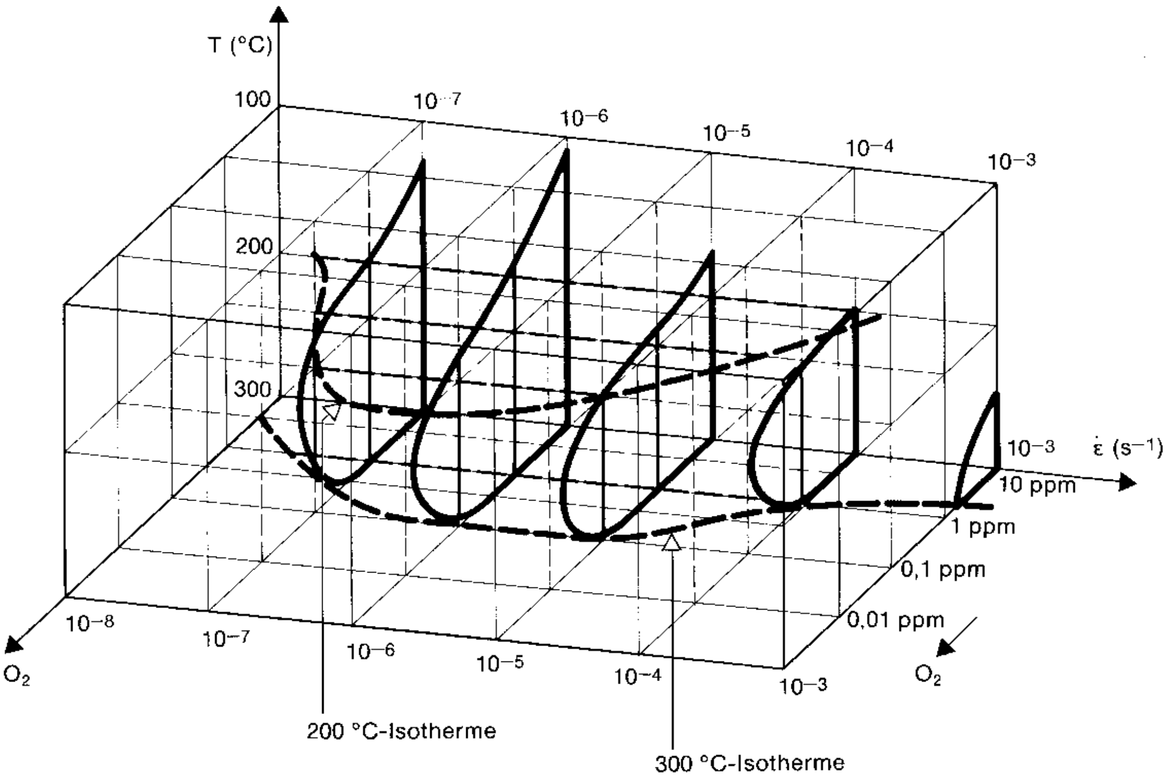

Fig. 2-13: Susceptibility diagram for SICC of low-alloy steels in HT water [2-8]

Operating experience shows that the simultaneous presence of these critical conditions in laboratory tests alone is not sufficient to trigger SICC. This can be explained in particular by the fact that the mechanical stresses on components during plant operation are significantly lower than in the usual SSRT/CERT laboratory tests, in which the samples are mechanically stretched until they break.

Based on operating experience, the following additional factors must be present for the development of SICC:

- Pitting corrosion with surface layer formation or
- geometric disturbances (e. g. notch effect due to weld imperfections, wall thickness transitions, stiffness transitions in tight curves, edge misalignment, etc.) or
- residual welding stresses (in addition to operational stresses).

2.4.1 Common test techniques for investigating the different types of crack corrosion

In order to test the simultaneous effect of medium and tensile stress on a material, suitable specimens are mechanically stressed in the relevant operating medium or in a relevant model medium during laboratory tests. Tensile specimens with smooth, macroscopically crack-free, and defect-free gauge lengths are generally used to investigate crack initiation. Crack growth is usually investigated using fracture mechanics specimens with an existing fatigue crack. The loading with a tensile stress (or strain) is constant or variable over time. An overview of typical test methods shows Tab. 2-3.

Tab. 2-3: Types of crack corrosion and their testing for crack initiation and crack growth in the laboratory

Mechanisms	SCC		SICC		CF	
Type of test	constant load or constant deflection	constant load or constant deflection	SSRT (also for SCC)	VLCF	LCF	LCF
Type of specimen	unnotched	precracked	unnotched	unnotched	unnotched	precracked
Loading mode	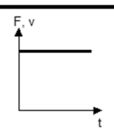	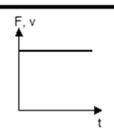	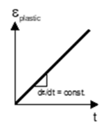	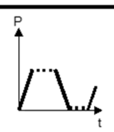	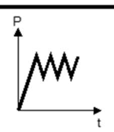	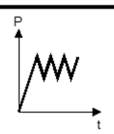
Result	time to failure 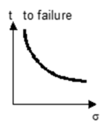	da/dt 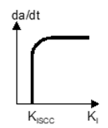	reduction of area to fracture 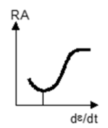	cycles to initiation 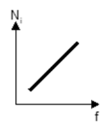	Δ stress/strain to initiation 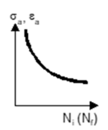	da/dN 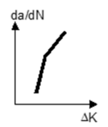
Objective, application	susceptibility, material selection	safety margins	susceptibility, mat'l selection, env. parameters	optimization of start-up procedure	design	evaluation of Δa and safety margins
Height of loading	variable (up to full plastic load)	linear elastic	increase to fracture	variable (up to full plastic load)	variable (up to full plastic load)	linear elastic
Applicable to component behaviour	yes	yes, if conditions of LEFM are fulfilled	qualitative indications	yes	yes	yes

The aim of the investigations to determine the crack corrosion behaviour is either to make quantitative statements on the time until crack initiation on smooth surfaces as a function of the acting stress or on the speed of growth of existing cracks as a function of the stress intensity factor. This usually results in typical curves in technically common corrosion systems, e. g. materials in chemical industry media (see. **Fehler! Verweisquelle konnte nicht gefunden werden.** and **Fehler! Verweisquelle konnte nicht gefunden werden.**).

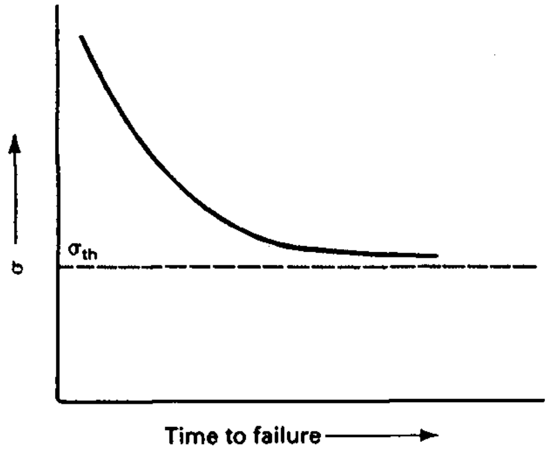

Fig. 2-14: Schematic representation of the usual progression between applied stress and failure time in stress corrosion cracking [2-3]

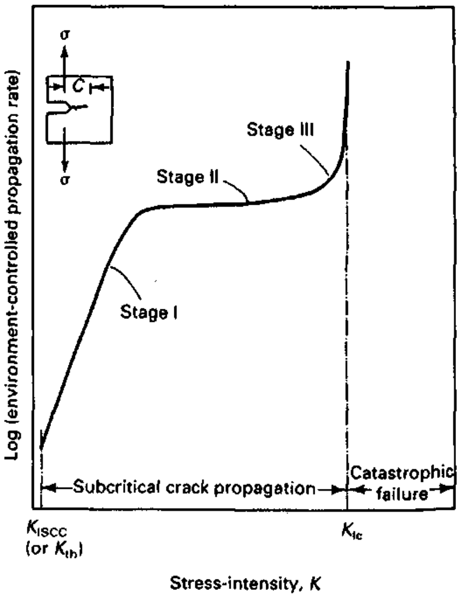

Fig. 2-15: Typical progression of the crack growth rate as a function of the stress intensity factor with subcritical crack propagation due to stress corrosion cracking [2-3]

A well-known test method for investigating the SICC is the tensile test with a slow strain rate in the medium, which is referred to in the technical literature as Slow Strain Rate Test (SSRT) or Constant Extension Rate Tensile Test (CERT). These tensile tests, in which smooth or notched tensile specimens are deformed at a very low strain rate, typically in the range of 10^{-5} s^{-1} ... 10^{-7} s^{-1}, with continuously increasing elongation until the onset of forced fracture, are suitable both for the basic, conservative determination of the medium effect in a corrosion system and for parameter studies of relevant influencing variables.

Extensive and systematic investigations using the SSRT technique in HT water have been carried out, for example, by Lenz et al. [2-8], Choi et al. [2-29] and Congleton et al. [2-31].

It is generally shown that the medium influences the macroscopically measured deformation behaviour of unalloyed and low-alloy steels and leads to reduced values of the macroscopically measured deformation parameters, see Fig. 2-16 (Note: at a constant strain rate, the “Time” parameter is proportional to the strain).

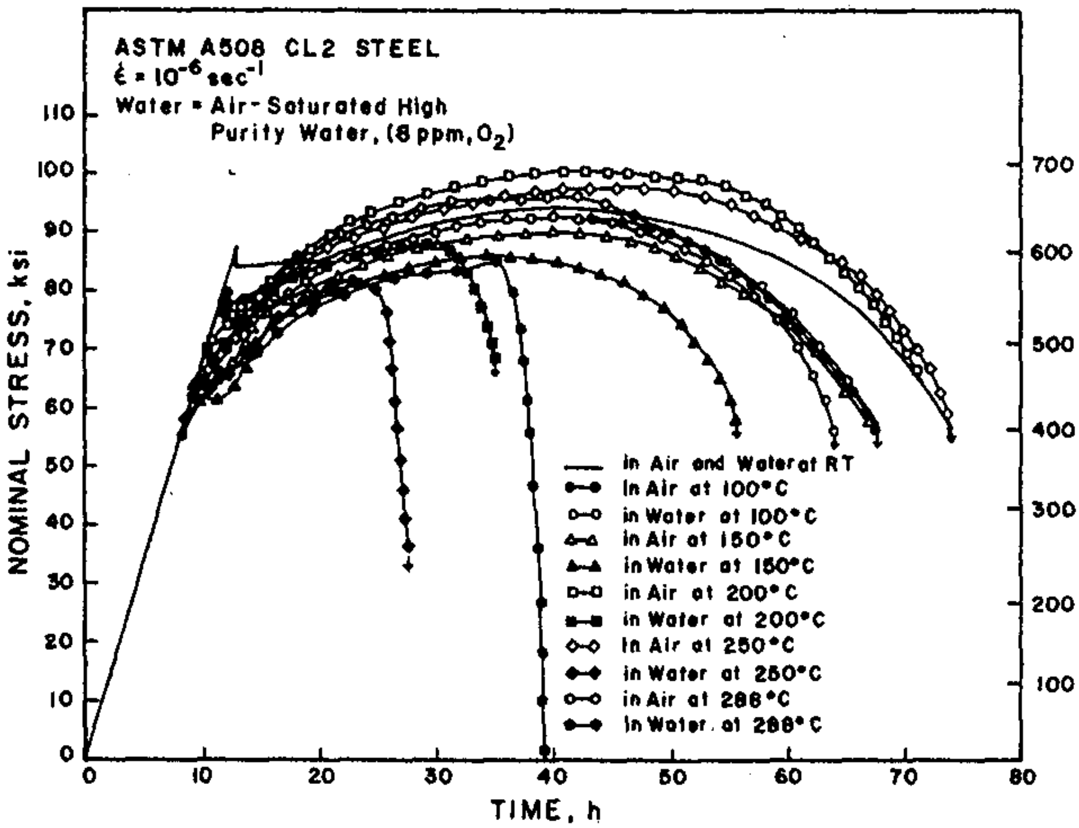

Fig. 2-16: Stress-strain curves of SSRT tests ($d\varepsilon/dt = 10^{-6}$ s^{-1}) in air and in oxygen-containing, high-purity HT water (8 ppm O_2) [2-29]

It should be expressly pointed out that the measured, apparent reduction in elongation at break and constriction at break does not represent a change in the plastic material behaviour per se, but that it is an effect of the deformation behaviour of the sample.

2.5 Illustration of possible crack growth rates

2.5.1 General preliminary remarks

The conditions and criteria that lead to crack growth due to SICC or low-frequency and low-cycle corrosion fatigue depend on the relevant boundary conditions of the corrosion system with material, medium and mechanical stress.

The following chapters show examples of which cyclic crack growth rates occur in the case of SICC or the physically corresponding cyclic crack growth and can therefore serve as a basis for conservative crack growth considerations. Crack growth analyses and evaluations of components are not included in the regulations for fossil-fired thermal power plants with a water-steam cycle.
For this purpose, a technical-scientific limit analysis of the SICC crack growth rates possible under laboratory conditions is carried out and subsequently compared with values from component damage and da/dN values.
These values are to be regarded as overly conservative for real pressurized components in steam power plants due to the design and construction-related lower or only short-term possible stresses and should therefore not be used as constant values over time for the evaluation of these components.
For the pressurized, water-flow components in fossil-fired steam power plants, a hydrogen influence on the mechanism of the SICC and thus the H-SICC can generally be assumed as a potential mechanism. Quantitative statements regarding the influence of hydrogen are not yet available. A separation between the merging mechanisms SICC and H-SICC is more of an academic nature here, as in practice a separation of the mechanisms in fossil-fired power plants is not possible and is also not necessary regarding the remedial measures.

2.5.2 Crack initiation by SICC

According to the findings from laboratory tests, cracking can occur due to SICC if the three primary parameters for strain rate, temperature and dissolved oxygen in the medium are exceeded simultaneously. However, operational practice has shown that these are necessary, but not sufficient conditions for triggering SICC in real components. The mechanical deformation of pressurized components and systems is limited by design (stress) and function (kinematics). In practice, further SICC-promoting factors are therefore required for the occurrence of SICC damage, as described above.

2.5.3 Crack growth estimation based on the Ford-Andresen model

The Ford-Andresen model [2-17] is based on sulfur as the key to the entire electrochemical process.

From the illustration of the Ford-Andresen model (see Fig. 2-2), it can be deduced that crack growth is maximized at a strain rate applied externally to the sample or component because the Mn Sulfides present in the microstructure are exposed more quickly. Accordingly, the theoretical crack growth rate for this load, which is basically only possible in the laboratory, is between approx. 4×10^{-6} mm/s and 8×10^{-5} mm/s (equivalent to between approx. 130 mm/a and 2500 mm/a) depending on the stress intensity factor.

2.5.4 Theoretical crack growth rates from SSRT/CERT tests

In SSRT/CERT tests, very high crack growth rates in the order of magnitude of the theoretical high sulfur line (see Fig. 2-2) are theoretically possible for short periods. In individual cases, however, the crack growth rates cannot be determined precisely without knowledge of the crack depth and the proportionate test time for active crack growth.

Rippstein et al. [2-19] have found that crack initiation in SSRT/CERT tests (i.e. under high loading exceeding operational conditions!) only occurs shortly before the tensile strength is reached. This considerably shortens the time of possible crack growth. The maximum crack growth rates determined by Rippstein et al. on this basis are approx. 6×10^{-6} mm/s or approx. 200 mm/a (Fig. 2-17).

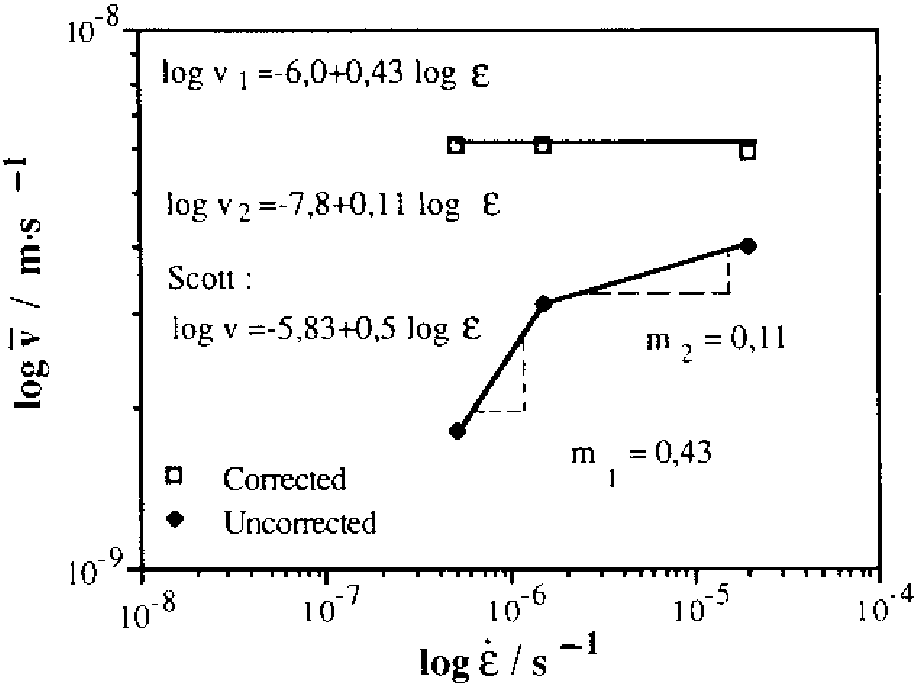

Fig. 2-17: Crack growth rates determined from SSRT tests with a low-alloy steel in HT water [2-19]

The crack opening rate has the main influence, whereby the measured crack growth rate can shift by around three orders of magnitude from approx. 10^{-9} m/s to 10^{-6} m/s under otherwise identical conditions. Specifying a SICC crack growth rate for certain environmental conditions does not appear to make sense if the crack opening rate of a defect to be evaluated is not precisely known.

2.5.5 Findings that can be derived from operating experience

In a SICC case that occurred in practice, which led to leakage in a BWR feedwater pipe with a wall thickness of 18 mm in at least 3 to 5 load cycles (start-up processes) [2-32], the crack growth rate can be narrowed down as follows:

- Penetration of the wall thickness occurred in at least 5 stages with an average of 3.6 mm crack propagation each time.
- Evaluations of the operating data show that the primary parameter values for O_2 content, temperature and strain rate required to trigger SICC are present for at least 10 h during start-up. A particularly "gentle" slow start-up can extend this time and therefore be counterproductive.

If it is assumed that existing defects or cracks immediately show crack growth, the crack growth rate required to produce this finding is calculated as follows

$$3.6 \text{ mm} / 10 \text{ h} = 1 \cdot 10^{-4} \text{ mm/s} \approx 3200 \text{ mm/a} \qquad \text{Equation 2-1}$$

This value is in the range of the theoretically determined high-sulfur line (see Fig. 2-4) and corresponds to the range of maximum crack growth rates that can be estimated from laboratory tests and that can be achieved in the short term.

In summary, it can be concluded that with SICC the maximum possible short-term crack growth rates in the component can be at the level of the high-sulfur line of the laboratory samples, which is why this can be regarded as a conservative enveloping limit curve for the physically possible crack growth due to SICC.

However, it is not technically sensible or expedient to use these short-term maximum possible values as constant values over time for the evaluation of real components, but their use for limit considerations may be adequate in individual cases.

2.6 Proposals to reduce the SICC/H-SICC

Effective remedial measures against SICC result from the known effect of the individual parameters for material, medium and stresses.

2.6.1 Material selection based on the sulfur influence theory

- Use of a low-S steel or a steel with a fine, homogeneous distribution of Mn sulfides. Steels with an S content of ≤ 0.005 mass-% are generally referred to as "low sulfur" in the literature;
- Use of a steel and a weld metal with a low susceptibility to DSA. The degree of susceptibility can be qualitatively determined in tensile tests with a slow strain rate in air at elevated temperature.

2.6.2 Material selection based on the H-SICC theory

- H-SICC leads to a decrease in elongation at break in the SSRT test for all common materials for the water vapor cycle at 200 °C to 300 °C (e. g. P-steels, 15Mo3, 13CrMo4-5, WB 36). This can be interpreted as an H embrittlement effect. The analysis of SICC damage regarding different materials still shows no significant differences in frequency. Although materials have different elongation at break values under the same SICC conditions, this is of no practical benefit. This means that changing materials is not a viable option for reducing susceptibility to SICC.
- In principle, materials with a sensitivity to H-SICC, e. g. higher-strength materials such as X20CrMoV12-1 or 10CrMo9-10 welded without post-weld heat treatment, cannot be used in this area of application. See also [3-21].

2.6.3 Constructive and procedural measures

- Avoid tearing of the magnetite layer (low-alloy materials) through soft inner contours and homogeneous temperature distribution and not too high temperature transients, resulting in corresponding thermal stresses (magnetite protective layer criterion according to TRD 301, Annex 1 [3-5]).
- If a cracked magnetite layer is detected (usually visually via hematite bleeding) without crack formation in the material, these must be ground while avoiding material hardening (localized removal of the magnetite layer) and the absence of cracks confirmed with Surface Crack Testing;
- Achieve a temperature distribution that is as uniform as possible with few, small temperature transients that are as short as possible;
- The SICC/H-SICC-relevant temperature range should be passed through as quickly as possible; a gentle approach can be counterproductive here;
- Avoidance of excessive stress and strain relief;
- Minimization of residual welding stresses and notch effects in weld seams (e. g. through design, weld seam preparation, weld seam geometry, welding technology and appropriate heat treatment);
- Avoidance of mechanical overloads (with plastic deformations).

2.6.4 Medium

- Avoidance of local increases in conductivity, e. g. by maintaining a slow flow and avoiding stagnant medium;
- Avoidance of stagnant corrosion through suitable preservation;
- Maintaining the limit concentration of dissolved oxygen, depending on the steel and medium conditions, including flow velocity, i.e. minimizing corrosion potential, but maintaining the formation of a surface layer to avoid flow-assisted corrosion (FAC, also known as erosion corrosion EC);
- Avoidance of the critical temperature range (approx. 150 °C < T < 250 °C) if this is technically possible.

2.7 Conclusions for SICC from test results and operating experience

Despite the large number of studies, there is currently no scientifically founded and complete overview of all influencing parameters and their interactions that allows an analytical, quantitative, and unambiguous assessment of the susceptibility of components to crack growth in the context of SICC. Practical predictions and assessments have therefore not yet been possible without an engineering assessment.

Specifically, there are still gaps in the database regarding the influence of strain restraint and thus the influence of local strain rates, which are significantly affected by this.

A large number of cases of damage due to environmentally assisted crack formation on components made of unalloyed and low-alloy steels in German power plants can be attributed to SICC, as it has been proven that crack initiation and growth occurred in particular during the start-up of the plant. During this time, strain changes are caused by the increase in temperature and pressure. These already existing and unavoidable stresses can also be superimposed by additional strain changes caused by thermal stratification of cold and hot media. These additional stresses can be reduced by design and operation.

An engineering criterion of 80 % of the hot yield strength at operating temperature was used as the threshold value for susceptibility to SICC for the evaluation of Nuclear Power Plant (NPP) components regarding crack initiation by SICC. This can be derived both from the results of laboratory tests and from operating experience, as crack initiation only occurs at stresses in the range of the respective hot yield strength of the material or above.

If crack growth occurs due to SICC, then due to the short-term, locally extreme mechanical stress, it can be conservatively assumed that the theoretical maximum crack growth rate is quickly reached, which results in the form of the high-sulfur line from the slip-step dissolution model. In plant operation, such stresses are always limited to a few hours.

In the international discussion outside of Central Europe, SICC, which represents a borderline case of fatigue corrosion cracking at very low loading frequencies, does not play an independent role as a separately considered type of crack corrosion. The effects observed in the laboratory, which can be attributed to the influence of strain changes at a slow rate, are considered abroad in the context of fatigue. This applies both to crack initiation, which is considered as part of component design, and to crack growth, which is analysed and evaluated as part of in-service measures.

3 Operating experience

3.1 Regulations

General

Historically, the consideration of corrosion effects on fatigue strength in nuclear regulations (ASME Code, JSME-CODE, RCC-M Code, KTA regulations) was first and still today primarily considered in the fatigue life calculation of components and systems of nuclear power plants under the specific material-side, temperature-side (characteristic relevant temperature range between 150 °C and 300 °C) and medium-side operating conditions (pressurized water reactor, boiling water reactor). Due to publications by the Argonne National Laboratory (USA) from the beginning of the 1990s, the question of the discrepancy between the design fatigue curves provided in the regulations for verification – derived from laboratory tests in air – and the medium conditions actually prevailing locally at the component to be verified was raised. Even the simple assumption that the fatigue strength of the materials used under reactor coolant conditions would not differ greatly from the behavior in air due to the fact that high-purity water would be used could not be substantiated. Two Japanese studies [3-1] and [3-2] investigated the question in depth and proved on the one hand the sensitivity of the materials to this corrosive medium effect. However, there has been no evidence in practice worldwide of premature, fatigue induced component failures of properly designed and manufactured NPP components under operating conditions that conform to specifications.

The main influencing parameters in the laboratory test with clear and strong influence were

- Temperature;
- Strain rate;
- Dissolved oxygen content in water and
- Sulfur content in the case of ferritic steels.

The EPRI "Fatigue Management Handbook" from 2009 [3-3] refers to the significance of environmental effects and corrosion fatigue in accordance with the correlation

Corrosion fatigue = interaction between corrosive environment and cycling

is referred to. The interaction of both effects can be more damaging than the separate effect of both mechanisms. On the one hand, the cyclic load can increase the corrosive effect and on the other hand, the corrosion effect can accelerate the mechanical fatigue process. The reduction in fatigue strength under the influence of the medium is shown qualitatively in the Wöhler diagram in Fig. 3-1. It is also clear from this diagram that medium-free conditions are only guaranteed in a vacuum and that, strictly speaking, the air environment – for which the fatigue curves ("in air" fatigue curves) are usually recorded – already represents a medium with a potential for reduction. Nevertheless, the “in air” fatigue curves are still regarded as a pragmatic reference for quantifying medium-related corrosive reduction effects in the form of reduction factors F_{en}.

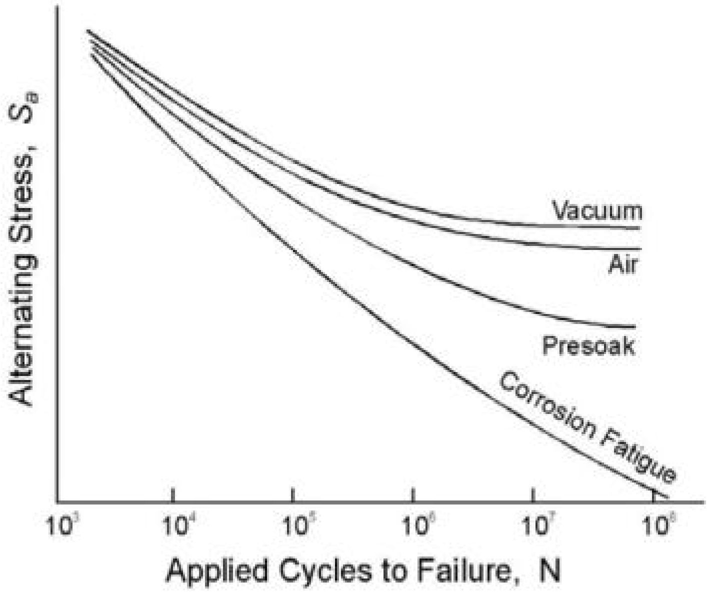

Fig. 3-1: Wöhler diagram under different ambient conditions according to [3-3]

These are defined – established in the NUREG/CR-6909 Guide [3-4] as an essential technical basis of the above-mentioned current nuclear regulations – as the quotient of the achieved number of load cycles at room temperature in air to the achieved number of load cycles at operating temperature in the medium

$$F_{en} = (N_{RT,air}/N_{Medium}) \qquad \text{(Equation 3-1)}$$

and when determining degrees of exhaustion (CUF = Cumulative Usage Factor) for each load spectrum k and the associated actual number of load cycles n_k multiplicatively according to

$$CUF = \sum_{k=1}^{n} \frac{n_k}{N_{k,RT,air}} \cdot F_{en,k} \qquad \text{(Equation 3-2)}$$

linked. $N_{k,RT,air}$ represents the permissible number of load cycles to be taken from the fatigue curve according to the stress level of the load spectrum k. This is exemplified for two load spectra of the equivalent stress ranges $\Delta\sigma_{eqv,1}$ und $\Delta\sigma_{eqv,2}$ corresponding to

$$CUF = \sum_{k=1}^{n} \frac{n_1}{N_1} + \frac{n_2}{N_2} + \cdots + \frac{n_k}{N_k} \qquad \text{(Equation 3-3)}$$

shown in Fig. 3-2.

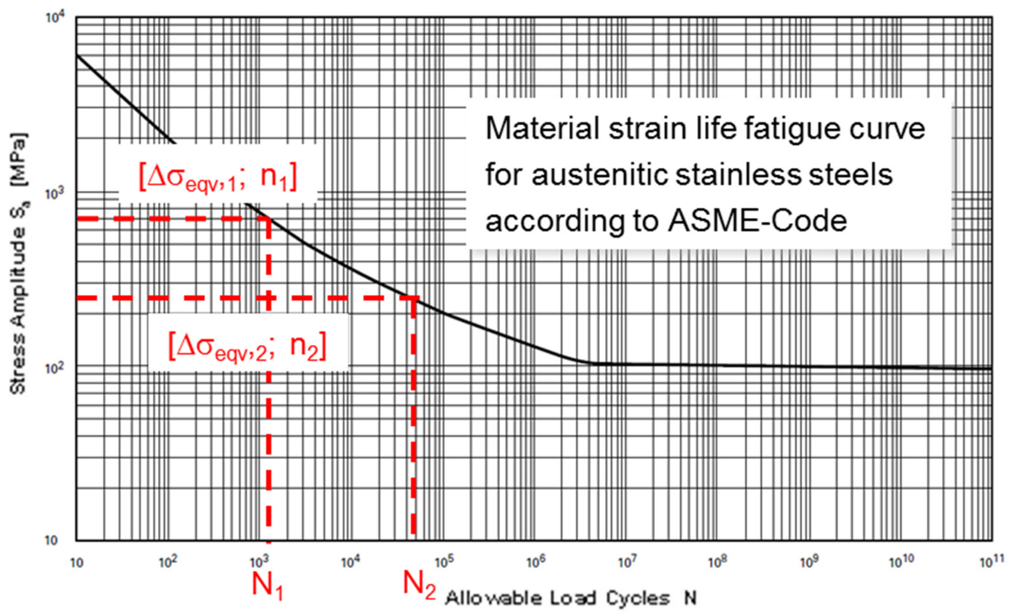

Fig. 3-2: Exemplar determination of the degree of exhaustion CUF for two load spectra

An example of the formula set for austenitic CrNi steels according to [3-4] shown in Fig. 3-3.

$F_{en} = \exp(-T^* O^* \varepsilon^*)$ for $\varepsilon_a > \varepsilon_{th} = 0.1\ \%$,

$T^* = 0$ $(T \leq 100\ °C)$
$T^* = (T - 100) / 250$ $(100 < T < 325\ °C)$

$\varepsilon^* = 0$ $(\dot{\varepsilon} > 10\ \%/s)$
$\varepsilon^* = \ln(\dot{\varepsilon} / 10)$ $(0.0004 \leq \dot{\varepsilon} \leq 10\ \%/s)$
$\varepsilon^* = \ln(0.0004 / 10)$ $(\dot{\varepsilon} < 0.0004\ \%/s)$

$O^* = 0.29$ (DO < 0.1 ppm) all wrought and cast SSs and heat treatments
$O^* = 0.29$ (DO > 0.1 ppm) sensitized Hi-C wrought SSs and cast SSs
$O^* = 0.14$ (DO > 0.1 ppm) all wrought SSs and treatments except sensitized Hi-C

Fig. 3-3: Set of formulas for determining F_{en} factors for austenitic CrNi steels [3-4]

Conventional regulations

Conventional regulations essentially specify calculation formulas that are intended to ensure the preservation of the magnetite protective layer on parts made of non-austenitic steels that come into contact with water. Section 5.1.4 of TRD 301 states that [3-5]:

In the case of parts made of non-austenitic steels that come into contact with water, particular attention must be paid to the preservation of the magnetite protective layer. The stress limits for these parts are therefore additionally restricted as follows:

$$\check{\sigma}_i \geq \sigma_{ip_4} - 600\ N/mm^2 \qquad \text{(Equation 3-4)}$$

$$\hat{\sigma}_i \leq \sigma_{ip_4} + 200\ N/mm^2 \qquad \text{(Equation 3-5)}$$

$$\sigma_{ip_4} = \alpha_m\,(p_4) \cdot p_4 \cdot \frac{d_m}{2\,s_b} \qquad \text{(Equation 3-6)}$$

Here, p_4 stands for the operating pressure in N/mm^2, α_m represents the associated stress increase factor and d_m and s_b denote the mean diameter and wall thickness in mm.

In section 13.4 of AD-Merkblatt S2 [3-32], a corresponding reference is made to TRD 301 Annex 1 [3-5]:

For parts in contact with water made of ferritic and martensitic steels that are operated at temperatures above 200 °C, care must be taken to preserve the magnetite protective layer. See TRD 301 Annex 1.

This is also confirmed in the explanations to AD-Merkblatt S2 [3-6]:

For the design of components in contact with water made of non-austenitic steels (e.g. waste heat boilers in chemical plants, rock hardening boilers), reference is made to the corresponding stress-limiting regulations in accordance with TRD 301, Annex 1.

The criteria of TRD 301 Annex 1 [3-5] were also adopted in DIN EN 13445-3 [3-7] in section 18.4.6. A note is added in [3-7]:

NOTE: It is assumed that the protective layer is stress-free under the operating conditions under which the magnetite protective layer is formed.

This also applies analogously to DIN EN 12952-3, section 13.4.3 [3-8].

Environmentally Assisted Fatigue (EAF) in nuclear regulations

KTA-Codes

In the current Western nuclear codes and standards for light water reactors, reference is made to the principles addressed in the “General” section.

In the context of the German safety standards of the Nuclear Safety Standards Commission (KTA), information on the consideration of the influence of the medium was introduced for the first time with the November 2013 edition of KTA safety standard

KTA 3201.2 (“Components of the Primary Circuit of Light Water Reactors, Part 2: Design, Construction and Calculation”). In Section 7.8.3 concerning fatigue analyses, “attention thresholds" based on typical operating transients are defined for the first time by applying the criteria from NUREG/CR-6909 [3-4] to consider the influence of the medium as follows:

If a medium-induced reduction in fatigue strength cannot be ruled out, consideration of the medium on fatigue is required from an attention threshold D = 0.4 by the following measures:

a) inclusion of the affected component areas in a monitoring program in accordance with KTA 3201.4 or
b) experiments close to operation or
c) mathematical verifications considering medium-related reduction factors and realistic boundary conditions.

Possible measures in power operation are therefore linked to KTA safety standard KTA 3201.4 ("Components of the primary circuit of light water reactors. Part 4: In-service inspections and operational monitoring”), version November 2010. Parallel to KTA 3201.2, a corresponding regulation was also introduced in the November 2013 edition of KTA 3211.2 (“Pressure- and Activity-Retaining Components of Systems Outside the Primary Circuit, Part 2: Design, Construction and Calculation”). These regulations were also integrated into KTA Safety Standard 3204 (“Reactor Pressure Vessel Internals”), version November 2017.

The attention threshold is therefore based on the degree of depletion “D” (corresponding to the Cumulative Usage Factor (CUF)). This should not be confused with the thresholds that apply to the activation of the medium-induced stress factors F_{en} according to [3-4] with regard to temperature, strain rate and strain amplitude, see Fig. 3-3 (there for austenitic CrNi steels).

The methods for considering the influence of the medium on the fatigue analysis that are anchored in the KTA rules are discussed in detail in [3-9].

<u>ASME-Code</u>

Within the framework of the ASME Code, the formulae of NUREG/CR-6909 Rev. 1 [3-4] are used to determine the F_{en} factors to take into account the influence of the medium on fatigue in accordance with equation (3-1). Code Case N-792-1 “Fatigue Evaluations Including Environmental Effects” [3-10] covers this procedure.

Note: The ASME Code Case N-917 “Fatigue Crack Growth Rate Curves for Ferritic Steels in Boiling Water Reactor Environments, Section XI, Division 1” contains optional fatigue crack growth curves for ferritic steels under BWR conditions for various water chemistry operating modes [3-11].

RCC-M-Code

Like other nuclear codes, the French AFCEN RCC-M Code has responded to international developments regarding the consideration of the medium effect on fatigue and has integrated two “Rules in Probationary Phase” (RPPs), called “RPP-2” and “RPP-3”, with the 2016 edition [3-12]. RPP-2 consists of an adaptation of the design fatigue curve for austenitic and duplex steels as well as nickel alloys and at the same time represents the basis for RPP-3, which contains guidelines for the inclusion of F_{en} factors in the calculation of damage levels CUF. Compared to the already addressed NUREG/CR-6909 [3-4] methodology, however, the F_{en} factor is reduced by a factor of 3, based on years of targeted experimental investigations. This margin, known as the “integrated F_{en} factor”, is made possible by the proven over-conservative quantification of the surface influence under medium conditions, which is already part of the “in air” design fatigue curves as one of several margin factors. This was demonstrated on the basis of numerous targeted investigations under medium conditions on small samples with rough surfaces [3-13] to [3-16]. The application of this alternative calculation method is currently being consolidated based on a comprehensive benchmark [3-17].

3.2 Design

The damage mechanism of strain-induced crack corrosion occurs exclusively in the area of the water vapor cycle, in which water is also at least temporarily present in the liquid phase. It requires a complex combination of boundary conditions in order to be effective. However, this also means that it is difficult to take this mechanism into account in the design.

The following case studies provide information on the selection of remedial measures:

Case 1: SICC on the inner housing of a boiler circulation pump

A boiler circulation pump will always be exposed to increased temperature gradients. Likewise, according to the boiler formula, increased wall thickness is required due to its large internal volume. For this reason, it is advisable to design and manufacture the inner contour with as few notches as possible. In addition, temperature gradients should be reduced in the process.

Case 2: SICC in drain pipes

In drainage pipes, pipe bends and horizontal pipe sections are particularly affected.

Pipe bends exhibit ovality after being produced by cold bending. The diameter in the area of the neutral fiber is increased and reduced in the tension and pressure area. Due to the ovality, an internal pressure load causes increased tensile elongation in the area of the neutral fiber. The increased elongation can cause the magnetite layer to fail and gradually promote a SICC crack. For this reason, the ovality should be kept as small as possible.

In the horizontal straight pipe area, the duration of exposure to standstill corrosion is often relevant. Inadequate drainage can cause the medium to stand for longer, leading to a concentration of corrosion-promoting water constituents and thus trigger pitting corrosion during standstill phases. If sufficiently deep pits are created, the SICC can start from there with crack propagation. For this reason, the process engineering concepts for the discharge lines must be reviewed. Stagnant medium with an air cushion should be avoided, as this accelerates corrosion when cold.

Countermeasures can be derived from the consideration of favourable boundary conditions:

- Limit the mean stress by limiting the stress utilization during dimensioning;
- If condensate forms, do not lay pipes horizontally, but with a sufficient gradient for draining. The gradient must be maintained in cold and warm operating conditions;
- If condensate forms, a sufficient number of drainage positions must be planned;
- Drain lines must be laid in an optimized manner to reduce the length of the pressurized line;
- Avoiding large notches on the inside to reduce local expansion amplitudes in alternating operation;
- If possible, provide weld seams with low edge offset and low root notch. This can be implemented, for example, by specifying assessment group “B” in accordance with DIN EN ISO 5817 for discontinuities in the root area;
- Develop and implement heat retention concepts for affected lines/components;
- The so-called “magnetite protection criterion” [3-5] is a quantitative boundary condition that can be used.

The magnetite protection criterion evaluates the damage step “thermomechanical failure and tearing” of the magnetite layer. Here, the influence of thermal transients in connection with the wall thickness of the component on the thermally induced differential strain between magnetite and metal is evaluated. If the strain limit is exceeded, the magnetite may crack or flake off and strain induced corrosion cracking may occur (see [3-5]).

3.3 Cases of damage

Two extreme cases of SICC damage frequency have been observed.

1. A system, for example a circulation circuit, experiences SICC damage to a large number of components over a period of years.
2. Only one single component in the system is damaged by SICC.

In case 1), process-related boundary conditions are the main cause.

In case 2), the design and operating mode of the component are relevant and must be questioned and, if necessary, optimized. Some case studies are presented below.

3.3.1 Historical cases of damage from 1960 onwards

In recent decades, a large amount of damage, including serious accidents, has been caused by SICC in fossil-fired power plants. As already described in the presentation of the state of knowledge on SICC in Chapter 2, damage due to SICC has also occurred in nuclear power plants, some of which have required extensive retrofitting. In the following, a categorization of the main components and systems in which historically relevant damage due to SICC has occurred is made. Reference is made to leading systems and the associated further literature as examples. As the damage in nuclear power plants has led to international R&D projects and an international exchange of experience that continues to this day, these are also included.

A systematic overview of historical cases of damage can be found in the EPRI report TR-106696 from 1997 [3-18]. It describes significant case studies from fossil-fired power plants as well as from nuclear power plants, each with a chapter on damage in German plants.

<u>Damage in fossil power plants</u>

Typical components and systems made of unalloyed and low-alloy steels with SICC damage worldwide are according to [3-18] (p. 2-1f.) state 1997:

- Feed water tanks and their degassing tanks;
- Feedwater preheater shells;
- Feedwater pump housing;
- Feed water pipes (see note);
- Economizer inlet manifolds and pipes;
- Boiler drum;
- Downpipes;
- Membrane wall of the boiler;
- Distributor in the lower membrane wall area (evaporator).

<u>Note:</u> A closer look at the cases of damage in German fossil-fuel power plants since 1960 shows that feedwater pipes are not affected in [3-18]. One possible explanation for this is the conservative design with avoidance of high-strength steels [3-18].

An evaluation of cases of damage in German fossil-fuel power plants as of 2000 [3-19] shows the following components and systems that are more or less fully exposed to the conditions leading to the occurrence of SICC, see Fig. 3 4:

- Steam generator heating surfaces and collectors in the eco-evaporator and separator system;
- Boiler drums;
- Circulation circuit;
- Start-up and shut-down system;
- Feed water tank;
- Injection cooler and lines;
- Minimum flow lines;
- Relief water lines;
- Emergency drain lines (secondary condensate);
- Draining and venting of the above systems.

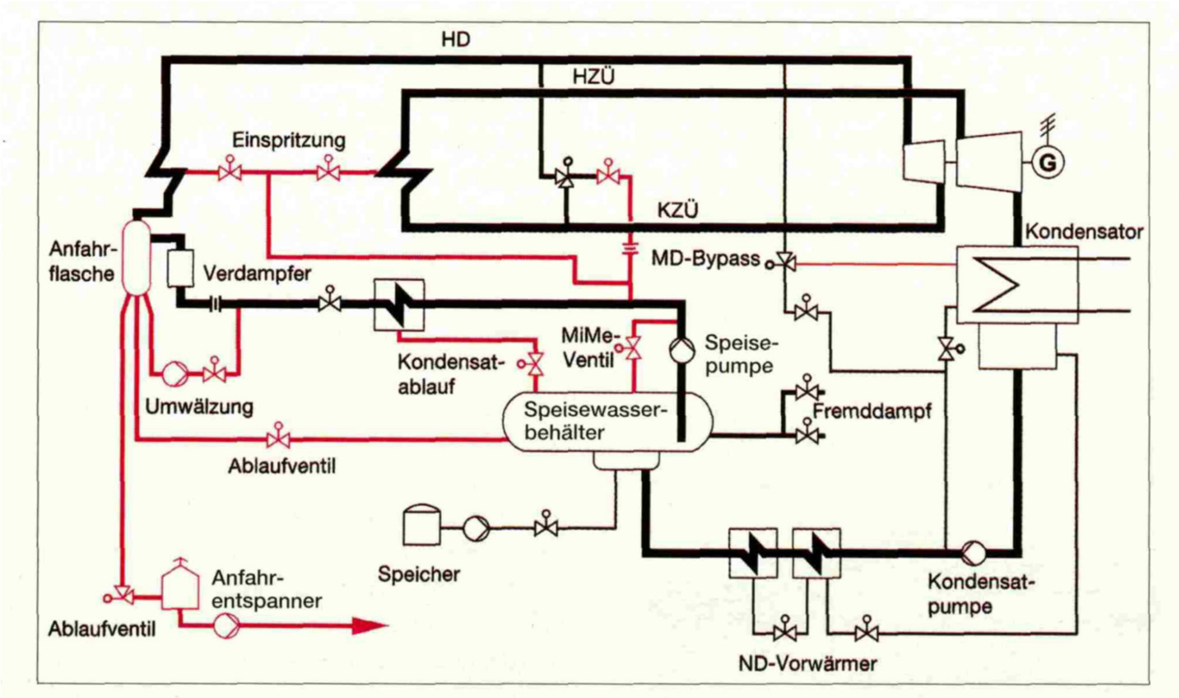

Fig. 3-4: Systems (in red) with conditions that can preferentially lead to SICC [3-19]

From today's perspective, the following should be added in particular:

- Boiler circulation pump housing [1-1]
- Drain lines, see chapter 3.3.2

According to [3-18] (p. 2-43 to 2-59), the main damage in German and European power plants from 1960 onwards with SICC as the cause of damage should be mentioned in particular:

<u>Feedwater tanks with the connected degassing tanks:</u>

Following cracks first discovered in 1966 in the feedwater tank/deaerator intersection area and a tear-off of a deaerator in 1971 in a southern German power plant with considerable consequential damage, systematic investigations were carried out on 55 feedwater tanks in the RWE lignite-fired power plants and published in 1977 [3-20]. Cracks were found in 16 of the 55 tanks. Operational cracking is therefore typical for this type of construction. Prior to the introduction of the term SICC in 1982 [3-21], the damage mechanism was referred to as stress-induced corrosion in conjunction with corrosion fatigue. The cracks were located exclusively at points with exceptional stress concentrations due to the design. The structural design was identified as being decisive for the occurrence of damage.

Systematic evaluations in Germany by VGB [3-22] and by NACE from 1984 onwards due to severe damage cases in the USA [3-23] and by EPRI [3-24] show the components potentially affected.

<u>Boiler drums:</u>

Beginning with damage in 1960 at the large power plant in Mannheim, damage was reported in boiler drums [3-25]. These were cracks on the inside of the drum in the perforated field area, preferably on the edges of the downpipe holes and in some cases also on the perforated surface. As of 1985, the merging concepts of stress-induced corrosion, SICC and crack corrosion at low expansion rates were named as the cause of the damage [3-25].

<u>Piping:</u>

Some examples of damage from 1960 onwards starting from the inside in piping in contact with water due to longitudinal cracking in pipe bends or due to circular cracks near rolling points are compiled in [3-19] as of 2000. This repeatedly led to the failure of downpipes with serious consequences. In the 1980s, areas of boiler systems that were difficult to access were increasingly affected, which led to the specification of inspections in VdTÜV Code of Practice 451 and in VGB Guideline VGB-R 509.

Four examples of damage from the 1990s, [3-25] and [3-19]:

- Bonn thermal power station: 1994 serious accident due to rupture of a boiling pipe directly under the drum, DN 80, 280 °C / 68 bar;
- 475 MW hard coal block in Saarland: 1995 longitudinal crack and pipe rupture of a drain pipe behind the water separator, ID 300 mm, 216 °C / 310 bar, see Fig. 3-6 upper part;
- 300 MW hard coal-fired unit in Denmark: 1995 tear-off of a flat bottom in a fitting of the start-up low load system, ID 300 mm, 300 °C / 210 bar;
- 300 MW hard coal block in Saarland: 1996 longitudinal crack with leakage in the bend of a blowdown pipe, ID 250 mm, 290 °C / 75 bar, see Fig. 3-6 lower part.

In the first two cases of damage, puddle formation in conjunction with prolonged shutdowns and inadequate shutdown preservation was one of the causes of the damage.

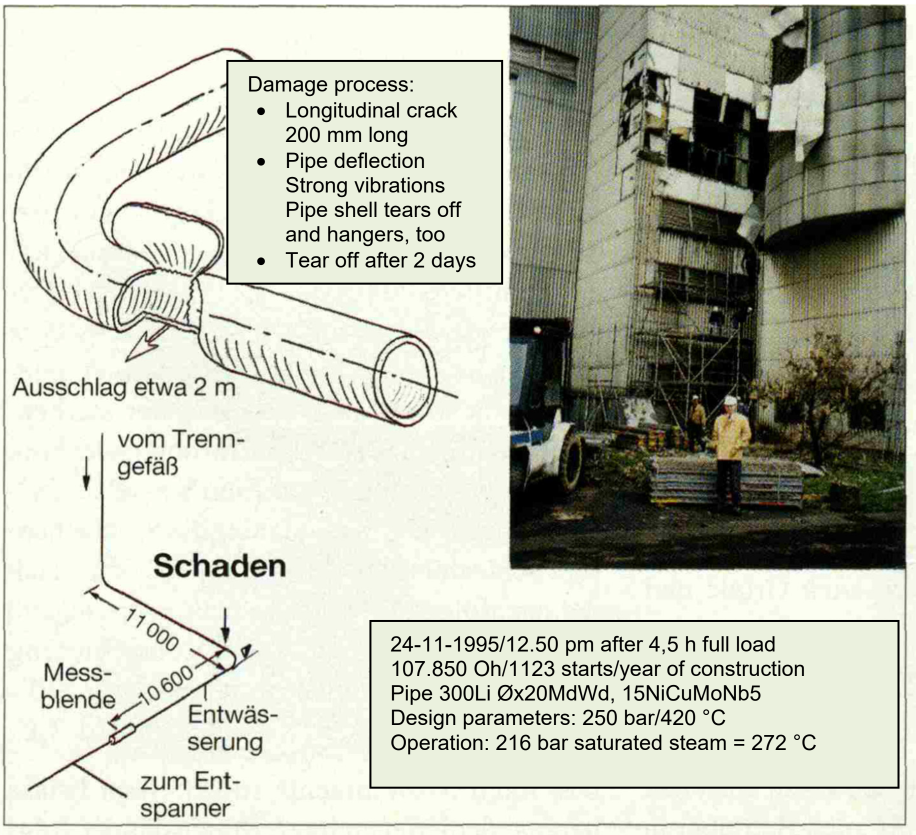

Translation	
German	**English**
Schaden	Damage
Ausschlag etwa 2 m	Deflection about 2 m
vom Trenngefäß	from the separator vessel
Messblende	Orifice plate
Entwässerung	Drainage
zum Entspanner	to the relaxer

Fig. 3-5 (1): SICC damage cases in pipelines
above: Longitudinal crack and rupture of a drain pipe ID Ø 300 mm
below: Longitudinal crack and leak of a blowdown pipe ID 250 mm [3-19]

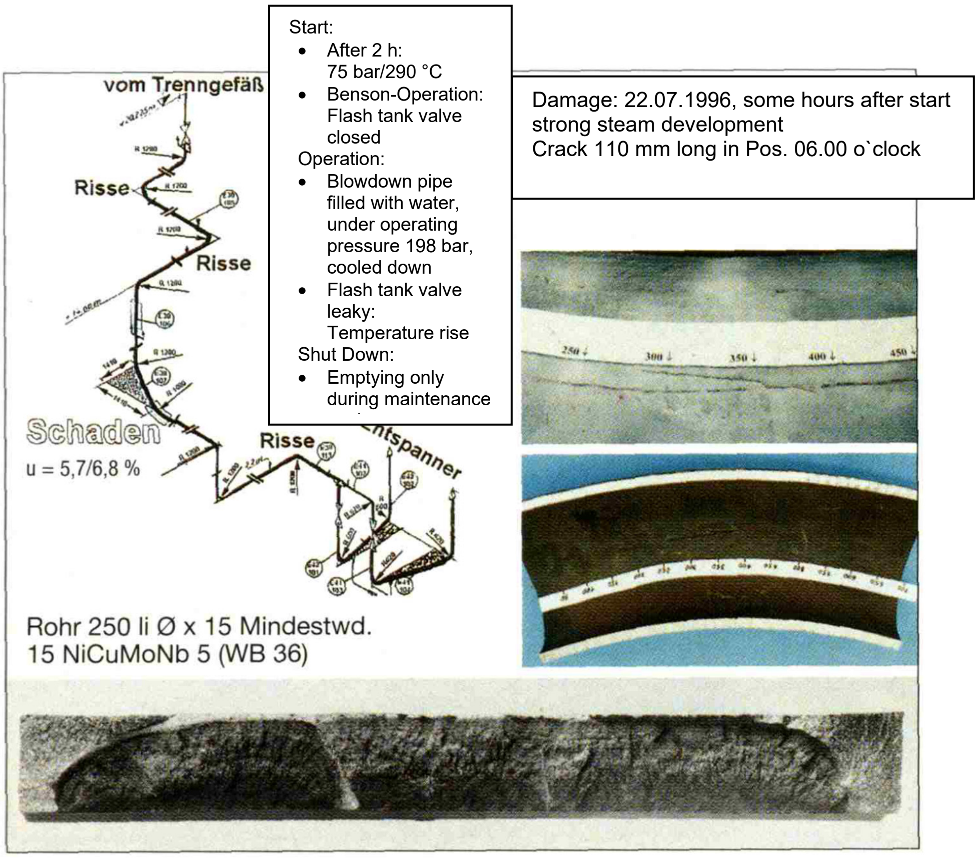

Fig. 3-6 (2): SICC damage cases in pipelines
above: Longitudinal crack and rupture of a drain pipe ID Ø 300 mm
below: Longitudinal crack and leak of a blowdown pipe ID 250 mm [3-19]

Translation:	
German	**English**
zum Trenngefäß	to the separator vessel
Risse	Cracks
Schaden	Damage
zum Entspanner	to the flash tank

As of the year 2000, reference [3-19] contains recommendations for monitoring pipelines regarding SICC with NDT (equivalent to NDE):

- Selection of pipe systems with a higher probability of damage;
- Definition of representative test points where SICC is most likely to be expected, preferably in the 6 o'clock position, if possible, supported by visual inspection (VT) of the inner surface;
- Radiographic testing (RT), ultrasonic testing (UT) for wall thicknesses from approx. 30 mm.

Damage in nuclear power plants

Typical components and systems made of unalloyed and low-alloy steels with SICC damage in NPPs internationally are according to [3-18] (p. 2-59 to 2-92) as of 1997:

- Thermosleeve welding areas in PWR components
  (reactor pressure vessel, steam generator);
- RPV feedwater nozzles and feedwater distributors in BWRs;
- Feedwater pipes in PWRs.

The experience with corrosion fatigue in German LWRs as of 1997 is described in [3-18] (p. 2-92 to 2-101). A current summary of the operating experience of LWR components and systems from Siemens/KWU LWR as of 2019 in [3-19] mentions the following major systems with damage caused by SICC:

- RPV feedwater nozzles in BWRs;
- Steam generator feedwater nozzles in PWRs;
- Feedwater pipes in BWRs.

Parallel to damages to feedwater tanks made of high-strength fine-grained steels in conventional plants, extensive cracking was found in the feedwater tank of the Biblis A PWR due to steam leakage, which led to early replacement in 1977 after only three years of operation with a change of material [3-20], [3-27]. As of 2005, [3-28] describes damage without and with leakages due to pitting corrosion and SICC on measuring lines in the water-steam cycle of PWRs. The three systems mentioned above must therefore be supplemented by:

- Feed water tanks made of high-strength fine-grained steels;
- Measuring lines in the water-steam circuit of PWRs.

Fig. 3-6 shows an example of the SICC damages to BWR feedwater nozzles found in the mid-1980s. By using a high-strength fine-grained steel from fossil power plant technology (17MnMoV64, WB35), the wall thickness of the pipe was minimized while at the same time achieving high stress utilization. This led to a jump in diameter with a significant edge offset and unfavourable weld seam geometry and thus to a significant local increase in stress. In addition, there were transient operational loads during start-up due to thermal stratification [3-29].

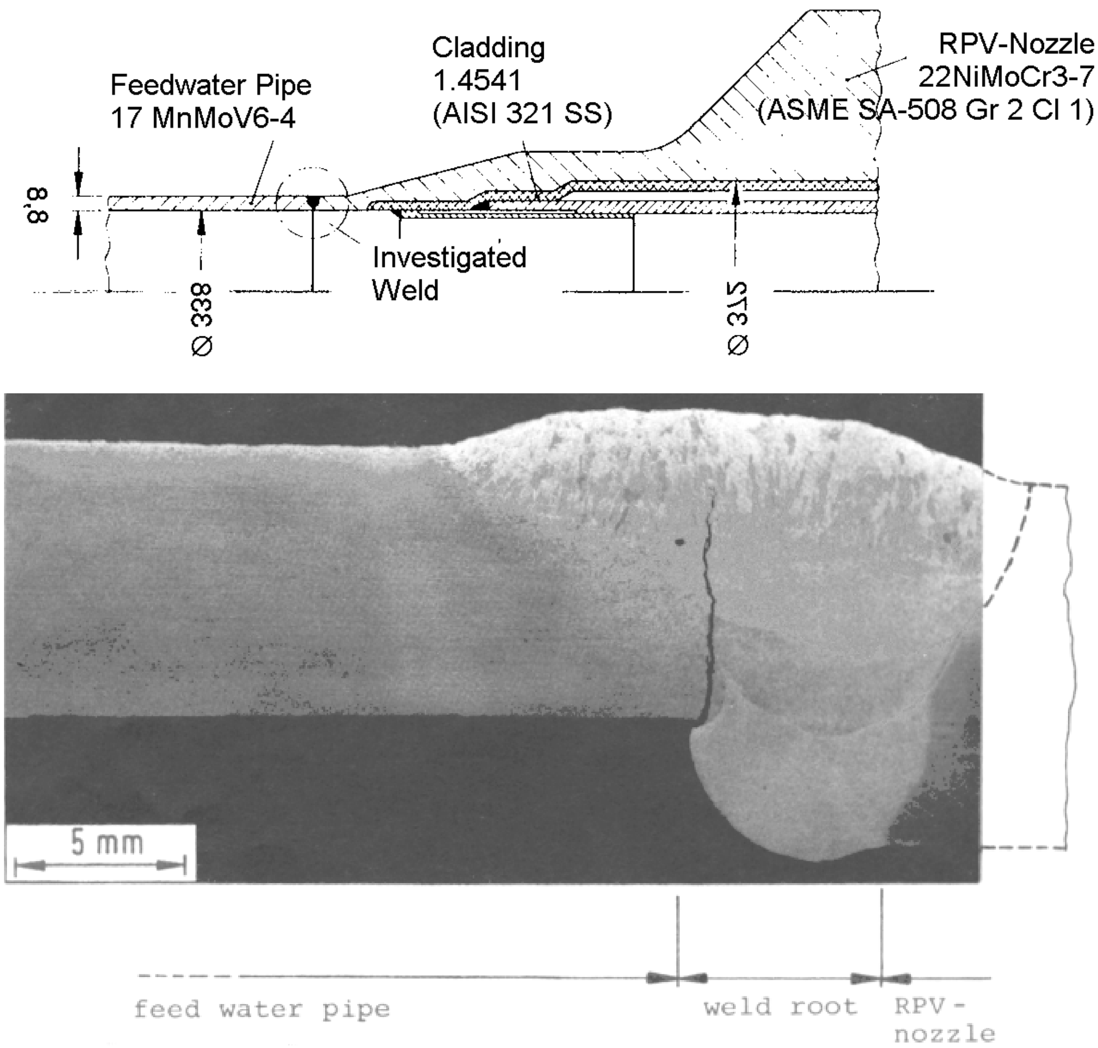

Fig. 3-7: Circumferential crack in a nozzle seam of a thin-walled feedwater pipe made of WB35 to a RPV nozzle of a BWR [3-29], [3-30]

Fig. 3-8 shows a typical crack formation in the circumferential direction in a steam generator (SG) feedwater nozzle, as it occurred from the late 1970s onwards. The similarity to Fig. 3-7 is striking. Analogous to the thermal fluctuations at the BWR feedwater nozzles during start-up, pronounced local cyclic transient loads occurred here during low-load operation due to thermal stratification at the unfavourably designed and manufactured nozzle seams. During retrofitting at the beginning of the 1980s, the process technology for start-up operation was substantially optimized by retrofitting newly designed low-load valves directly in front of the SG feedwater nozzles in addition to optimizing the welding technology [3-29].

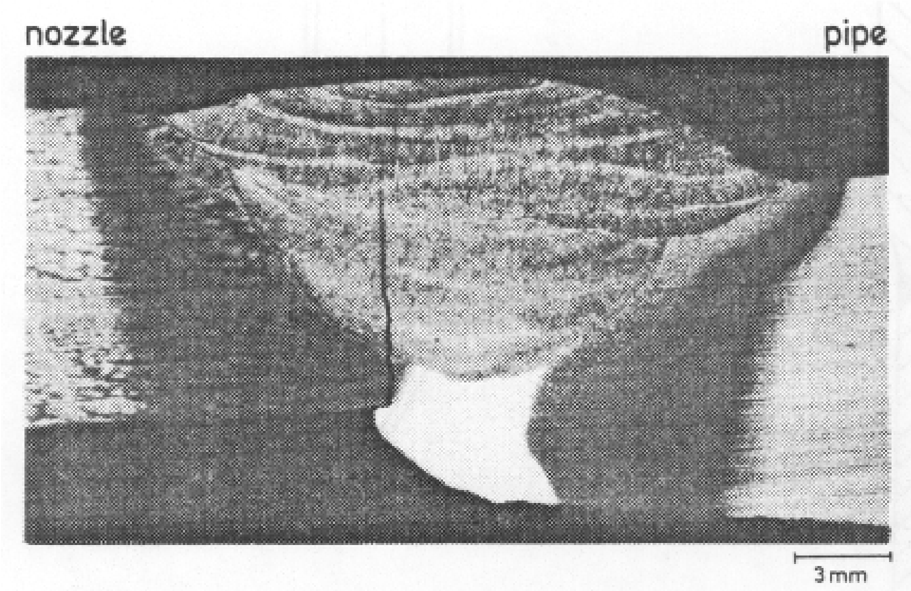

Fig. 3-8: Circumferential crack in a connection seam of a thin-walled feedwater pipe to the feed water nozzle of a PWR [3-27] (Presentation), [3-30]

Fig. 3-9 shows a typical crack formation in the weld metal of a BWR feedwater pipe. The axial cracks start here at corrosion pits [3-29]. It is worth mentioning that a correlation between the occurrence of SICC and the type of welding electrode used was established. The main influencing factor is the sensitivity of the weld metal to dynamic strain aging DSA, which depends on the alloy composition, see chapter 2.3.3.

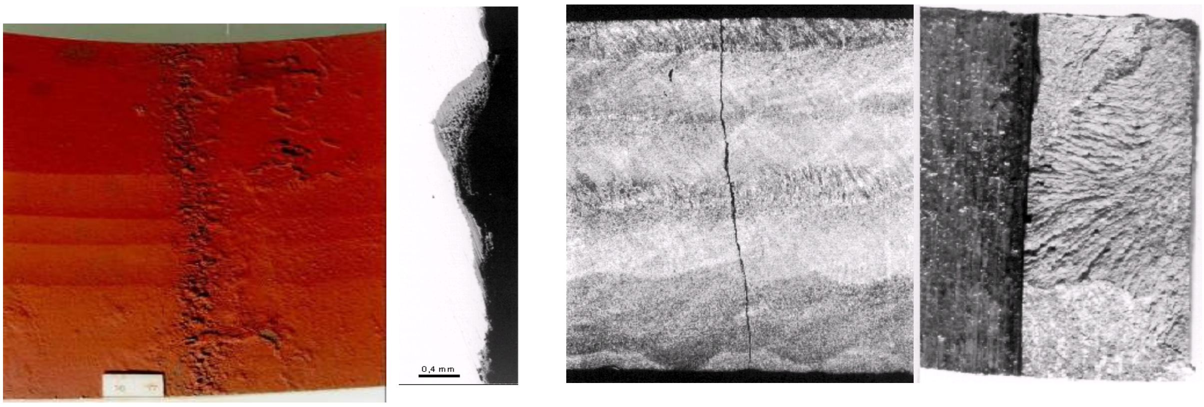

Fig. 3-9: Axial crack in the weld metal of a circular BWR feedwater pipe weld. [3-29], [3-31], left: pronounced surface damage (pit formation) due to water puddles during standstill phases, right: axial transcrystalline crack growth through the wall

Fig. 3-10 shows an example of SICC cracking in a pressure sensing line of a PWR live steam line DN 25 mm made of carbon steel St 35.8 caused by pitting corrosion [3-28]. This crack formation mechanism led to leakage elsewhere.

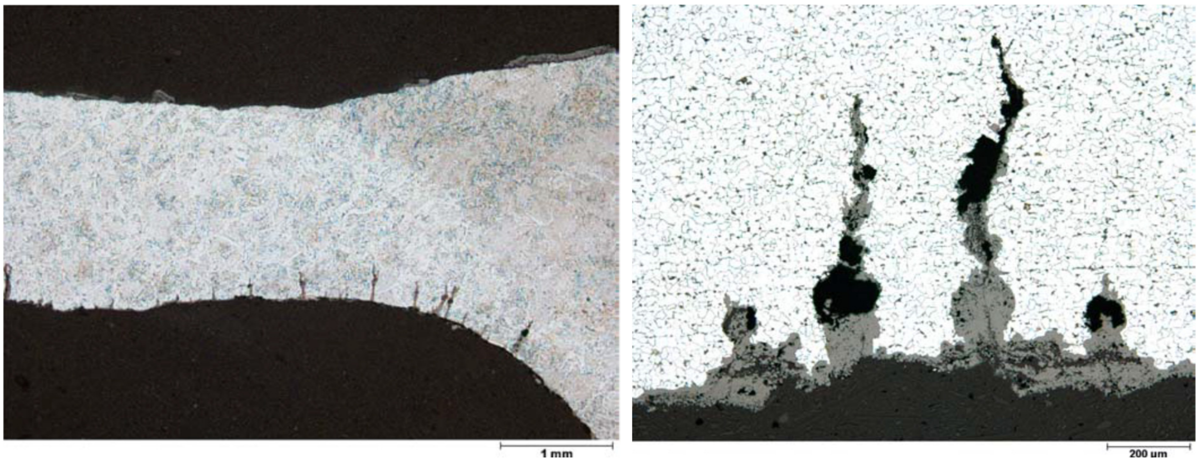

Fig. 3-10: SICC cracking in a pressure sensing line of a PWR fresh steam line DN 25 mm made of carbon steel St 35.8 due to pitting corrosion attacks [3-28]

3.3.2 Damage to a drain line

Drain lines for pressure components in the water vapor circuit are usually made from unalloyed or low-alloy steels such as P265GH, 16Mo3 or 13CrMo4-5. These materials are easy to weld and can be used well in the application due to the lower operational temperatures.

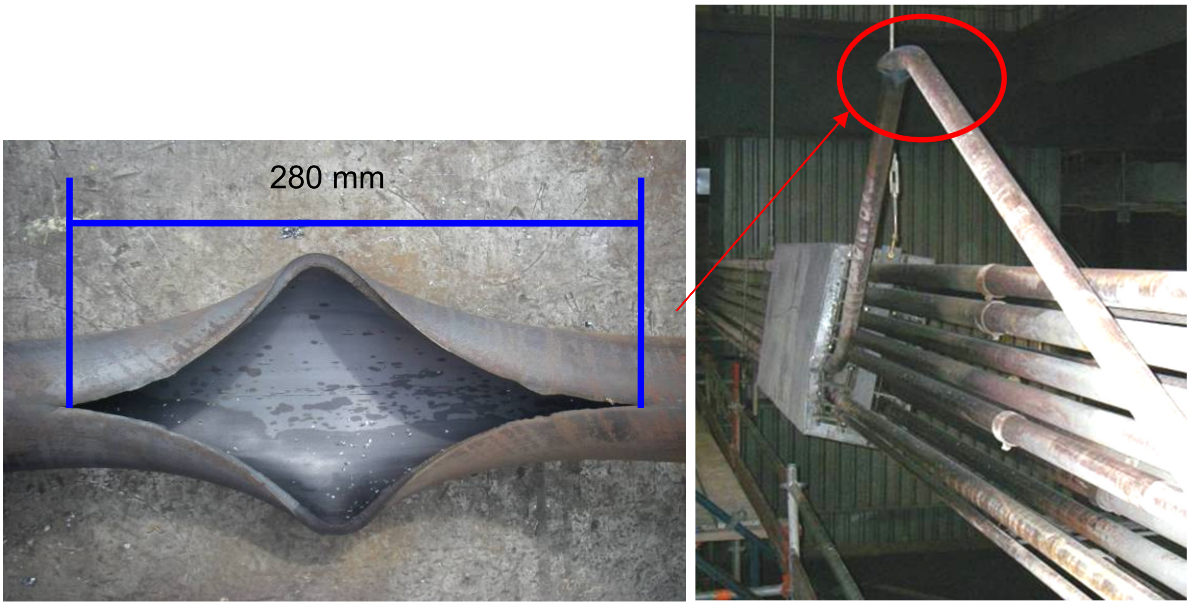

Fig. 3-11: Longitudinally torn open pipe of a drain line, crack position at 6 o'clock position in the horizontally laid pipe section (15Mo3, operating temperature 440 °C and operating pressure 230 bar)

Drain lines usually run close to stairs or inspection routes in the boiler house. The damage pattern in Fig. 3-11 shows the personal risk due to the large leakage area. Until the first damages to the drain lines in the 2010s, only a very low risk was seen, as the load caused by heat is rather moderate and the internal pressure is usually only temporary. It is therefore now recommended to include drain lines into the periodic inspection concept.

The fine linear crack can be seen on the longitudinally cut pipe segment at another point in the same pipe, Fig. 3-12. The crack is located exactly at the 6 o'clock position at the low point of the horizontally laid pipe. The crack also shows hematite bleeding, Fig. 3-11. Otherwise, the pipe appears almost unstressed. The material shows no abnormalities. It has a homogeneous ferritic-pearlitic microstructure and the crack is relatively straight, Fig. 3-13, Fig. 3-14. The crack shows no differentiated interaction with the various microstructural components.

The crack in Fig. 3-13 and Fig. 3-14 starts in a corrosion pit. It grows in a tensile stress-oriented manner and exhibits the internal corrosion scouring typical of SICC. These are caused in phases by stagnation corrosion in the crack tip. Fig. 3-15 shows an enlargement of the current crack tip area. The crack flanks are covered with a thick, partly porous oxide film.

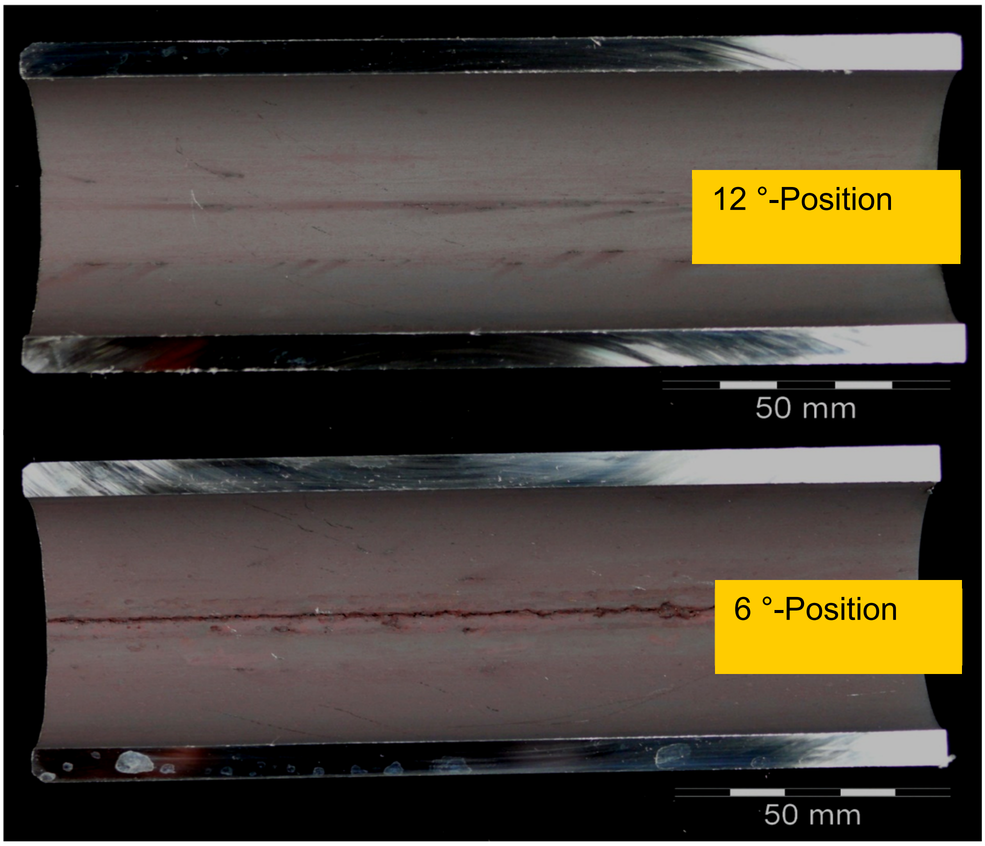

Fig. 3-12: Longitudinally cut pipe (15Mo3, 63.5x7.1 mm) of a superheater 2 drain line with crack findings at the 6 o'clock position

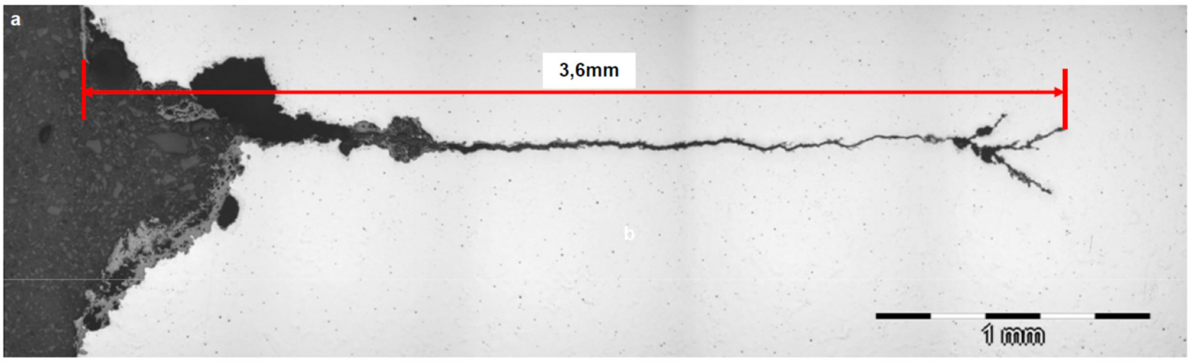

Fig. 3-13: Transverse section of the longitudinal crack from Fig. 3-12. The crack starts in a corrosion pit

It grows in a tensile stress-oriented manner and exhibits the internal corrosion scouring typical of SICC. In these phases, stagnation corrosion occurred in the crack tip.

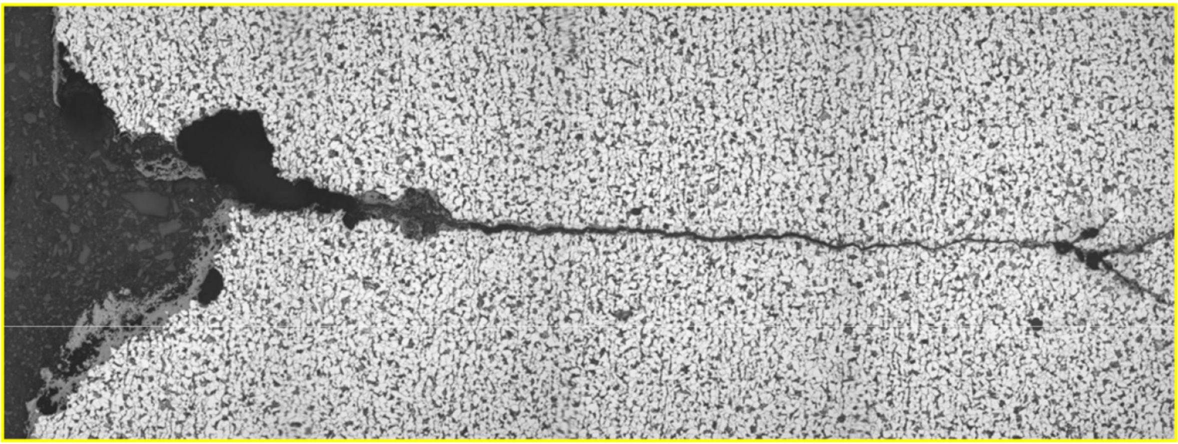

Fig. 3-14: The same SICC crack as in Fig. 3-13 etched with HNO_3. A uniform ferritic-pearlitic matrix is visible

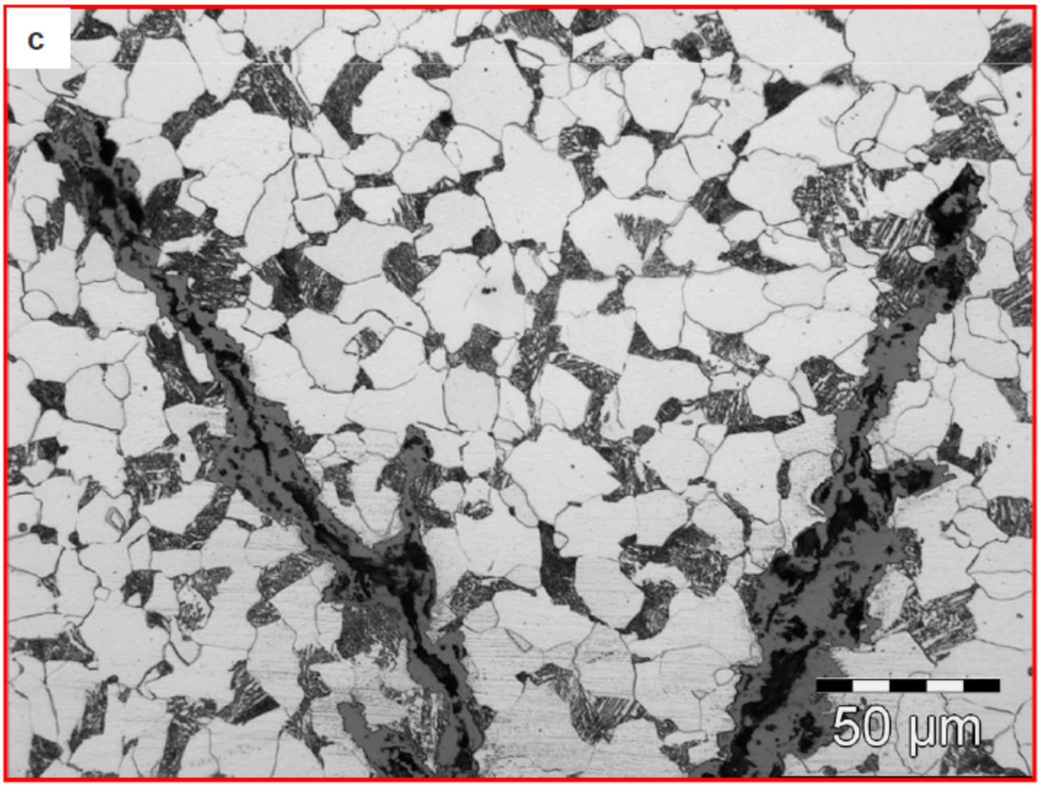

Fig. 3-15: Crack tips of the branched SICC crack. The flanks of the crack are covered with a thick, partly porous oxide film

3.3.3 Damage to a boiler circulation pump

The massive damage to the housings of the boiler circulation pumps (BCP), which has been known since 2014, is largely due to the damage mechanism of the SICC, see [1-1]. Fig. 3-16 shows the damaged components from the Staudinger power plant.

Based on an increased expansion behaviour and the corresponding media interaction, the damage is initiated in the so-called handling groove.

Fig. 3-17 shows a section of the fracture surface of the boiler circulation pump in question. The fracture surface is divided into an inner area of cyclic crack growth with a clear magnetite layer and an outer, larger area with a ductile residual force fracture. The normally bare residual force fracture surface shows flash rust due to its storage after the pump was salvaged.

Fig. 3-16: BCP Staudinger 2014

Fig. 3-17: Section of the fracture surface of the BCP plant of the Staudinger power plant from 2014;
Left – residual force fracture (honeycomb-shaped, ductile);
Right – cyclically grown SICC crack with magnetite layer

Detailed information can be found in VGBE-TW-530 “Recommendations for the operation and monitoring of boiler circulation pumps” [1-1]. Cracks have also been detected on the BCP housings in other power plants, as in the example in Fig. 3-18.

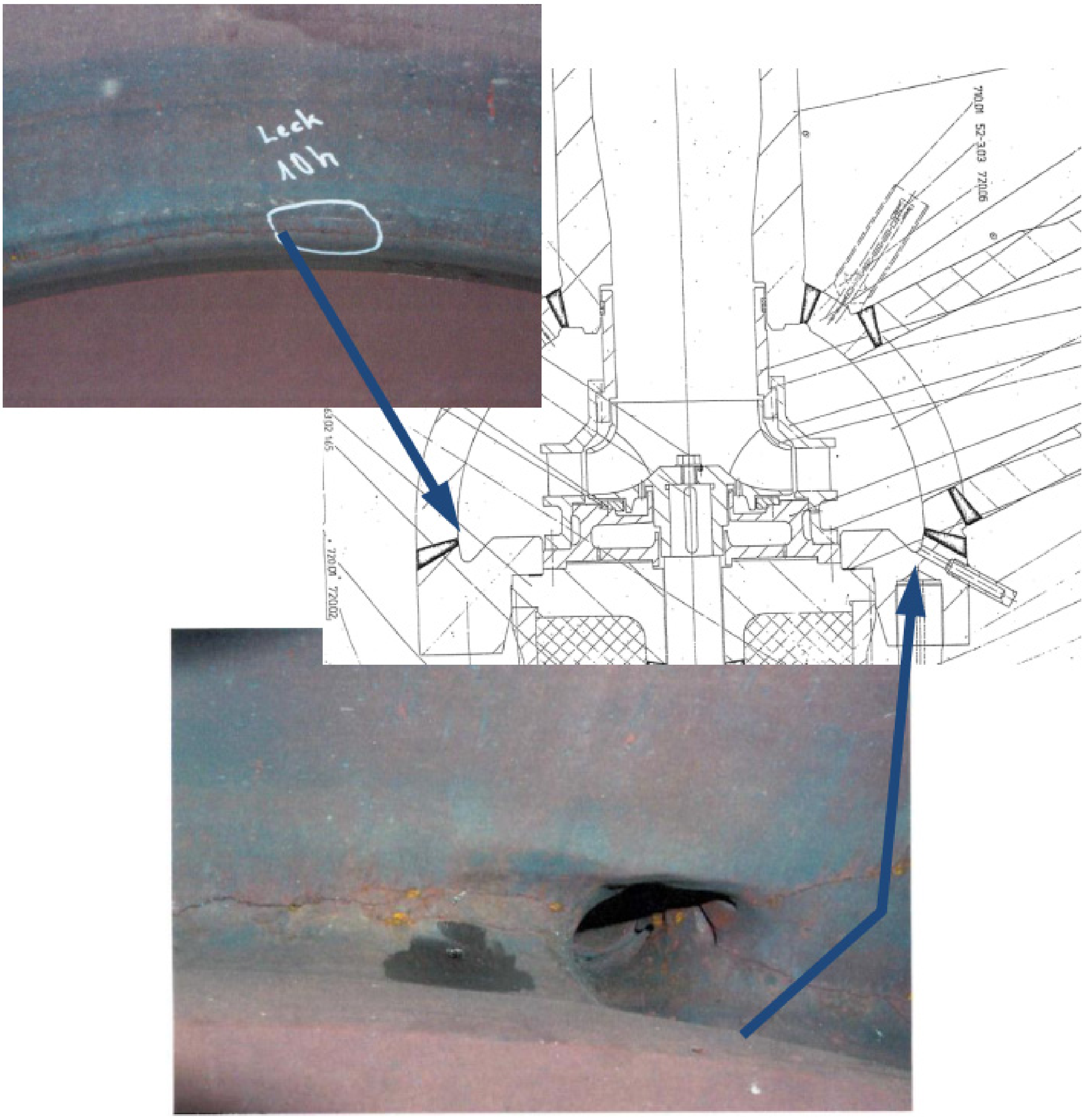

Fig. 3-18: Sectional drawing of a boiler circulation pump with two associated visual crack findings on the boiler pump housing

3.3.4 Damage to fittings/pipe bends in the circulation circuit

From 2010 to 2012, there were repeated minor leaks in the circulation circuit (240 bar, 388 °C) at a power plant. Various components and fittings in this system were affected. All components of the circulation circuit were made of the low-alloy steel WB36. The following illustrations Fig. 3-19 and Fig. 3-20 show a T-piece and a pipe bend with cracks.

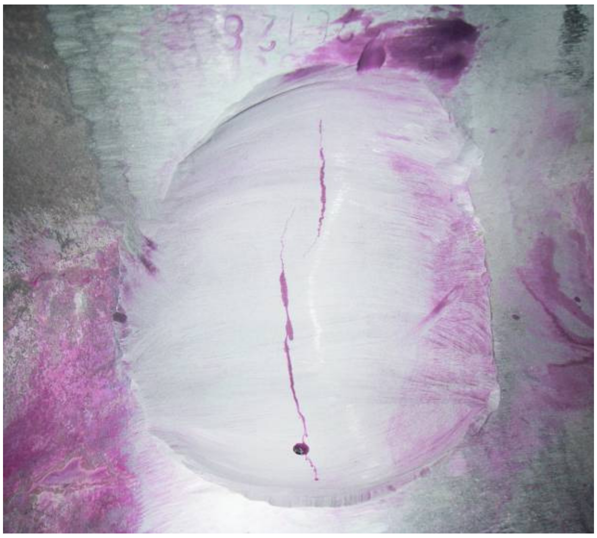

Fig. 3-19: Crack indications (PT) after leakage on a T-piece (WB36) from a recirculation system. The grinding work shows an increasing crack size towards the inner surface.

Fig. 3-20: Crack indications (PT) after leakage at the end of a pipe bend (WB36) in the neutral fiber from a recirculation system. The grinding work shows an increasing crack size towards the inner surface (identical system as in Fig. 3-19).

In another power plant, SICC findings were detected in 2022 with periodic inspections, particularly on shut-off valves and non-return valves made of low-alloy steel 15Mo3 as shown in Fig. 3-21 in the recirculation circuit.

Based on these findings, further valves were specifically inspected in 2023. In some cases, comparable SICC cracks were found.

The main thing here was the systematic, i.e. almost all fittings were affected. The cracks had reached a significant depth, but there was a sufficient distance to critical crack sizes. There were no leaks. Slow crack growth is therefore generally assumed for this damage.

Fig. 3-21: Non-return valve made of 15Mo3 in the circulation circuit (design: 280 bar, 405 °C, operating data: 245 bar, 400 °C)

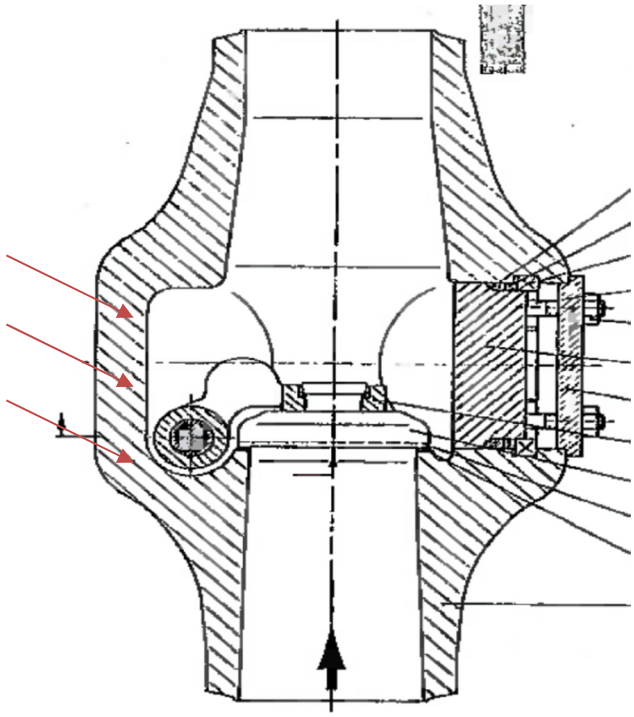

Fig. 3-22: The damaged area is made up of a flat surface in the rear inner area of the non-return flap, Fig. 3-21

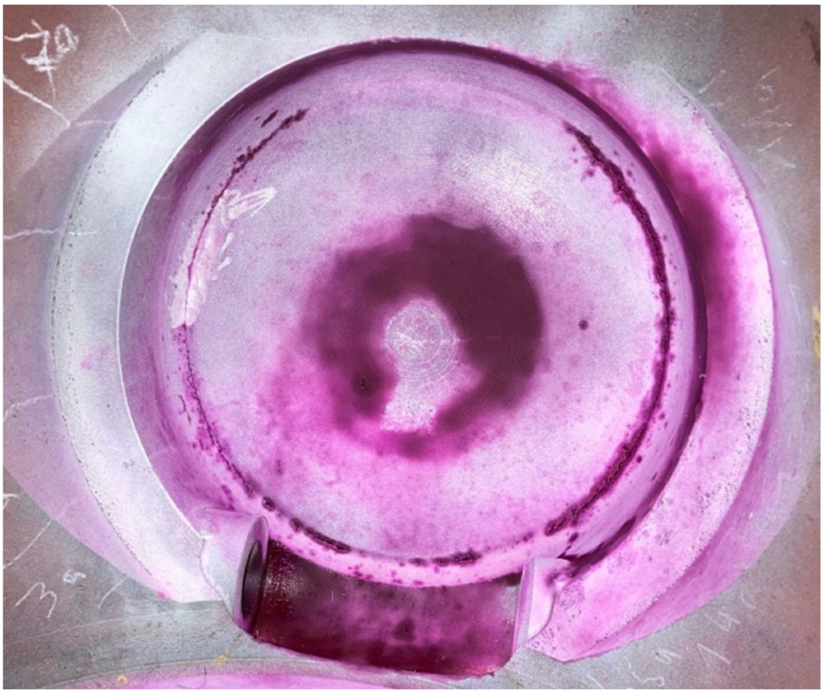

Fig. 3-23: After dismantling the non-return flap from Fig. 3-21, the red-white test showed an almost circumferential linear indication. This finding was unexpected in terms of depth and severity. Neither the material, the stress caused by pressure and temperature nor the internal geometry suggested this.

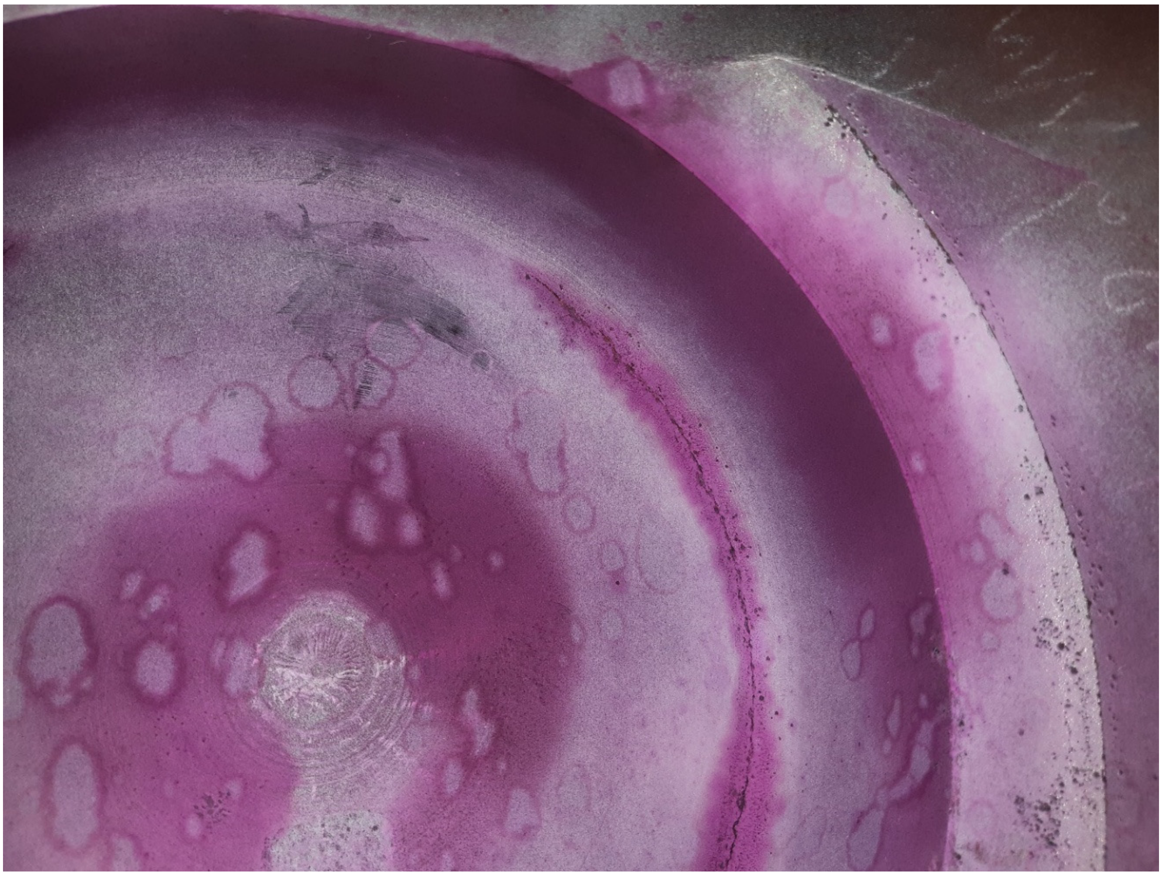

Fig. 3-24: Non-return flap 2021

3.3.5 Damage to a feed water tank

As described in Chapter 3.3.1, cracks were found in numerous feedwater tanks in German power plants from 1966 onwards. In addition to numerous crack formations at the connections of feedwater tanks and degassers, systematic crack formations in the circumferential welds up to leakage were found in several feedwater tanks made of high-strength steels in the 1970s, see also the examples in [3-21].

The following describes a typical case of damage to a feedwater tank made of high-strength steel.

In 2018, a leak occurred on a circular seam from the shell seam to the curved bottom of a feedwater tank. The leakage point on the horizontal feed water tank was in the 6 o'clock position. During a subsequent surface crack test on the inside, further crack indications were detected in all circumferential seams and on two nozzle seams. All crack indications were located in the water-wetted area of the feed water tank (4 o'clock to 8 o'clock position). The cracks were largely oriented transverse to the circumferential welds and therefore perpendicular to the largest main normal stress. Fig. 3-25 shows a sketch of the feedwater tank with the main dimensions. Tab. 3-1 contains information on the feed water tank and its mode of operation. Tab. 3-2 provides information on the material from which the feedwater tank was made.

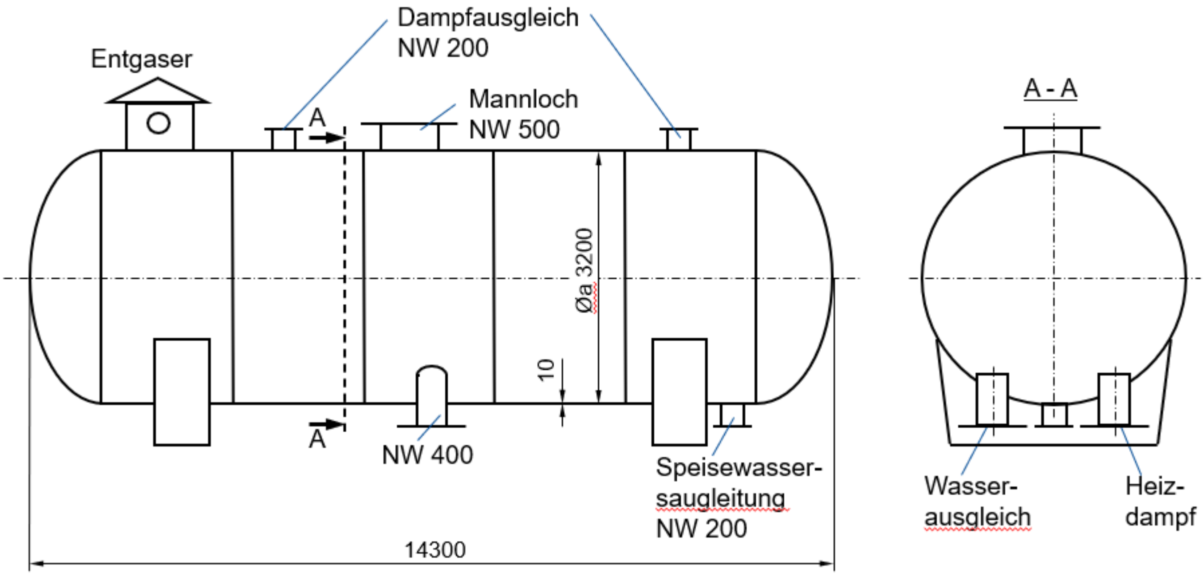

Fig. 3-25: Skizze des Speisewasserbehälters

Translation	
German	**English**
Dampfausgleich	Steam equalization
Entgaser	Degasser
Mannloch	Manhole
Speisewassersaugleitung	Feed water suction line
Wasserausgleich	Water equalization
Heizdampf	Heating steam

Tab. 3-1: Information on the feed water tank and its mode of operation

Year of construction	1964
Dimension	Ø 3200 mm x 10 mm x 14,300 mm; V = 100 m³
Operating temperature	157 °C
Operating pressure	4,7 bar(g)
Load change	1x Start-up/shut-down per year
Medium	Boiler feed water; alkaline with ammonia; pH 9.5; O_2 < 0.01 mg/L

Tab. 3-2: Information on the material and the welding process

Material designation:			BH 36 KW (Weldable fine-grained structural steel; similar: WStE 355)			
Mechanical-technological properties						
Tensile strength R_m	490 MPa – 630 MPa		Notched bar impact work KV with -20 °C			≥ 39 J
Yield strength R_e	≥ 355 MPa					
Chemical analysis in mass-%						
C	Mn	Si	P	S	N ≤	Al
0.18	1.2	0.45	0.02	0.04	0.05	0.05
Information on welding production (according to documentation):						
Welding process			E-Hand (electrode welding)			
Welding electrode			Union SH schwarz 3K			
Heat treatment after welding			No post-weld heat treatment			

Fig. 3-26 shows the position of the leak in the circumferential seam between the shell course and the curved bottom on the outside of the container.

Fig. 3-26: Position of the leakage point on the circumferential seam between the casing course and the curved base

A boat sample was taken from a circular seam between two shell sections at a point that showed crack-like indications during the MT test. The boat sample is shown in Fig. 3-27 and the position of the microsection made from it is marked.

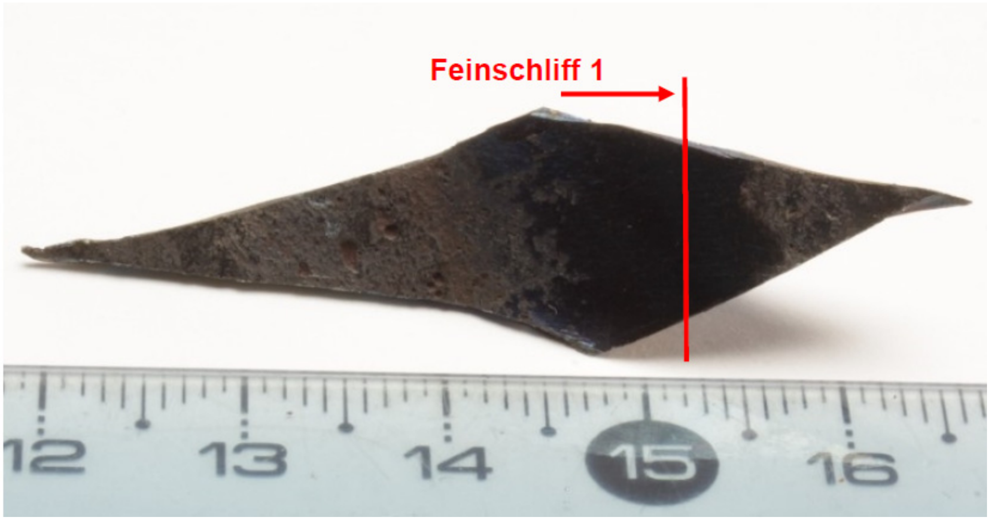

Fig. 3-27: Boat sample from the circular seam with MT displays

The crack shapes characteristic of SICC are already macroscopically recognizable in the unetched fine section. On the left in Fig. 3-28 a crack with scouring and on the right a carrot-shaped crack. Both cracks are filled with magnetite.

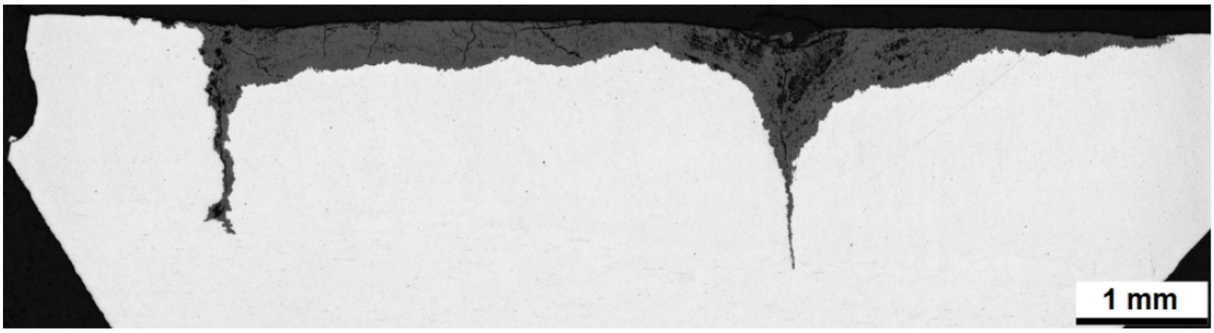

Fig. 3-28: Unetched fine grinding along the weld seam with typical SICC cracks

The thick magnetite layer is conspicuous in the cracked area of the inner surface.

Fig. 3-29 and Fig. 3-30 show an enlarged view of these two cracks in the etched fine section. The weld microstructure and the base material show no abnormalities.

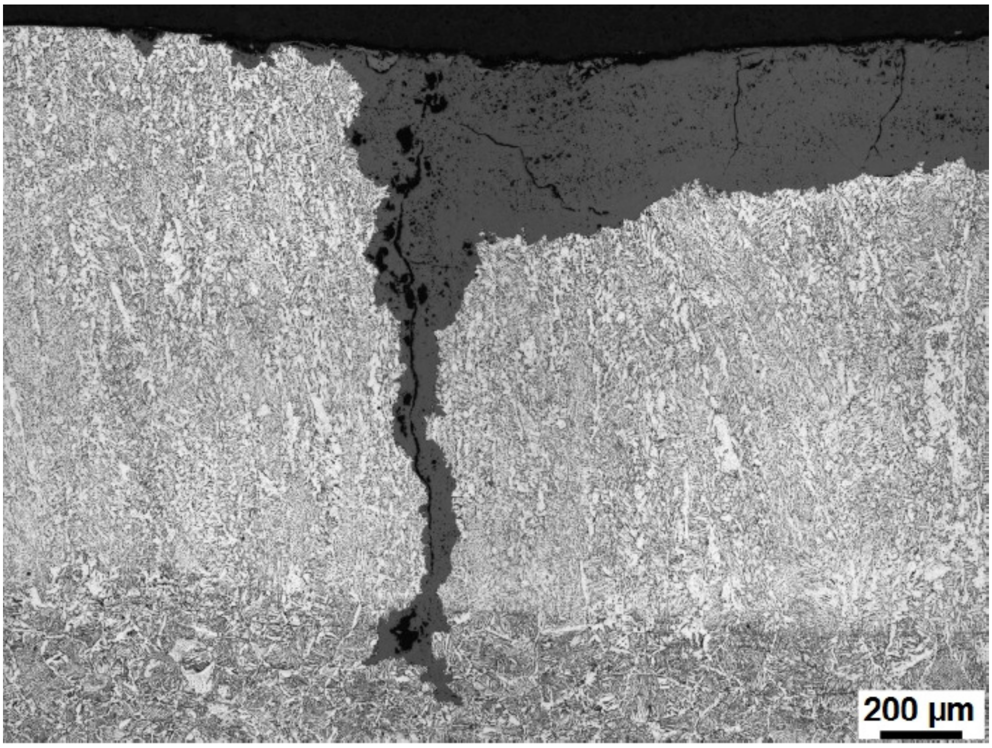

Fig. 3-29: Etched fine section shows the crack with scouring – detail from Fig. 3-28 left

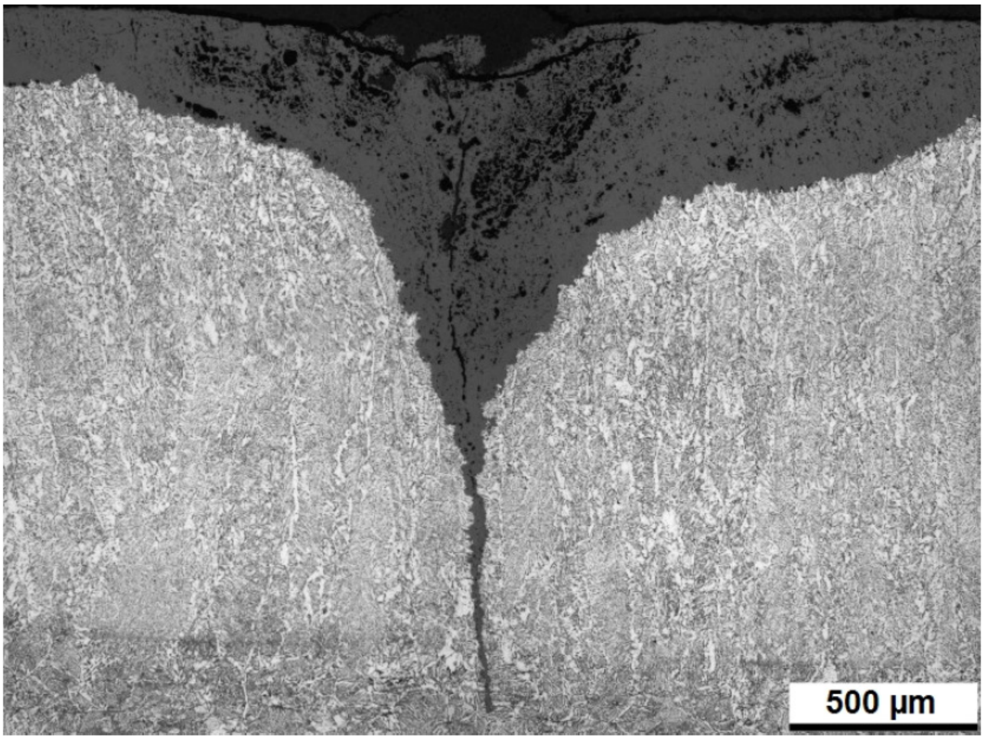

Fig. 3-30: Etched fine grinding shows the carrot-shaped crack – detail from Fig. 3-28 right

The following repair concept was implemented:

- The area of the leak was repaired by welding and then ground. Welding was carried out by the TIG process, using a preheating to 120 °C. The absence of cracks was then confirmed by means of a surface crack test (MT). In order to avoid the introduction of stress through local annealing and as it was not possible to achieve uniform heating of the installed feed water tank along the entire circumference, no post-weld heat treatment was carried out.
- All crack indications were ground out until they were free of cracks, whereby care was taken to ensure smooth transitions.
- If, after grinding out the cracks, the calculated minimum wall thickness was undercut, local build-up welding was carried out and then ground again.
- After one year of operation, the effectiveness of the repair was checked using surface crack testing (MT).

Due to the damage, the inspection concept was supplemented by a periodic MT inspection of the water-covered weld seams.

3.4 Remedial measures

The remedial measures are derived from the requirements of the SICC mechanism. As explained in detail in chapter 2.3, the decisive influencing variables are

- the mechanical stress, particularly the rate of expansion results from the time course of the pressure, the temperature, and the geometry of the component (e.g. ovality of the pipe);
- the medium;
- the temperature;
- the material.

If a triggering parameter is omitted, no SICC occurs.

The expansion behaviour of pipes can be influenced by an adapted support concept. It should be mentioned here that in the case of SICC in pipe bends, a soft installation may be preferable to reduce the expansion rate or to distribute the necessary expansion clearances over a larger pipe section. It is also an option to use bends with the lowest possible ovality to reduce the expansion amplitude in the event of pressure fluctuations. A limited possibility is to slow down the opening behavior of fittings to reduce the thermal transients (magnetite protection layer criterion).

Standstill corrosion plays a special role. This takes place at standstill, i.e. between 10 °C and 40 °C. It allows pitting corrosion attacks or corrosion cavities to form in the undamaged and virtually notch-free material, and SICC cracks can form at the base of these notches. Particularly damaging in this context is the formation of localized fluid accumulations in the bottom of the incompletely drained pipe or component, which can also be promoted by a local build-up at the weld seam geometry. This also leads to an increase in the concentration of corrosion-promoting ionic components.

For standstill corrosion to be possible, a previously created local disturbance in a magnetite layer due to overstretching or over-compression of the layer or an only slightly or poorly formed magnetite layer is a prerequisite. Avoiding standstill corrosion by taking suitable operational measures (see chapter 3.5) is therefore another method of preventing SICC.

Detailed information on remedial measures regarding the choice of material and medium is provided in chapters 2.6.1 to 2.6.4.

An additional note due to the increased relevance for conventional systems:

If the systems are ventilated during short shutdowns, the resulting oxygen-saturated water in these areas increases the potential for SICC damage during the next start-up.

The temperature range between approx. 150 °C and 250 °C, which is critical for SICC, should be avoided as far as possible or preferably passed through quickly during start-up. However, this statement does not refer to operational conditions that are absolutely necessary for process engineering, but to the avoidable cooling of the systems into the critical range. This can be ensured by a sufficient minimum flow rate or by improving the thermal insulation of the component.

3.5 Standstill preservation

In principle, the preservation measures of a pressure device, a pressurized pipeline or a steam generator cover the entire service life, from production, transport, storage (if necessary), installation and commissioning to operation, including interruptions.

In this section, the aspect of standstill preservation, i.e. preservation for interruptions in operation, is presented. See VGB-S-116 “Preservation of power plants” [3-32].

In the case of water-tube boilers for the water-steam cycle of conventional power plants, it has proven to be a good idea to determine the optimum preservation method taking the following aspects into account:

- Standstill time;
- Maximum time available until recommissioning;
- Effects on recommissioning;
- Degree of automation of the preservation equipment;
- Influence on other plant components;
- Disposal of preservatives;
- Occupational safety;
- Environmental protection.

The following preservation methods have proven themselves in practice, depending on the application and area:

- Wet preservation;
- Dry preservation;
- Inertization;
- Vapor phase inhibition;
- Preservation with film-forming amines.

All of these methods generally lead to good corrosion protection in the water-steam cycle when used correctly. Flue gas-side corrosion during system shutdowns must also be assessed.

3.5.1 Wet preservation

The wet preservation of systems is characterized by a minimal duration (a few hours) until recommissioning as well as low financial expenditure. It is not necessary to empty the system. Corrosion protection is usually ensured by degassed media, such as the operating medium or deionized water.

It is essential for this method that the system is completely filled, that air or steam cushions are safely avoided or replaced by inert gas and that the preservation medium is degassed as far as possible. At the same time, there are system-specific requirements for cleanliness to avoid undesirable interactions with the surfaces in contact with the medium. As a rule, relevant media properties (e. g. oxygen concentration ≤ 0.05 mg/kg, conductivity ≤ 5 µS/cm, pH value > 10) that can be easily determined using operating measurement technology are defined here.

Wet preservation by heat retention is characterized by particularly short recommissioning times. This requires the permanent circulation of the feed water in the water-steam cycle using sufficiently dimensioned feed water pumps and the maintenance of a minimum temperature (usually > 70 °C).

The preserved system also requires cyclical monitoring during shutdown to maintain preservation to monitor any leaks and carry out appropriate replenishment. The regular system measurement technology is generally sufficient for this.

Care must be taken to ensure that the preservation medium does not freeze. In general, no antifreeze can be added, as there is a risk of acidic decomposition products.

Based on the pressure maintenance, possibly at elevated temperatures, repair measures on the system are only possible to a limited extent.

3.5.2 Dry preservation

Dry preservation is characterized by a short duration (a few days) for recommissioning and low financial expenditure. It is necessary to empty the system, but preservation must be initiated while the system is in operation. Corrosion protection is ensured by the absence of an electrolyte film on the surfaces to be protected. When the systems are shut down, the residual heat present is used to evaporate all the water contained. All drains and vents must be opened for this purpose.

It is essential for this method that the system is completely drained and dried on the surfaces in contact with water and steam, that there are no hygroscopic deposits on the surfaces to be protected and that the relative humidity on these surfaces is less than 30 %.

A disadvantage of this method is the potential concentration of corrosive ionic impurities in the residual puddles. These can lead to localized pitting corrosion in unalloyed and low-alloy steels, which in turn can be potential starting points for the initiation of SICC. See also the examples of damage in Fig. 3-9 to Fig. 3-15.

The conservated system requires cyclical monitoring during standstill to maintain preservation to prevent the temperature from falling below the dew point by taking suitable measures.

3.5.3 Inertization

The inerting of systems is characterized by a minimum duration (a few hours) for recommissioning. The system must be drained to replace the inerting agent, usually nitrogen. Corrosion protection is ensured by the absence of oxygen.

It is essential for this method that the system is technically oxygen-free (< 0.5 vol. %) and that there is a nitrogen overpressure (usually > 20 mbar) during the preservation period.

The conservated system also requires cyclical monitoring during the standstill to maintain preservation, in order to monitor any leaks and carry out appropriate replenishment of the inerting agent.

3.5.4 Preservation with vapor phase inhibitors

Vapor phase inhibitors can be used where wet or dry preservation is not feasible. For this purpose, sublimating substances are used, which are deposited on the metallic surface and thus prevent the corrosion reaction. The vapor phase inhibitors are applied as a powder or emulsion, for example. Complete dewatering is not necessary, as the surface reaction also takes place through surface condensates. A prerequisite for long-term effectiveness is that there is no air exchange in the system to be protected. Deconservation is generally achieved by rinsing with water.

4 Inspection concept

One task of non-destructive testing (NDT, equivalent to NDE) within a periodic inspection program is to detect damage caused by corrosion-supported crack formation mechanisms in general and by SICC in particular in good time before leakage or serious damage occurs. In this context, information on the typical manifestations of SICC in real components and systems is relevant, see the damage cases in chapter 3.3, in order to assess the effectiveness of NDT.

SICC damage depends on the stress on the component, i.e. the geometry of the component and the load characteristics (including internal pressure, temperature, medium). In the following sections, the NDT-relevant characteristics of SICC are presented and classified in test scenarios in connection with endangered components. Based on this classification, inspection approaches are presented that systematically improve the probability of detecting SICC.

4.1 Damage pattern

Crack position:

The SICC always starts from the medium side, i.e. from the inside. In pipelines and components that are not accessible from the inside, the detection of cracks from the accessible outer surface is therefore only possible using volume testing methods. These include ultrasonic testing (UT), radiographic testing (RT) and eddy current testing (ET). Surface testing methods such as magnetic particle testing (MT), dye penetrant testing (PT) or visual testing (VT) do not provide any information about the inner surface. Only wall-penetrating cracks can be detected with these test methods.

If components are accessible from the inside, as is the case with feed water tanks in particular, the surface test methods can be used to inspect the inner surface.

Crack characteristics and crack detection:

In most cases, a very fine and sometimes slightly branched crack forms starting from a pitting corrosion attack. The cracks induced by SICC were often detected at locations with changes in the inner contour, changes in wall thickness and scoring of the inner surface [1-1]. Crack growth follows the tensile stress state, which is present at stresses within 150 °C to 280 °C. For a straight pipe, this usually means growth perpendicular to the inner surface. As these are planar defects, it is difficult to detect them using RT, as this requires optimum irradiation conditions for each crack.

Crack detection from the inside is possible using endoscopy/videoscopy. Large vessels can be inspected with direct visual inspection. Corrosion cavities and hematite bleeding provide indications of SICC. It is not possible to test the depth of the cracks with VT.

Technical progress in ultrasonic testing technology, including evaluation technology, in particular phased array testing technology (PA-UT), currently offers additional advantages in the use of UT for the detection of SICC cracks. In addition, the accessibility for ultrasonic testing is much easier than for radiographic testing.

The following testing methods have proven themselves to date:

- From the inside: Direct VT in the case of accessible test positions, VT with aids such as endoscope and borescope; indirect VT with videoscope;
- From the inside: Surface crack testing with MT or PT if accessible;
- From the outside for wall thicknesses from approx. 4 mm: UT preferably using phased array (PA-UT);
- RT can generally be used locally from the outside, in particular to verify UT findings.

The difficulty of the UT inspection task due to the fineness of the crack and the possible form echoes should not be underestimated. This has been shown by the experience gained from boiler circulation pump (BCP) investigations [1-1]. Where applicable, mechanized ultrasonic testing is used to improve the test results by means of image-based evaluations of the ultrasonic data stored true-to-location.

4.2 Test cycles and test ports

According to the German Ordinance on Industrial Safety and Health, all work equipment is subject to periodic inspections. Depending on the inspection task, the inspection cycle can be within hours or years. For example, routine inspections in the form of so-called integral visual inspections (VT) are common in power plants at hourly intervals.

The inspection cycles must be defined in such a way that cracks within these intervals do not lead to component failure.

By selecting representative test locations based on the damage mechanism of the SICC, the testing effort can be reasonably reduced. At the same time, the reliability of the tests is significantly improved.

SICC can occur as a systematic active damage mechanism in piping systems if the design, manufacture, and loading provide the appropriate boundary conditions for triggering SICC. Tab. 4-1 gives a brief overview of possible test areas. Some examples are also given.

Tab. 4-1: Boundary conditions that promote SICC and can therefore be used for a preselection of test locations (no claim to completeness)

Boundary condition	Value/Areas	Examples
Liquid phase in the water vapor system	150 °C < T < 280° C	Circulation system (incl. fittings and pump housings), Minimum flow line, Emptying lines from collectors
Increased local tensile strain or shear strain, which can lead to cracking of the magnetite layer	Ovalized pipe bends	Pipe bends usually have an ovality. The neutral fiber of the bend is subject to increased tensile elongation under internal pressure load
	Notches	Machining grooves, root notches
	Contour notches in fittings	Inner edges, e.g. in slide valve housings, the handling groove in typical housings of boiler circulation pumps, perforated edges of boiler drums
	Wall thickness and contour transitions	Housing of boiler circulation pumps, dampers, valves, and fittings
Areas in which Shut-Down corrosion is possible due to insufficient condensate drainage	Horizontal pipe sections	Condensate can remain in the 6 o'clock position under unfavourable conditions
Systems that quickly achieve oxygen saturation of condensate/liquid phase through aeration, even when not in operation for a short time	Leaking valves, open and wet systems at Shut-Down	Emptying system
Piping systems without continuous flow		Drain line

4.3 Test procedure

A combination of tried and tested inspection techniques is recommended for the creation of a SICC-related inspection plan. The methods that can be used so far are

- VT of the inner surface;
- Surface crack testing (PT, MT) of the inner surface with accessibility;
- UT of the volume up to the inner surface (from the outside);
- Local RT of the volume from the outside.

All methods have their advantages and limitations and can lead to misinterpretations, which is why professional planning, valid personnel certification (e. g. DIN EN ISO 9712) for the respective test method and, in particular, practical experience with the respective test technique in comparable test tasks are essential.

4.3.1 Visual Testing (VT)

Direct visual inspection is the simplest technical option for inspecting accessible internal surfaces. If accessibility is limited, the technically more complex direct visual inspection using an endoscope or borescope as an aid and the indirect visual inspection using a videoscope are suitable. These are used in particular when inspecting pipe sections or boiler drums. To do this, an opening must be created, either by cutting a pipe section or, for example, an inspection nozzle. Pipe pigging systems are also used for very long pipe systems, but these have not yet been used to locate SICC.

Endoscopy and videoscopy are imaging procedures. This means that optical distortions are possible. Modern systems have an auto-zoom for focus adjustment but cannot avoid optical distortions. The optical findings can be over-interpreted due to the different magnification. The certification and experience of the inspector/evaluator from comparable inspection tasks are essential here.

During the visual search, damage to the magnetite layer is assessed. If these are elongated and also show iron hydroxide or hematite bleeding, a SICC should be suspected. However, scaling and deposits on the magnetite layer can also lead to misinterpretation. Alternatively, linear indications can be verified with endoscopy, videoscopy or ultrasonic examination. Instead of this verification, the affected pipe section can also be replaced directly to minimize costs. This was carried out, for example, in the case of findings on drain lines.

4.3.2 Ultrasonic Testing (UT)

Ultrasonic testing methods and techniques utilize the reflection of sound waves at interfaces, which are represented with characteristic display patterns. The following reflector types are examples of interfaces for ultrasonic testing:

- Crack flanks, planar;
- Porosity, volumetric;
- Pits.

Depending on the ultrasonic testing parameters, such as testing frequency and wave type, the different reflector types are displayed with different characteristics. Classic ultrasonic testing is not an imaging test method, such as radiographic testing with X-ray tubes or isotopes. Special methods of ultrasonic testing, e. g. phased array testing or ultrasonic testing with mechanized data acquisition, provide visual representations of the test object by projecting the ultrasonic signals into the test object or onto its surface.

SICC-typical defects in the form of cracks can be detected using adapted ultrasonic testing techniques. The testing technique is adapted by selecting test parameters and scanning directions depending on the shape and wall thickness of the test object. The usually ferritic material and its acoustic properties remain of secondary importance for SICC detection. The surfaces to which the ultrasonic probes are coupled must be prepared for testing prior to the test.

Ultrasonic testing for SICC-typical indication patterns is possible with test frequencies from 1 MHz and can be increased to higher test frequencies of up to approx. 10 MHz depending on the component and its surface quality. With higher test frequencies, the requirements for the quality of the surface to which the ultrasonic probe is coupled increase. The contact surface of the ultrasonic probe must be adapted to the surface of the component. This applies in particular to positions where, for example, pipes are tested for cracks that extend longitudinally and are inspected with the probe in the circumferential direction of the pipe.

Ultrasonic testing as a surface and volume method always includes the entire cross-section of the test object, including the surfaces. Ultrasonic testing must be adapted to the zone to be tested and the test sensitivity must be adjusted to detect certain defects. For the detection of cracks typical of SICC, the inner surface away from the probe is defined as the test zone and the test sensitivity is adjusted, for example, on representative test specimens with artificial reflectors in the form of slots or eroded grooves. The component contour and the local wall thickness must also be taken into account.

Ultrasonic inspection techniques can be designed as search or analysis inspection techniques depending on the respective inspection situation. This distinction is helpful where large areas are tested in a short time and analyses are only required at indication locations, e. g. to determine the depth of crack indications.

Adapted ultrasonic tests, also qualified on representative test specimens with artificial defects, are used to determine and document the lengths and depths of SICC indications in a traceable manner. The imaging methods of mechanized or partially mechanized ultrasonic testing provide true-to-location projections of the indication positions and enable optimal testing for alterations in the findings left in place.

The characteristic manifestations of SICC in the form of crack fields with prominent individual cracks, some of which exhibit typical scouring, can be reliably detected with ultrasonic testing due to the expected gap widths > 20 µm. Initially, the cracks usually run without branching and are transcrystalline. The following test conditions must be given:

- Sufficient clearance on the outer surface for coupling and guiding the ultrasonic probes;
- The surface must be clean, free of scale, loosely adhering particles, and coatings for coupling the probes;
- Sufficient surface quality (evenness, roughness);
- Insulation must be removed.

Nevertheless, there are detection limits and possibilities for misinterpretation. The most important impairing boundary conditions are:

- Sound-influencing, inhomogeneous, and coarse microstructure in the test area or in the sound path to the test area (cast microstructure, especially weld seams);
- Form echoes from the inner contours of the test objects or the roughness of the inner surface;
- limited possibilities for attaching the probes from the outside (edges, changing radii, poor accessibility).

Above all, experience from tests on boiler circulation pump housings has shown that correct interpretation is difficult when the aforementioned effects are considered.

Adapted probes, such as SE probes (transmitter-receiver probes), must be used on thin-walled pipes with small diameters, which are used in particular for drain lines.

The use of phased array ultrasonic testing techniques (PA-UT) and mechanized data recording increases the reliability and reproducibility of the test results.

4.3.3 Surface crack inspection (SCI)

Surface crack testing with MT or PT is mostly used to verify visual findings on openly accessible internal surfaces. Magnetic particle testing (MT) is generally recommended for ferritic components regarding the test results. For the frequently used dye penetrant testing (PT), two things should be noted:

- Grinding can cause cracks in soft, easily deformable materials to be smeared shut and subsequently no longer be detectable using PT;
- The detection limit of PT is inferior to MT.

4.3.4 Eddy Current Testing (ET)

Eddy current testing (ET) is a test method that uses deviations in electrical conductivity as a test statement. Eddy current testing is basically a surface method for detecting discontinuities in the near-surface area. On test objects with wall thicknesses < 5 mm, eddy current testing can include the mating surface in the test. These include, for example, heat exchanger tubes in steam generators, heat exchangers and condensers. Under favourable conditions and with specially adapted test equipment, test results are possible down to depths of around 20 mm. For meaningful test results with eddy current testing, surface quality requirements must be met that are at least equivalent to those for ultrasonic testing. Under good surface and material conditions, fine cracks can be detected with eddy current testing. The detection and resolution capacity decreases rapidly with increasing depth. As a manual test, eddy current testing is not an imaging test method, but eddy current data can be recorded with spatial coordinates using suitable semi-mechanized or mechanized testing equipment and output as display images in the same way as with mechanized ultrasonic testing.

Reference bodies with identical material and dimensions must be available for the component to be tested, which make it possible to interpret the electromagnetic deviations.

One advantage of the method is the fast and effective testing of long pipe sections.

A disadvantage is the extensive preparation required, including the creation of reference test specimens, and the low level of dissemination and experience for mobile testing in conventional energy systems.

Eddy current testing can only be used to detect typical SICC cracks on very thin pipes in exceptional situations.

4.3.5 Radiographic Testing (RT)

X-ray tubes and isotopes can be used to detect typical SICC indications from the outside. Radiographic testing (RT), like ultrasonic testing, is an NDT method for volume testing that can be used to detect imperfections on the surfaces and inside test objects. RT is an imaging method that uses the blackening of a photographic film or a digital electronic detector placed on the opposite side of the component to visualize positions in the test object that are more permeable to X-rays or gamma radiation due to lower attenuation. Such positions are, for example, smaller wall thicknesses, voluminous cavities or planar separations. Cracks caused by SICC are planar separations that can be detected with radiographic testing if they are optimally positioned in the beam path, i.e. aligned as parallel as possible to the plane of incidence. For the result of the radiographic test, it is favourable if indications of cracks are as close as possible to the film or to the detector of the digital radiography. The quality of the test results decreases as the wall thickness of the radiographed test object increases. From a wall thickness of around 30 mm, cracks can only be detected if they are optimally positioned in relation to the beam path. Test locations without changes in the wall thickness of the test object are advantageous for radiography.

Advantages:

- Visual evidence of the findings;
- Simple documentation and qualitative testing for alterations possible;
- Low requirements are placed on the surface quality.

Disadvantages:

- Relatively high space requirement when using an X-ray tube;
- Relatively precise alignment to the possible SICC crack required to detect the crack;
- Several images required when testing the entire circumference of a circumferential weld;
- Area must be cordoned off during exposure times due to work safety.

4.4 Crack Size Determination

- If an indication has been assessed as unacceptable, the next step is to check whether grinding until crack-free, temporary continued operation, repair or replacement is possible and/or necessary.
- Determining the crack depth can be important for this decision. According to previous experience, it is possible to determine the crack depth using UT, PA-UT, or potential probe methods. As described above, the test is influenced by various boundary conditions. It is therefore important to make a precise estimate of the detection limit for the areas to be tested in advance. It can be useful to define different test zones on the component that describe different detection limits.

- As a very fine crack usually forms, it is a particular challenge to analyse the depth of the upper flaw edge (crack tips). For this purpose, additional display patterns are evaluated using ultrasound technology, the so-called tip diffraction echoes.

4.4.1 Periodic crack size determination

- If a fracture mechanical integrity verification analysis has been carried out on the basis of a crack size determination (see chapter 5) and the component or system has thus been released for further operation for a limited period of time, a retest must be carried out in accordance with the specifications from this integrity verification analysis, such as the number of cycles and operating time. It must be ensured that the accuracy of the measurement is known and considered. Crack alterations within the measurement accuracy are difficult to interpret. A more complex evaluation, such as a comparison of the overall images of both measurements, can be helpful. The same quality of both measurements is a basic prerequisite for this comparative analysis.
- In practical cases, it has already happened that a system with improved accuracy and detection limit was used for the follow-up measurement. This can make it difficult to interpret the possibly different measurement results, both positive and negative. The cause may be due to the change in testing technology.

4.5 Examples of NDT on SICC-damaged components

4.5.1 SICC-damaged valve body

PT was used to determine indications on a gate valve housing (material: 15Mo3, dimensions: 450 mm x 45 mm) at positions on the inner contour that are typical for SICC. To illustrate the initial position, the housing was digitized with a 3D scan, see Fig. 4-1. The component has larger dimensions, as shown in Fig. 4-2.

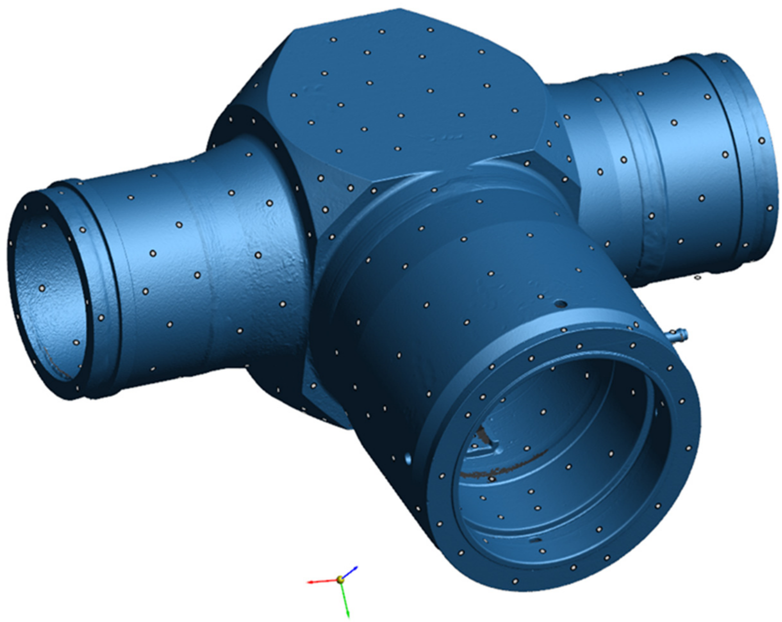

Fig. 4-1: 3D scan for contour mapping of a valve damaged by SICC

Fig. 4-2: Preparation for the mechanized UT (mPAUT) on the slider housing of Fig. 4-1

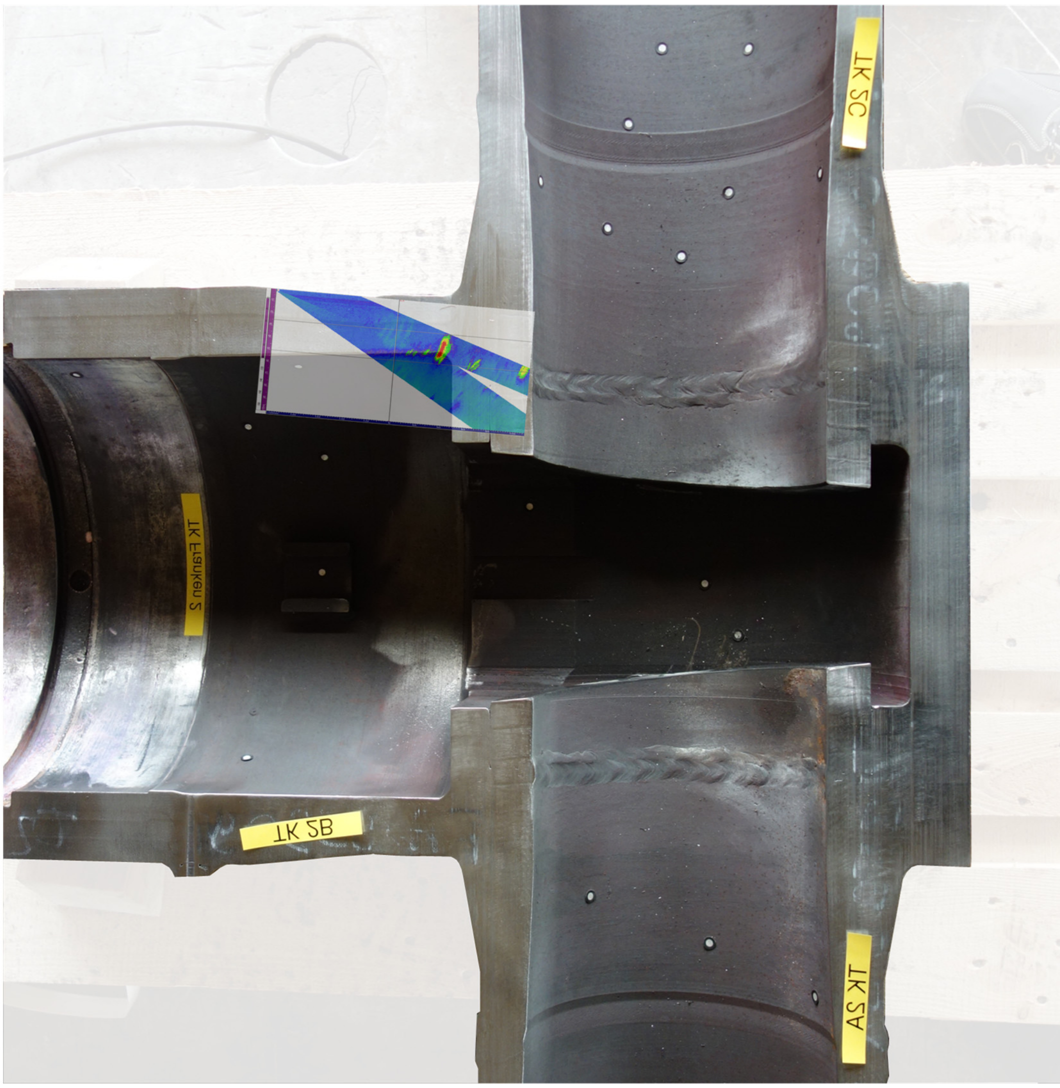

Fig. 4-3: Sliced housing of the valve damaged by SICC with a superimposed mPAUT result display

The data from the mechanized PA-UT test (mPAUT) recorded before the housing was separated was transferred to the cross-section of the housing. The ultrasonic displays were projected onto the internal contour transition with a good signal-to-noise ratio, see Fig. 4-3. This housing position is susceptible to SICC due to the contour transition and the different wall thicknesses.

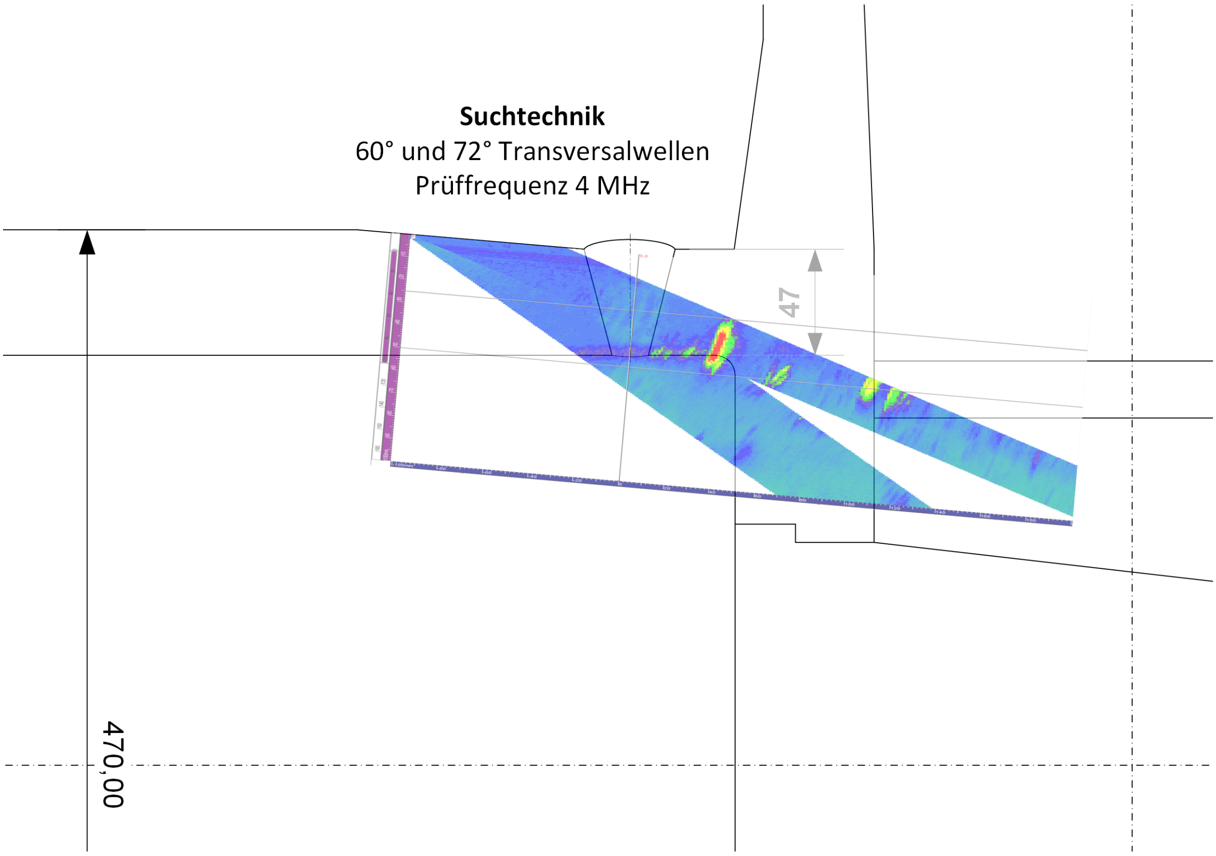

Fig. 4-4: Component sketch of the valve housing with superimposed mPAUT result display with beam angles of 60° and 72° and 4 MHz test frequency

Translation	
German	**English**
Suchtechnik	Search technology
Transversalwellen	Transverse waves
Prüffrequenz	Test frequency

In Fig. 4-4, the shape displays from the component contour and the defect displays can be interpreted simultaneously on the evaluated sound field images.

This component contour is complex for mechanized ultrasonic testing. Due to the external cone and the circular housing seam, the probe cannot simply be moved up to the display location. For this reason, the probe must be coupled to the outside of the conical contour and the ultrasonic signal pass through weld metal so that it reaches the display location. The evaluation shows characteristic display patterns, see Fig. 4-4:

- from the weld metal of the housing circumferential weld;
- shape indications of the inner surface;
- the indications of the defect with a clear signal-to-noise ratio.

These defect indications are displayed with different intensities along the entire circumference. The differences result from the locally different coupling conditions on the outer surface and from the locally different reflectivity of the defect. From the display position and the characteristic reflection of the flat incident sound field, a planar defect with a connection to the inner surface is assumed to be the cause of this display pattern. A shape indication from the shape of the housing cannot be the cause of this pattern at the reconstructed display position. It can be concluded that it is a typical crack indication.

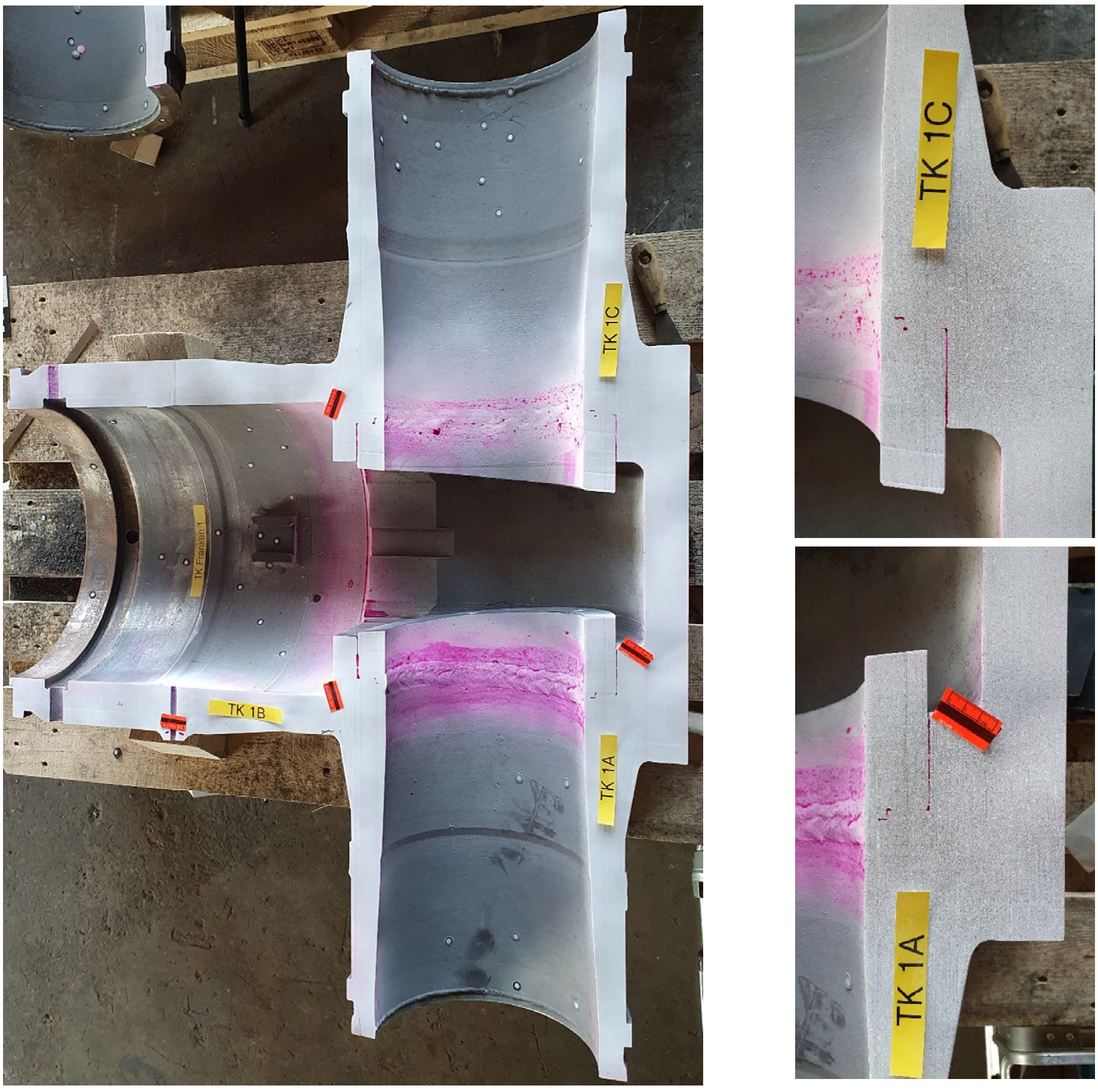

Fig. 4-5: Cut surfaces of the fitting housing with PT results

After separating the valve body, the accessible inner surface and the cut surfaces were tested using dye penetrant testing (PT). As expected, the result of this test shows the positions on the weld seams with a red background, as these positions were not machined before the test, see Fig. 4-5. The PT indications on the cut surfaces, which only become clear in enlarged views, show typical bleeding at the gap positions of the housing construction. In addition to these indications, linear indications are shown at the contour transition of the drive housing to the base body along the entire inner circumference, which are evaluated as a coherent indication.

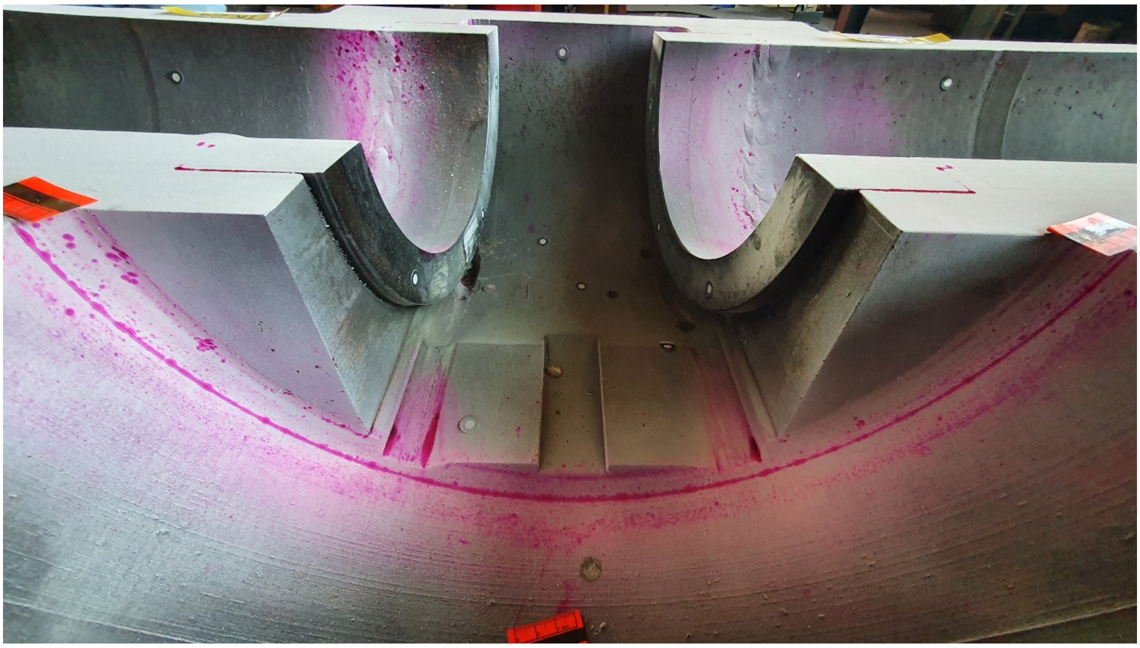

Fig. 4-6: Cut surfaces of the valve body and inner surface of the body (identical to Fig. 4-5, looking from the valve insert connection) with PT results

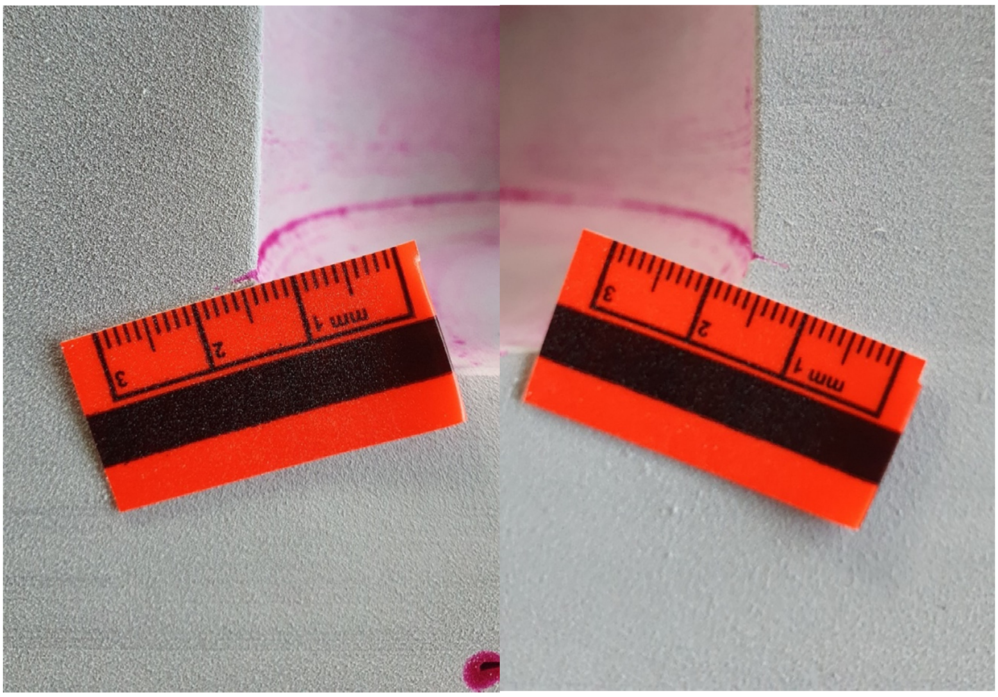

Fig. 4-7: Enlarged view of the linear PT indications on the inner surface and on the cut surfaces of the fitting housing of Fig. 4-5 and Fig. 4-6 at the contour transition of the actuator housing to the base body

The two enlarged sections in Fig. 4-7 (with circumferential positions offset by approx. 180°) of the PT indications on the inner surface of the valve housing and the cut surfaces at the position of the contour transition from the actuator housing to the base body of the valve show the linear character of the indications in the housing wall along the entire inner circumference. The depths of the crack indications of approx. 3 mm to 4 mm can be determined on both sides using the glued-on scales. These crack depths and the alignment of the crack surface normal to the inner contour are the reason for the clear ultrasonic indications. Linear defects, which are connected to the inner surface and extend almost vertically in the direction of the wall thickness, are optimal reflectors for ultrasonic testing. Due to the complex scanning conditions at this position of the valve body, ultrasonic testing could only compare the crack depth from the ratio of the echo heights of the crack indications to that of the alignment reflector. The reflectivity of the ultrasonic display corresponds approximately to that of a three millimeter deep, eroded rectangular groove in the adjustment body.

4.5.2 Housing of a boiler circulation pump with SICC crack indicators

In the forged housing of a boiler circulating pump (WB36), mechanized phased array ultrasonic testing (mPAUT) detected fault indications. For this reason, the housing was removed and tested again with mPAUT before further processing (Fig. 4-8). These tests confirmed the fault indications in the transition from the cylindrical flange to the spherical upper part of the housing.

Fig. 4-8: Front view of the boiler circulation pump in dismantled state with mPAUT test manipulator

This revealed indications of pits and cracks. The indication locations were reconstructed in the test zone on the rounded inner surface of the cylindrical flange and the spherical upper part of the housing. The ultrasonic data stored with location coordinates were evaluated and showed that the indication patterns of the two deepest cracks can be detected along the entire circumference, see Fig. 4-9. The maximum determined depth extension reached approx. half the wall thickness at individual circumferential positions.

After testing in the dismantled state, the housing was cut at the circumferential position with the determined depth maxima of the two crack indications. The fluorescent surface crack test of the cut surface with the color penetrant test (PT) confirmed the crack indications detected with mPAUT in their crack depths and height positions.

The distributions of the mPAUT and PT test results on the inner contour of the housing show a clear correlation. The two neighboring cracks (Fig. 4-10), which lie “on top of each other” in the section, are each shown with considerable lengths in the mPAUT (Fig. 4-11). In addition to the two main cracks at the fillet, further cracks are determined using both test methods. The crack depths of the secondary cracks are considerably smaller than those of the main cracks (see Fig. 4-11). The crack depths are not determined here in the direction of the wall thickness, but in each case along the almost straight, non-branching course of the crack indications. The macroscopic view of the sectional plane shows that the cracks are aligned approximately normal to the inner contour and run approximately perpendicular to the main stress direction, see Fig. 4-11.

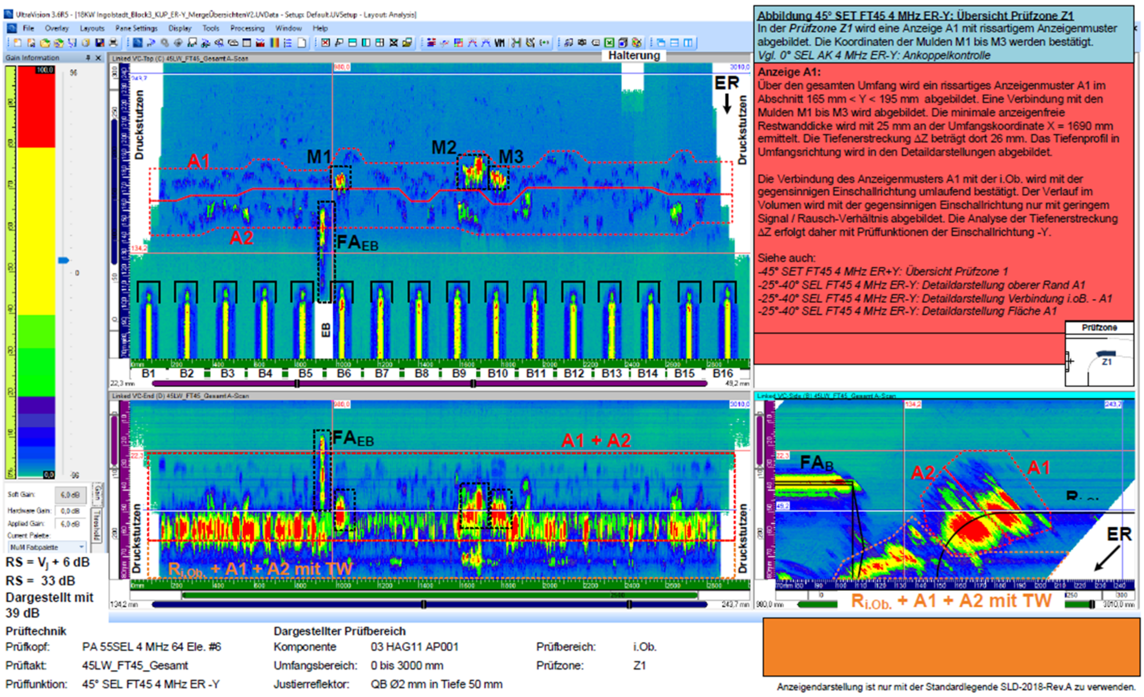

Fig. 4-9: mPAUT result display of the boiler circulation pump in the installed state

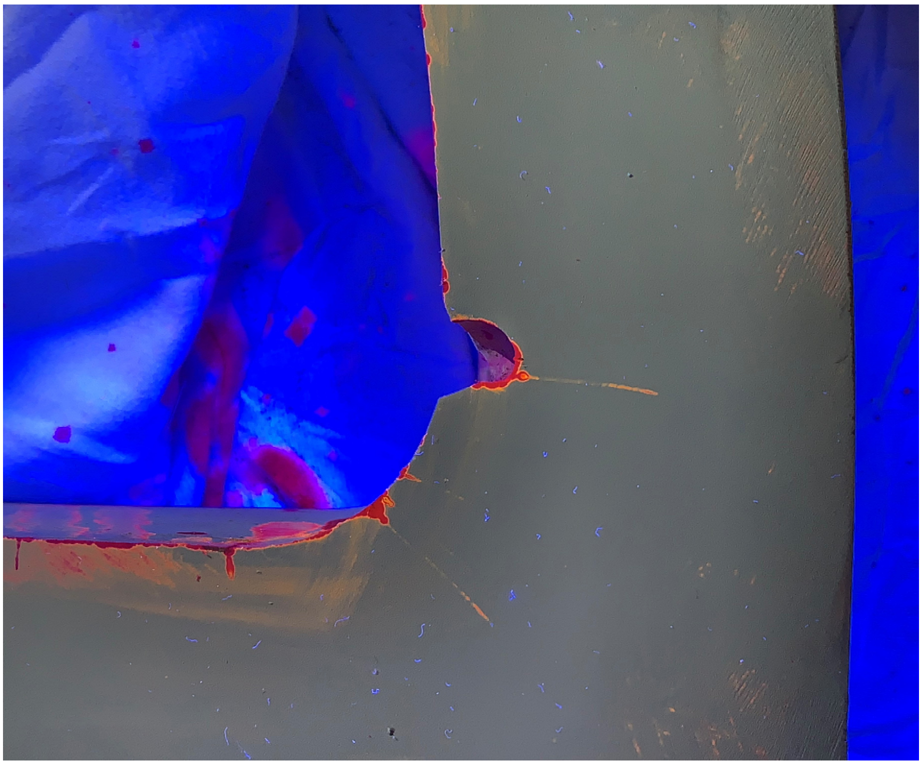

Fig. 4-10: MT displays on the inner surface and the cut surface of the BCP housing

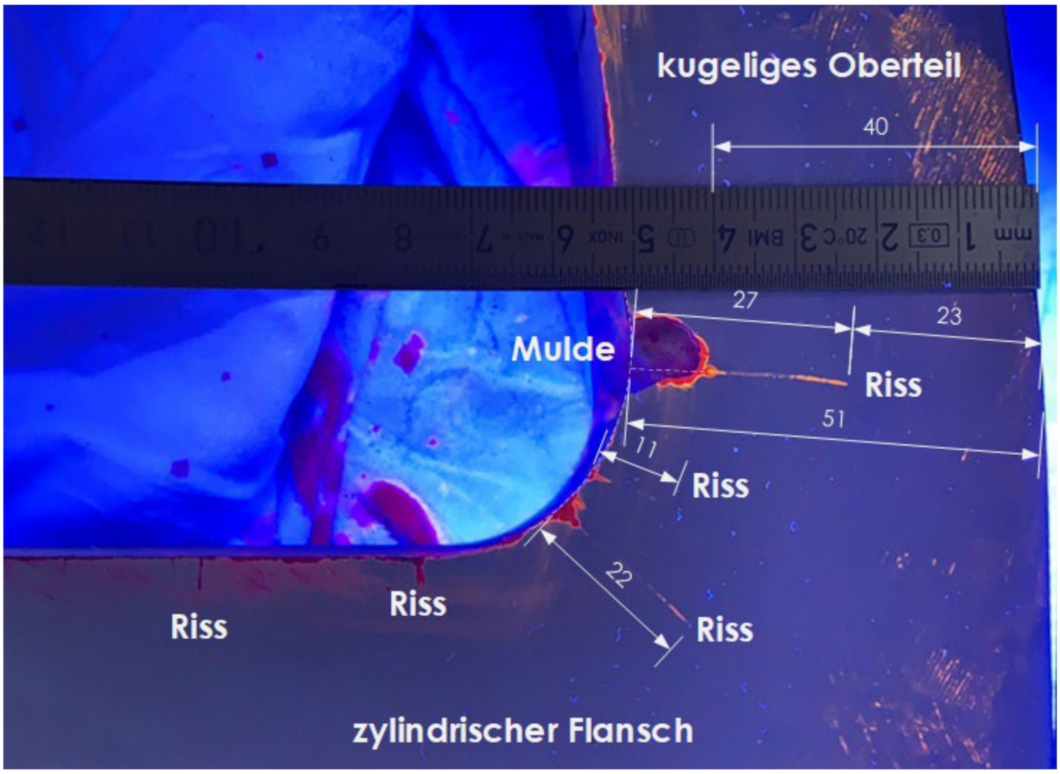

Fig. 4-11: Measured cracks starting from the inner surface

Translation	
German	**English**
Kugeliges Oberteil	Spherical upper part
Mulde	Pit
Riss	Crack
Zylindrischer Flansch	Cylindrical flange

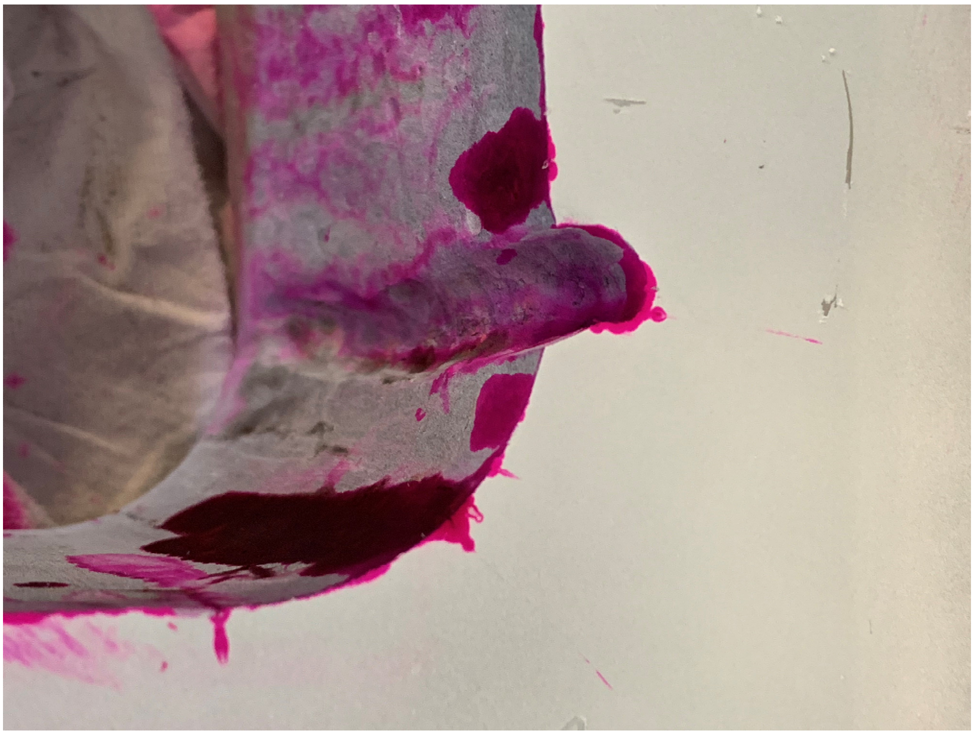

Fig. 4-12: The same cracks as in Fig. 4-11 visualized by a simple PT

The position of the crack indicators on the rounded inner contour of the boiler circulation pump shows another conspicuous feature. The ultrasonic data recorded on the installed pump show the indications of the two main cracks simultaneously. This effect can only be explained by the local permeability of the crack flank for the ultrasonic signals. This effect is confirmed by the results of the PT test, as parts of the crack are very difficult to detect. It follows from this that the crack flanks are pressed together without internal pressure load in such a way that they become permeable to ultrasonic signals (transverse waves) with test frequencies of 4 MHz and 6 MHz. This effect is also known as a “kissing bond”. In testing practice, this results in the need to analyse the ultrasonic data so finely that comparable display patterns can be identified as segments of connected crack indications, see Fig. 4-13.

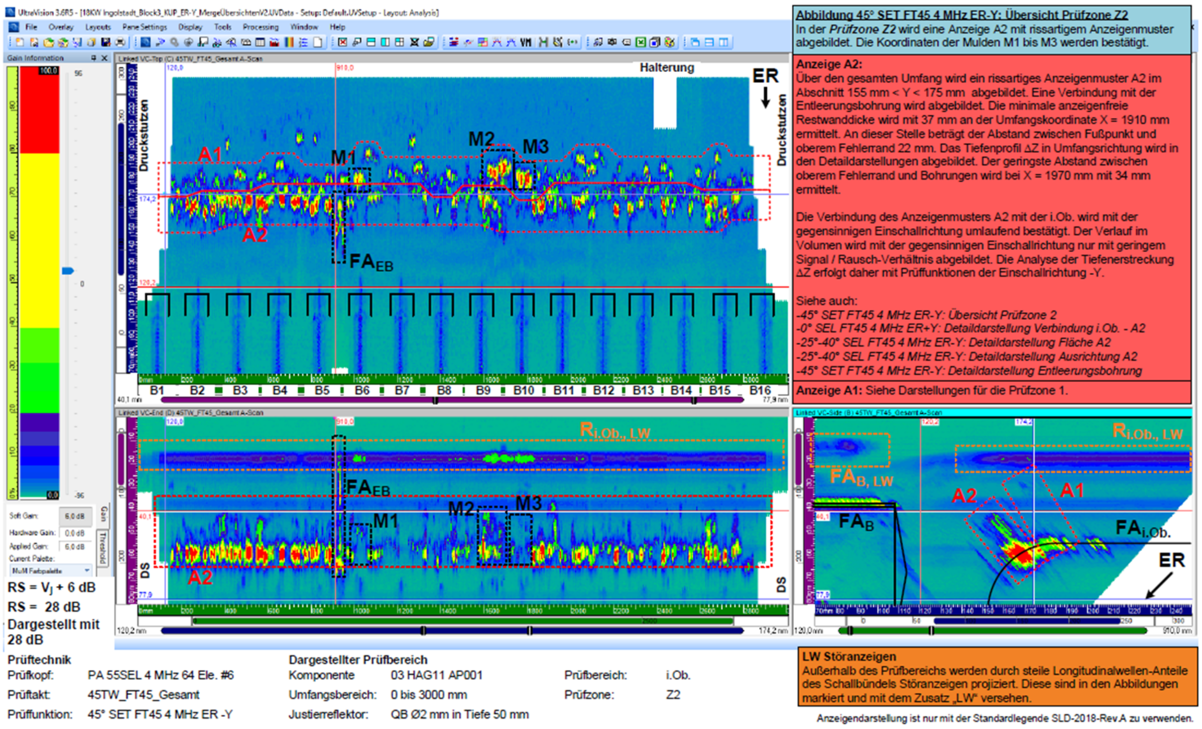

Fig. 4-13: mPAUT result display of the built-in pump

Fig. 4-13 shows the results of the mPAUT test with a 45° transverse wave probe at 4 MHz. The side view visible in it, bottom right, is shown enlarged and optimized for the component geometry in Fig. 4-14. The superimposed PT result and the sketched ultrasonic probe illustrate the local permeability of the crack flanks for the ultrasonic waves.

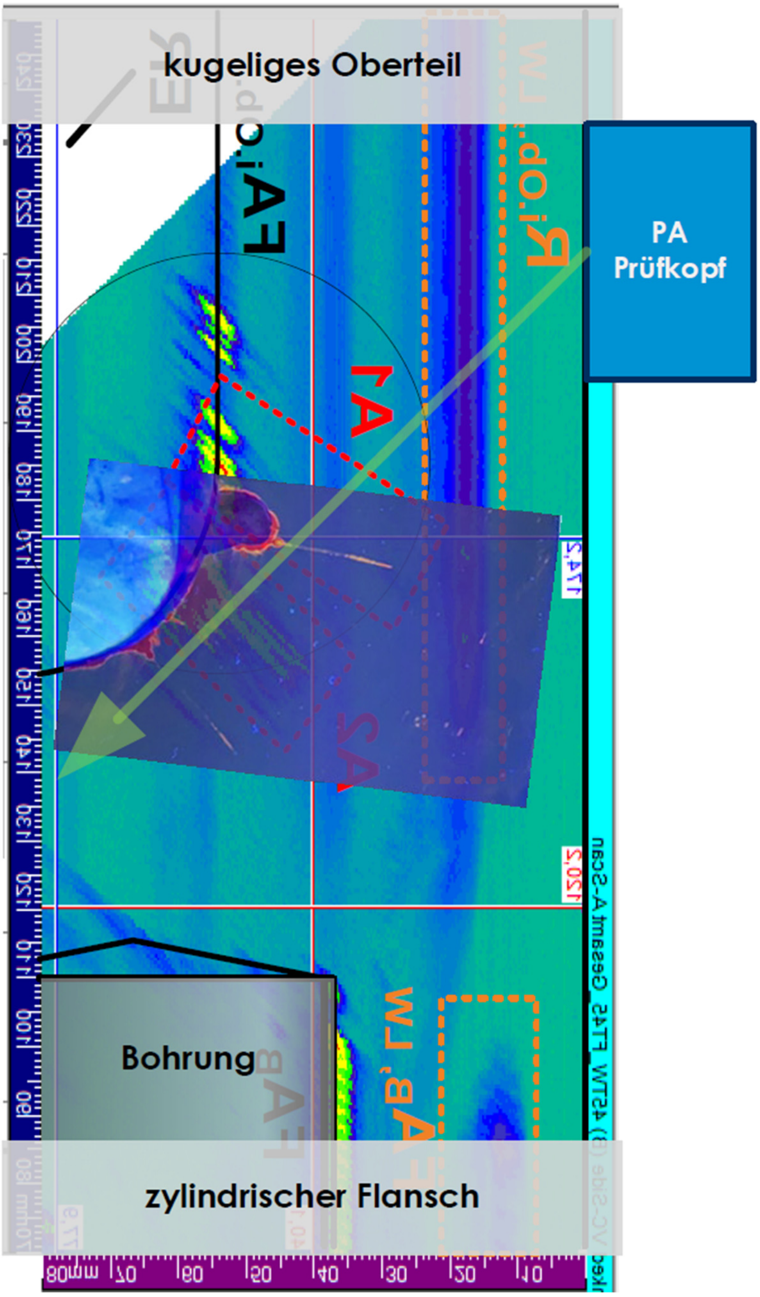

Fig. 4-14: Superimposed display of the mPAUT and PT test results with partially ultrasonic permeable crack indications

Translation	
German	**English**
Kugeliges Oberteil	Spherical upper part
Bohrung	Drill hole
Prüfkopf	Test head
Zylindrischer Flansch	Cylindrical flange

4.5.3 Screening with an expert system

Knowledge of the plant operation and the typical stresses in the various parts of the plant allows a preliminary assessment of which damage mechanisms could potentially be effective in which parts of the plant. To support the know-how of the operating team, expert systems can also be used to define the test concept for specific damage mechanisms, e. g. the COMSY software platform [4-1][4-2][4-3], which was originally developed for the ageing management of NPPs.

This is a software product with a modular architecture in which each module is used individually or in combination with other modules to predict damage processes. In addition to the database and data management function, a series of analytical functions are provided that allow critical locations to be identified and component-related damage rates and remaining service lives to be determined. On this basis, inspection intervals and maintenance activities can be optimized.

The ageing-relevant component data is linked to an integrated power plant model. This allows up to seven different groups of damage mechanisms to be addressed, both below the temperature range relevant for creep and for creep and creep fatigue, Fig. 4-15.

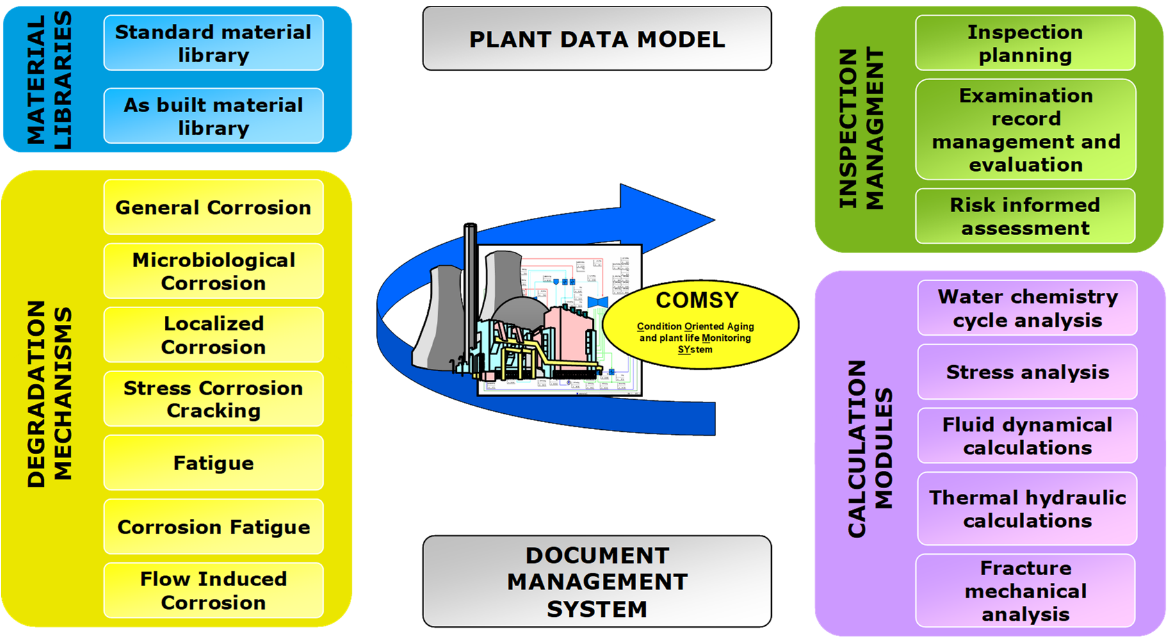

Fig. 4-15: Ageing management of mechanical components with an expert system [4-1]

Strain induced corrosion cracking is one of these mechanisms. To determine system areas potentially affected by SICC, a simulation of the water-chemical cycle in each system and sub-system with respect to pH and oxygen concentrations is carried out, in which the distribution of alkalizing agents and oxygen is calculated based on the respective distribution characteristics.

To perform this analysis, the heat balance diagram of the entire power plant is first modelled, including the system parameters for all relevant system areas. This model is then used as the basis for the above-mentioned analysis of the water chemistry cycle, considering the associated thermal-hydraulic parameters. Taking into account the materials used in each case and, if applicable, the thermomechanical stress conditions, the system areas can then be examined regarding their degradation potential for the damage mechanisms as shown in Fig. 4-15.

<u>Screening for strain induced corrosion cracking:</u>

The sub-model used to evaluate SICC and directly linked to the overall power plant model is shown schematically in Fig. 4-16.

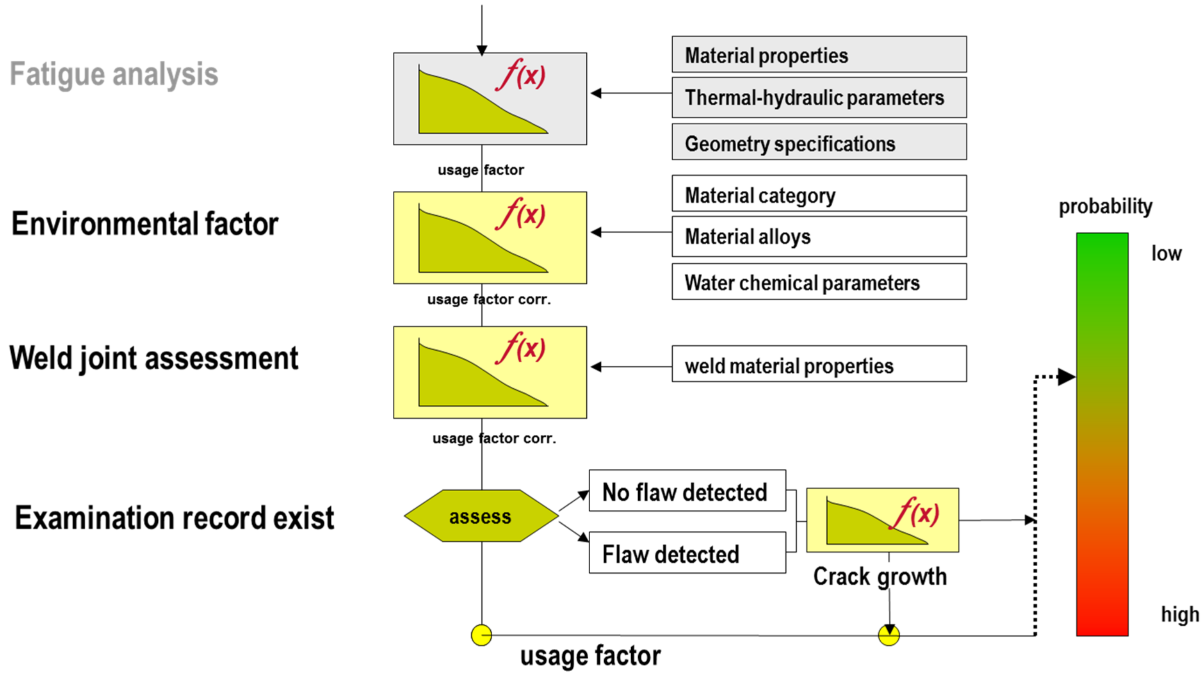

Fig. 4-16: Sub-model for screening with regard to strain induced corrosion cracking

The three main influencing parameters – ambient medium (dissolved oxygen), temperature and (estimated or precisely determined) strain rate – can be used to make a local estimate of the susceptibility to SICC. If a load specification or real load cycles are available, an approximate degree of fatigue can also be specified or an estimate of the residual fatigue life can be made.

This provides a computer-aided option to support the screening of an entire power plant regarding the susceptibility to SICC of individual plant areas, systems, or components. Once identified, the test methods and test measures described in subsections 4.1 to 4.4 and, in particular targeted fatigue monitoring based on measured operating data in the temperature range below the creep range can then be used.

This expert system is successfully used in several fossil power plants worldwide to assess the potential for various damage mechanisms such as FAC. Concrete practical applications for SICC prediction have so far been carried out in the context of NPPs, taking into account the operating conditions there [4-1][4-2][4-3][4-4].

5 Integrity assessment for SICC findings

If linear indications are identified on the inside of the component using non-destructive testing methods (NDT), these can also be assessed by means of an integrity analysis to determine whether continued operation is permissible for a limited period of time instead of immediate component replacement. The verification of the integrity analysis is carried out with non-destructive testing after a defined period of time or after a defined number of cycles or after a defined load collective at a point in time at which the failure determined by calculation can still be ruled out with a reasonable degree of certainty.

Literature on the methodology of the fitness-for-service (FFS) analysis can be found in the FKM guideline [5-1], in the ASME BPV Code Section XI for NPPs [5-2], in BS 7910:2013+A1:2015 [5-3], in API 579-1 2021 ed. [5-4] and in the VdTÜV data sheet MB DAMP 0468:2022-10-15 [5-5].

A specific recommendation of a methodology is not made in this report. In the following, however, the special features of an integrity analysis are discussed, in which the SICC is assumed to be the damage mechanism determining the further crack propagation.

The basic procedure of an integrity analysis is to determine the permissible flaw size resulting from the highest stress to be assumed based on the maximum flaw size determined by means of NDT using fracture mechanics calculation methods. The operational crack growth for the assumed active damage mechanism is then calculated and thus the operating time until the permissible flaw size is reached is determined. A suitable test interval until the first non-destructive repeat test is then determined. If it is determined during this evaluation that the defect size has already reached the permissible defect size, a failure cannot be ruled out mathematically. In this case, either a repair measure must be initiated or the operational stresses must be reduced.

When calculating the permissible defect size, the mechanism that led to the crack growth is not relevant. Only the fracture mechanical resistance of the material counts here.

Operational cyclic fatigue crack growth is usually the driving mechanism for crack growth. Sufficient technically validated material parameters are available for the steels of pressurized components in steam power plants. The use of crack growth curves in the medium is generally a suitable basis for evaluating corrosion-supported crack growth.

The following subchapter 5.1 contains examples of corresponding material parameters for the evaluation of permissible defect sizes and cyclic crack growth in the medium in the low-alloy steels WB 36 (15NiCuMoNb5) and GS17CrMoV5-11.

As described in detail in Chapter 2, the level of technical and scientific knowledge on operational crack growth is currently significantly lower for SICC than for cyclic fatigue crack growth. The use of SICC crack growth rates determined in the laboratory (see

Chapter 2), in conjunction with increased safety factors, therefore generally leads to an overly conservative assessment of the damage mechanism with the possible consequence of unnecessary replacement of the component under consideration.

The assessment of cracked components in conventional power plants due to active SICC is therefore carried out as a case-by-case analysis with the following possible components:

- Determination of defect size using an NDT method qualified for the component geometry;
- Determination of the operational stresses including temperature and medium in the affected area;
- Determination of the permissible defect size using representative material properties and, in the case of defects in the weld metal, considering residual stresses using recognized fracture mechanics evaluation methods;
- Best possible prediction of SICC crack growth in the form of a fatigue crack growth calculation with characteristic values in the medium;
- Evaluation of the distance between the defect size at the next inspection and the permissible defect size;
- For cracks close to the permissible dimensions, it is recommended to install a leakage monitoring system, e. g. using temperature sensors, video monitoring or acoustic sensors;
- Periodic inspection must be carried out to verify the predictions of crack growth.

The operating time until the next periodic inspection is determined for the two parallel criteria:

1. operating time;
2. number of cycles.

With the limited crack growth verified on the real component, the crack growth analysis and thus also the length of the operating time for the subsequent cycles can be adjusted. In the event of increased, progressive crack growth, component replacement is recommended.

It is recommended that the area in question be checked for access restrictions during power operation and during start-up and shut-down.

5.1 Basic input parameters for fracture mechanics calculations

In general, the following input data is required for a fracture mechanics evaluation of findings (including SICC findings):

- Findings size and the crack postulate derived from it;
- Dimensions of the component;
- Loads (max. load, load in normal operation, load cycles);
- Fracture mechanical material parameters.

The fracture mechanical material parameters required for a fracture mechanical evaluation of findings are described below. This evaluation generally consists of two calculations:

- Determination of the critical crack size;
- Determination of the crack growth for the planned test interval.

The input variables required to determine the critical crack size depend on the assumed failure mechanism (ductile fracture, brittle fracture, limit load failure) and the complexity of the analysis. This ranges from conservative analytical evaluations (level 1) to the use of numerical micromechanical models (level 3). The more complex the analysis effort, the lower the conservatism of the results, see Fig. 5-1 for a ductile fracture assessment as an example.

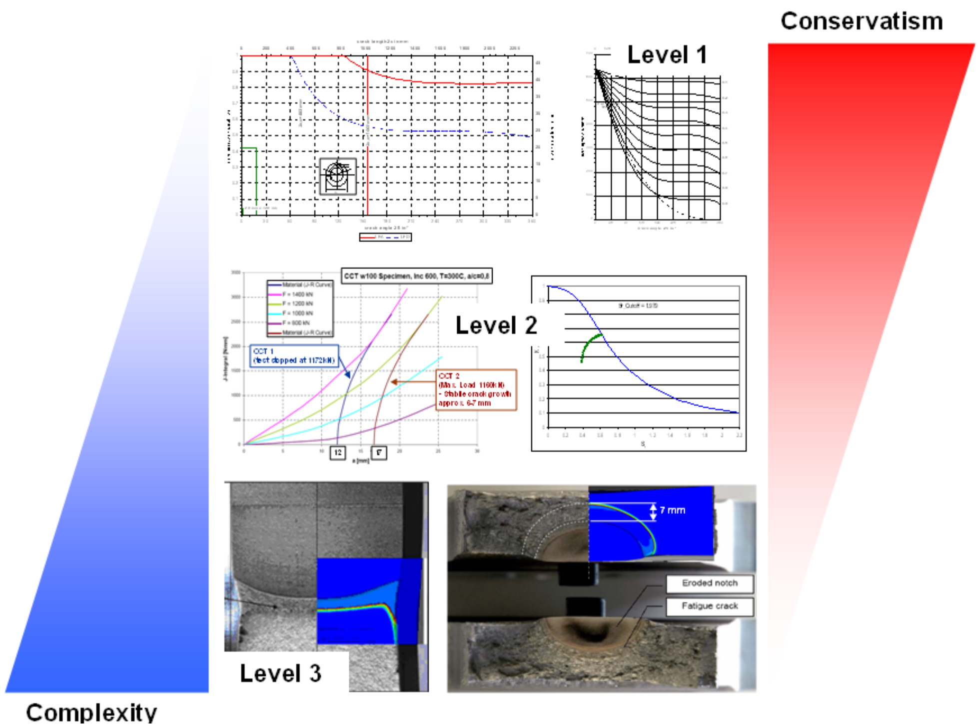

Fig. 5-1: Complexity and conservatism of a ductile fracture analysis (Framatome GmbH)

Depending on the complexity of the analysis, the following material parameters are required to determine the critical crack size:

- Strength parameters (yield strength, tensile strength);
- Fracture toughness;
- Crack resistance curve (J-R curve);
- Parameters for micromechanical models (e. g. Gurson model).

To determine the crack growth for the planned test interval, the associated material parameters are required for the relevant stable crack growth mechanisms. The stable crack growth mechanisms include

- Fatigue crack growth due to mechanically or thermally induced alternating stress, usually in the form of the Paris law $da/dN = C \cdot \Delta K^n$;
- Corrosion-assisted crack growth (SICC, H-SICC, SCC, etc.), usually as a function of time da/dt or as a modified dependency da/dN;
- Creep crack growth or creep fatigue crack growth.

5.2 Material characteristics for the materials WB 36 (15NiCuMoNb5) and GS17CrMoV5-11

The material properties for the materials WB 36 (15NiCuMoNb5) and GS17CrMoV5-11 are of particular relevance for power plants. This fact is reflected in the well-documented amount of data for these materials. For this reason, they are discussed in this subsection as examples of unalloyed and low-alloy steels.

For the copper-alloyed low-alloy steel WB 36 (15NiCuMoNb5), it has been known since the end of the 1990s [3-26] that thermal ageing due to finely dispersed copper precipitation occurs during long-term operation from around 350 °C, which has an effect on the mechanical properties.

As part of a research project [5-6], the influence of plastic alternating deformation at different temperatures on the copper precipitation process and the effects on the material toughness of WB 36 (15NiCuMoNb5) were investigated. The hardening behaviour was evaluated in LCF fatigue tests on different precipitation states (recovery annealed, stabilizing annealed and operationally stressed). It was found that the dislocation movement has an accelerating influence on copper precipitation. The behaviour of the recovery annealed condition approaches that of the operationally stressed condition with increasing strain range. Copper precipitation is promoted in the course of alternating deformation.

TEM investigations on WB 36 (15NiCuMoNb5) in [5-6] show that the increase in strength and decrease in toughness observed during long-term annealing or operational stress in the range of 350 °C are essentially due to precipitation processes of copper particles in the range of a few nanometres (nm).

In [5-7], the influence of temperature, the oxygen content of the high-temperature water and the strain rate on the susceptibility to strain-induced cracking corrosion for low-alloy steels used in LWR, including WB 36 (15NiCuMoNb5), was described as early as 1986 using a 3D model.

Fracture mechanical properties for static loading:

In [5-6], JR tests (20 % side-notched CT25 specimens, partial unloading method according to ASTM E813-89) were performed at different temperatures and physical crack initiation values were determined via the stretch zone measurement and engineering crack initiation values at a stable crack growth of 0.2 mm, Fig. 5-2.

At 0 °C, the material reaches its highest point in its initial state. The crack initiation value J_i is higher at 340 °C than at 250 °C and corresponds to the room temperature value.

The effect of operational exposure (57,000 h at 350 °C) is to cause the transition temperature to shift to higher values. At 340 °C, K_{IJ} (calculation based on the physical crack initiation value) is 125 MPam$^{1/2}$ for the material in the initial state and 84 MPam$^{1/2}$ after operational stress.

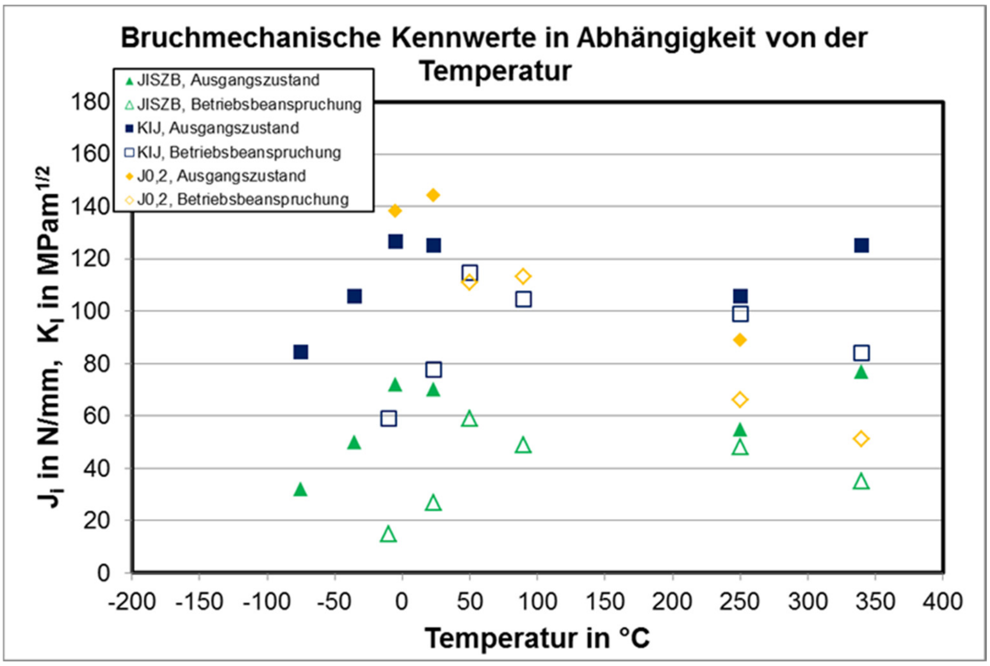

Fig. 5-2: Stress intensity factor and crack initiation values of WB 36 (15NiCuMoNb5) in the initial state and after operational exposure (57,000 h / 350 °C) [5-6]

Translation	
German	**English**
Bruchmechanische Kennwerte in Abhängigkeit von der Temperatur	Fracture mechanical properties as a function of temperature
Ausgangszustand	Initial state
Betriebsbeanspruchung	Operational stress
Temperatur	Temperature

In [5-8] and [5-9], these investigations were supplemented by the test temperature of 90 °C, Fig. 5-3. The crack initiation value J_i of 72 N/mm in the initial state is significantly higher than after the above-mentioned operational exposure (57,000 h / 350 °C) with J_i = 49 N/mm. The crack resistance curve after operation shows a significantly reduced resistance to stable crack growth.

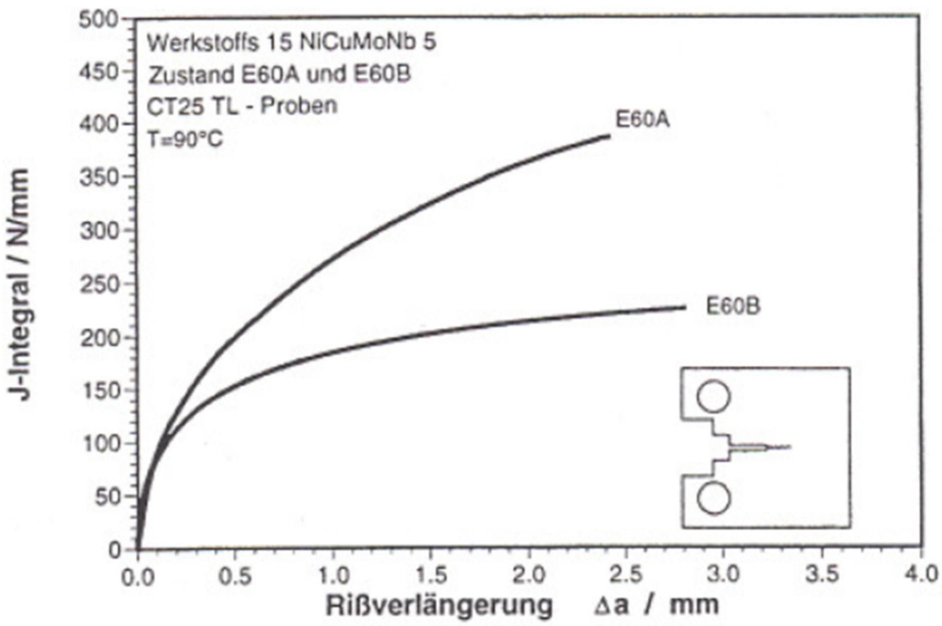

Fig. 5-3: Crack resistance of WB 36 (15NiCuMoNb5) [5-9]

Translation	
German	**English**
Werkstoff	Material
Zustand	State
Proben	Samples
Rißverlängerung	Crack extension

Annex C of KTA 3206 [5-10] contains, among other things, the J_{IC} values available from research projects and other material tests for WB 36 (15NiCuMoNb5) as a basic pipe material at elevated temperatures up to 250 °C for various defect positions from 76.2 N/mm to 176 N/mm, which can be formally converted into ductile fracture toughness values according to Eq. 5-1, Tab. 5-1:

$$K_{Jc} = \sqrt{\frac{J_{Ic} \cdot E}{(1-\vartheta^2)}} \qquad \text{(Equation 5-1)}$$

Tab. 5-1: Conversion of the J_{IC} characteristic values of WB 36 (15NiCuMoNb5) as a pipe base material at elevated temperatures up to 250 °C for various defect positions into ductile fracture toughness values K_{JC} [5-10]

Defect		**Orientation**	**J_{Ic}**	**K_{Jc}**
Orientation	**Type**	**Samples**	N/mm	MPam$^{1/2}$
axial	Surface crack	T-S	76.2	130.0
	Through wall crack	T-L	92.9	143.5
Circumference	Surface crack	L-S		197.6
			1st letter – load direction	
			2nd letter – crack propagation direction	

In [5-11], the influence of the stress velocity on the fracture toughness K_{IJ} was investigated. The fracture toughness K_{IJ} of the cyclic pre-cracked samples determined using the strain gauge method at room temperature shows values of approx. 150 MPam$^{1/2}$ up to a loading rate of 104 MPam$^{1/2}$/s. The impact fracture toughness of the material 15NiCuMoNb5 increases only slightly with the stress velocity. At room temperature, the transition region from ductile to brittle fracture is reached at a stress rate of more than 10^4 MPam$^{1/2}$/s. No results are available at higher temperatures. However, these highly dynamic stress velocities are not relevant in practice for steam power plants.

Fracture mechanical parameters for cyclic loading:

The da/dN-ΔK limit curves of low-alloy steels given in [5-12] for determining the remaining service life under cyclic loading are mainly based on measured values determined under PWR primary circuit conditions at low O_2 content, Fig. 5-4. While these limit curves conservatively cover the influence of the PWR medium, higher O_2 contents lead to accelerated crack propagation [5-13].

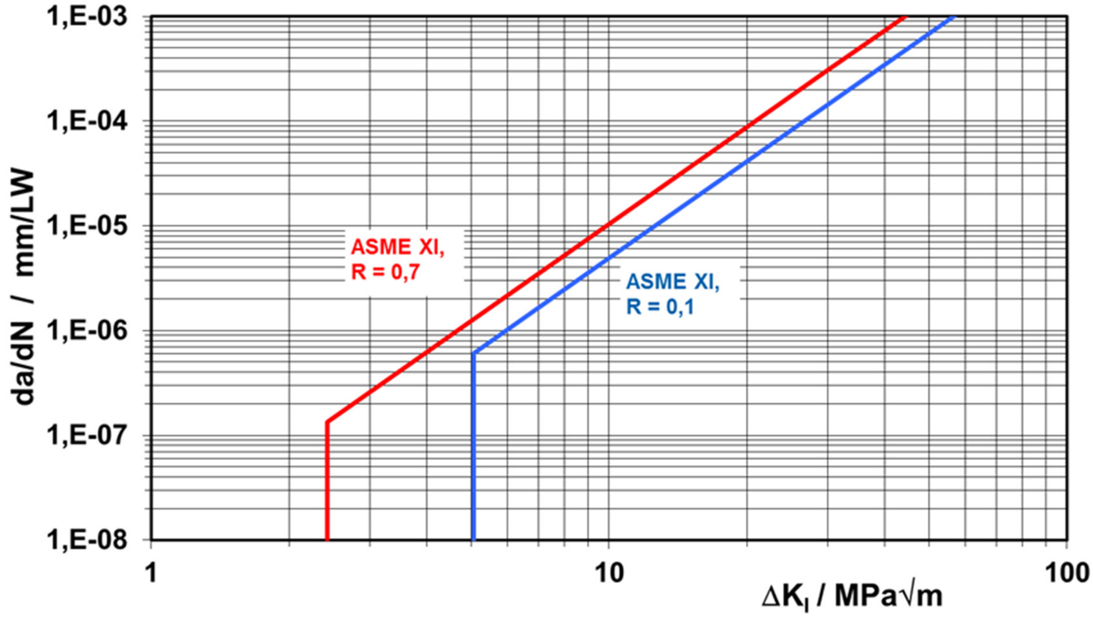

Fig. 5-4: Reference curves for the cyclic crack growth rate of reactor pressure vessel steels according to ASME Code Section XI [5-12]

Tests on the cyclic crack growth of the material WB36 (15NiCuMoNb5) were carried out in [5-14] on a pipe with a circumferential notch. The load was applied in three phases with different frequencies (1/15 min, 1/1 min, 4/1 min). The crack growth behaviour and the crack growth rate da/dN in the test phases are shown in Fig. 5-5.

By increasing the frequency from 1/15 to 1 load cycle per minute, the load cycle-related crack growth rate is reduced by a factor of 10, as the influence of corrosion practically no longer comes into play due to the increased frequency [5-15].

This aspect underlines the great significance of the load frequency on the crack propagation per load cycle and on the type of crack propagation (fatigue or fatigue with increasing corrosion influence). The phenomenon of slowing down the crack propagation per load cycle by increasing the frequency is also reflected in the crack surfaces [5-16]. A cyclic crack growth test on a Compact Tension specimen (specimen 15NiCuMoNb 5 taken from a tube and joined together to form a CT specimen by electron beam welding) was carried out in an autoclave under operationally similar water conditions at extremely slow load cycles (1/15 min) [5-16]. This showed that crack growth rates occur at slow load cycles that are about a factor of 5 above the limit according to ASME XI [5-12], Fig. 5-6.

While a typical corrosion-supported fatigue crack growth appears at low load frequencies, ductile striations appear at high frequencies [5-16].

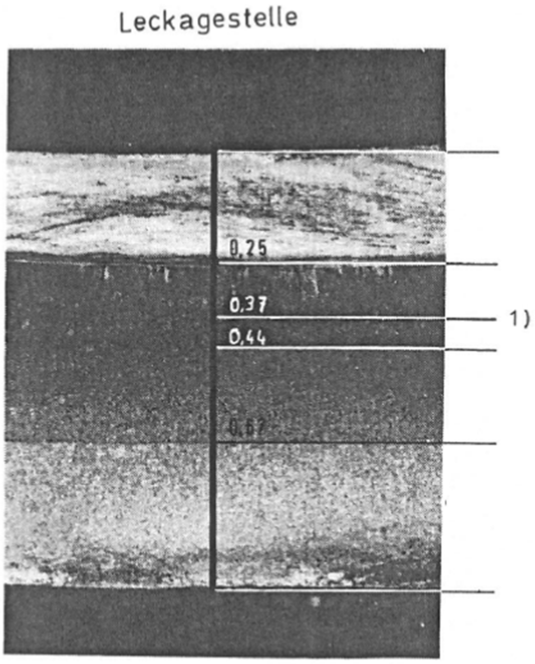

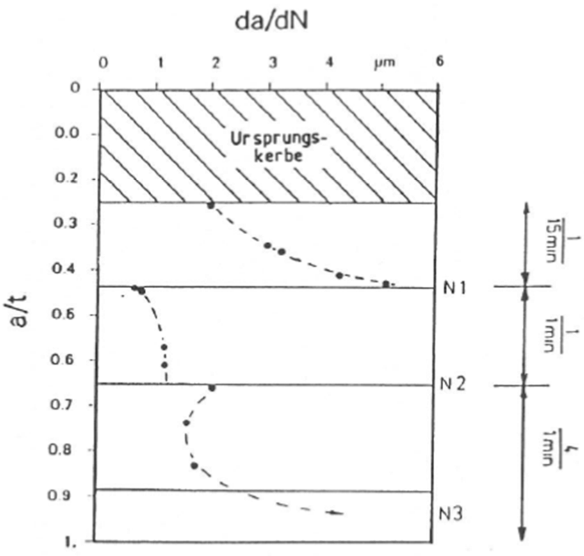

Fig. 5-5: Cyclic crack growth of 15NiCuMoNb5, pipe with circumferential notch [5-15][5-16]

Translation	
German	**English**
Leckagestelle	Leakage location
Ursprungskerbe	Original notch

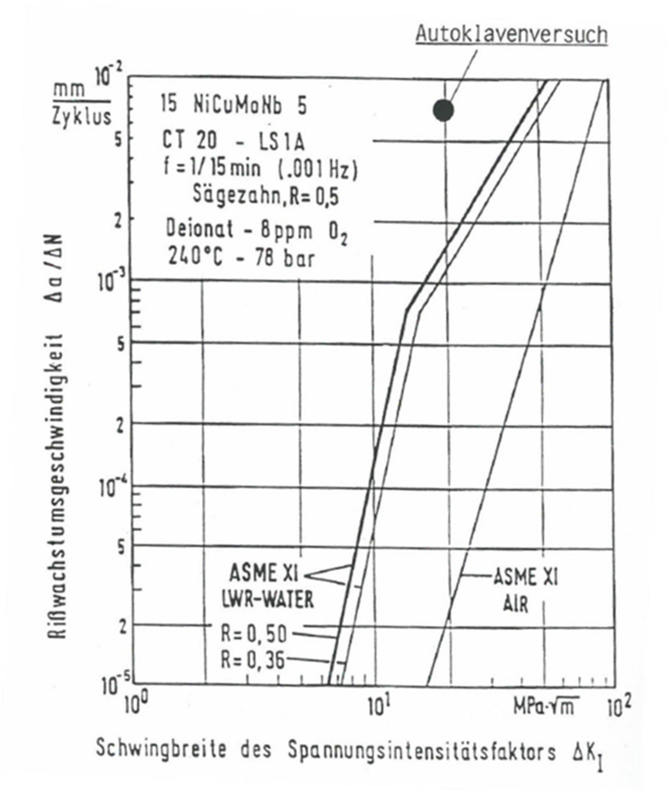

Fig. 5-6: Cyclic crack growth rate da/dN as a function of the amplitude of the stress intensity factor ΔK_I and comparison with ASME Code Section XI [5-12][5-16]

Translation	
German	**English**
Autoklavenversuch	Autoclave test
Rißwachstumsgeschwindigkeit	Crack growth rate
Schwingbreite des Spannungsintensitätsfaktors	Range of the stress intensity factor

Fracture mechanical properties under creep and creep fatigue stress:

Fig. 5-7 shows a creep crack test carried out at the MPA Stuttgart at 350 °C in comparison with scatter bands of other materials. Further test results on the creep and creep fatigue cracking behaviour of the materials WB 36 (15NiCuMoNb5) and GS17CrMoV5-11 are not known.

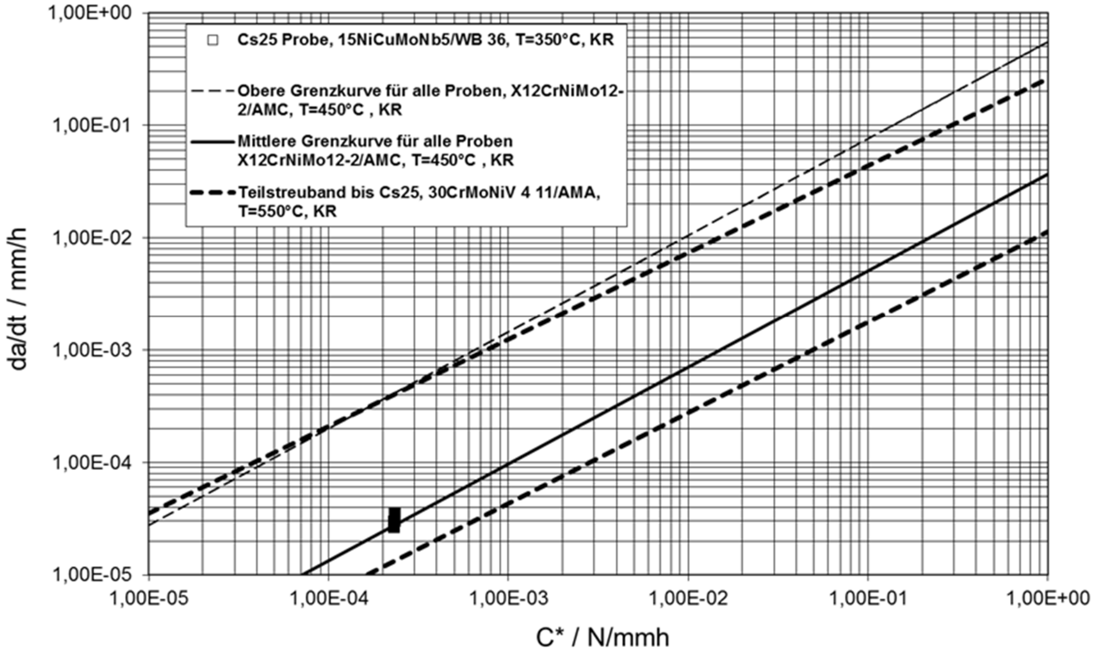

Fig. 5-7: Creep cracking test WB 36 (15NiCuMoNb5) at 350 °C in comparison to scatter bands of other materials [5-17]

Translation	
German	**English**
Probe	Sample
Obere Grenzkurve für alle Proben	Upper limit curve for all samples
Mittlere Grenzkurve für alle Proben	Average limit curve for all samples
Teilstreuband	Partial scatter band

Determination of material data in the LCF test:

At the MPA Stuttgart, low-cycle fatigue tests (LCF tests) and da/dN tests at different R-values under water conditions were carried out on WB 36 (15NiCuMoNb5) and GS17CrMoV5-11 materials subjected to operational stress [5-18][5-19].

The samples for testing under water conditions (280 °C, O_2 = 0.4 ppm) were pre-autoclaved for 100 h before the LCF test so that a magnetite protective layer could form. Fig. 5-8 shows the formation of the magnetite layer on WB 36 (15NiCuMoNb5) in the FIB cut as well as the surface of the layer.

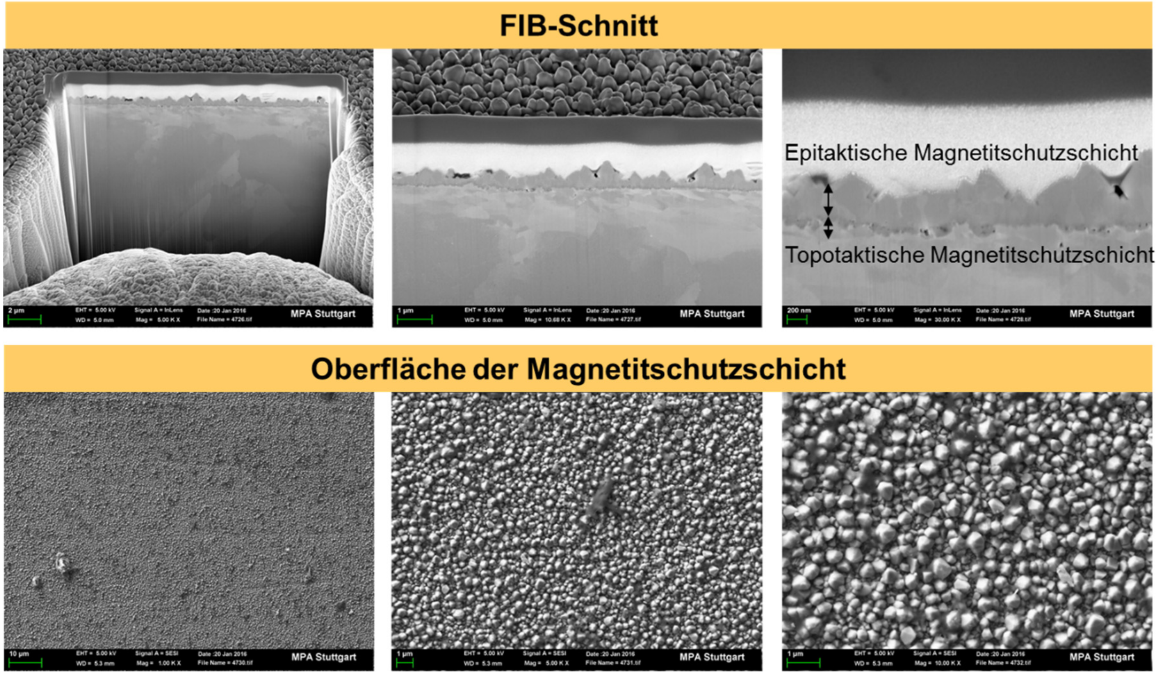

Fig. 5-8: Formation of the magnetite protective layer for the material WB 36 (15NiCuMoNb5)

Translation	
German	**English**
FIB-Schnitt	FIB cut
Oberfläche der Magnetitschutzschicht	Surface of the magnetite protective layer
Epitaktische Magnetitschutzschicht	Epitaxial magnetite protective layer
Topotaktische Magnetitschutzschicht	Topotactical magnetite protective layer

Fig. 5-9 shows the crack and the fracture surfaces of a sample tested under water conditions. Fig. 5-10 shows the classification of the results in literature values [5-6].

Fig. 5-9: Sample L8 (GS17CrMoV5-11) after LCF test under water conditions

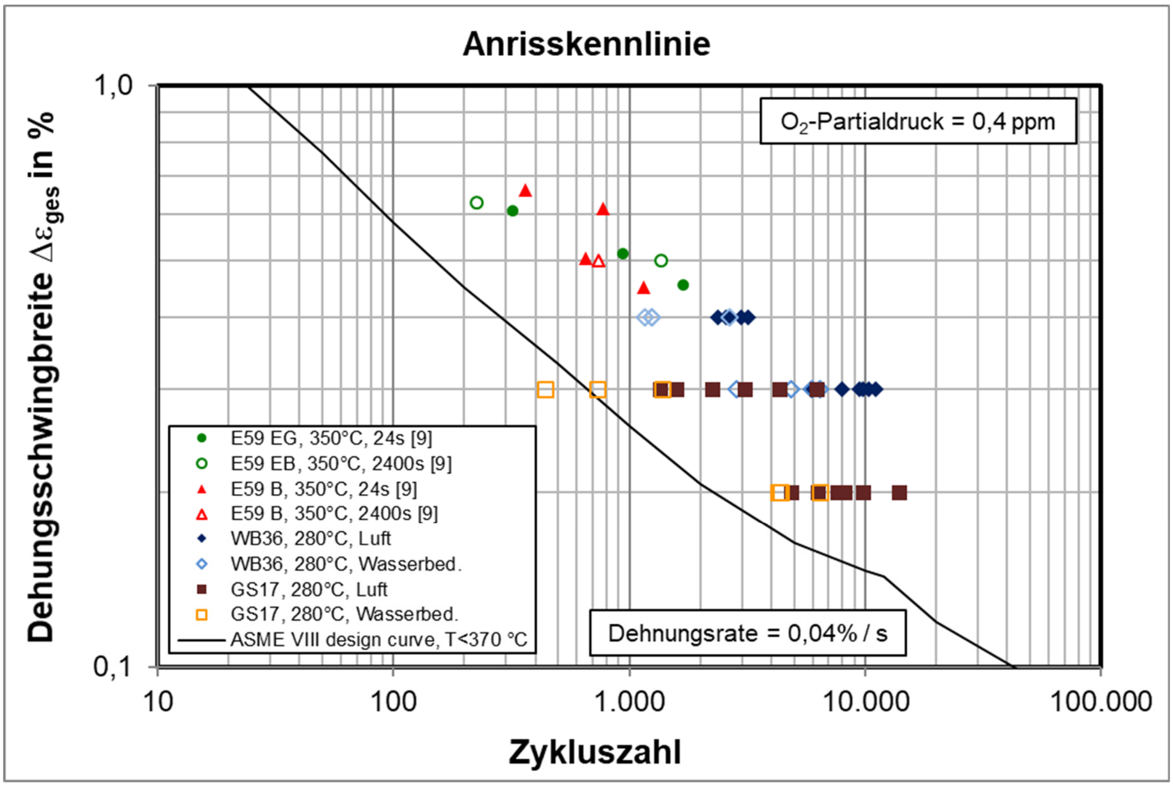

Fig. 5-10: Results of the LCF tests [5-6] [5-18][5-19]

Translation	
German	**English**
Dehnungsschwingbreite	Strain amplitude
O_2-Partialdruck	O_2 partial pressure
Dehnungsrate	Strain rate
Zykluszahl	Cycle number

The tests under water conditions were carried out for WB 36 (15NiCuMoNb5) with $\Delta\varepsilon$ = 0.3 % and $\Delta\varepsilon$ = 0.4 % and for GS17CrMoV5-11 with $\Delta\varepsilon$ = 0.2 % and $\Delta\varepsilon$ = 0.3 %. The test results of the samples of the cast steel GS17CrMoV5-11 show a larger scatter band than the results for the forged steel WB 36 (15NiCuMoNb5) [5-18][5-19].

While the WB 36 tests in air are in line with the literature data [5-6], the crack initiation curve for the GS17 tests is at lower numbers of cycles.

Under water conditions, the crack initiation curves for the WB 36 (15NiCuMoNb5) as well as for the GS17CrMoV5-11 cast material are shifted to lower numbers of cycles compared to the crack initiation curves in air [5-18][5-19].

da/dN tests under pulsating stress

Under water conditions, da/dN tests in accordance with ASTM E647-95 [5-20] were carried out on CT25 specimens made of WB 36 (15NiCuMoNb5) and GS17CrMoV5-11 [5-18][5-19]. The stress ratio in these tests was R = 0.1. The crack length during the test in the autoclave was determined using a direct current potential drop method, whereby the recorded measurement signal initially only allowed a qualitative assessment of the crack growth. To correlate the measurement signal with the crack growth during the experiment, the sample is broken open with liquid nitrogen after completion of the test and the actual crack growth is determined at equidistant intervals on the exposed fracture surface using a measuring microscope. The relationship between crack growth and signal change allows the crack growth to be visualized over the duration of the test, Fig. 5-11.

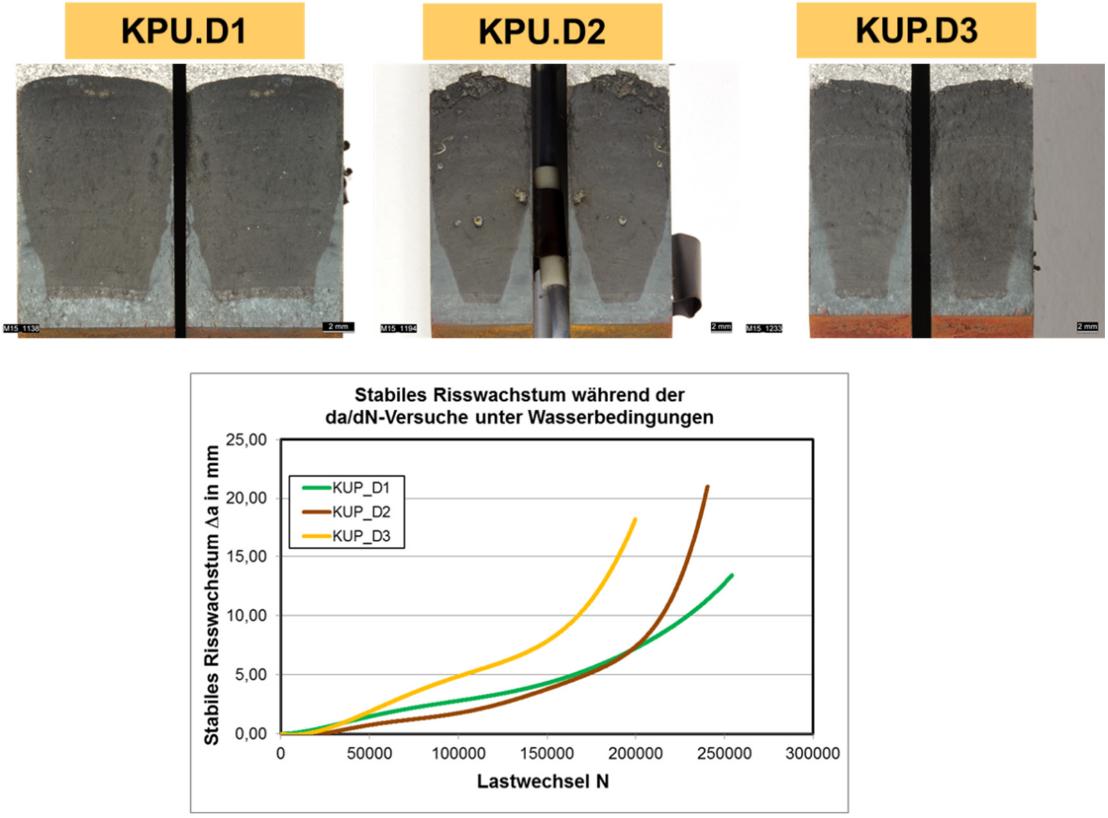

Fig. 5-11: Fracture surfaces of the CT specimens tested under water conditions; crack growth based on the potential measurement during the test

Translation	
German	**English**
Stabiles Risswachstum während der da/dN-Versuche unter Wasserbedingungen	Stable crack growth during da/dN tests under water conditions
Stabiles Risswachstum	Stable crack growth
Lastwechsel	Load cycle

da/dN tests under alternating stress

The da/dN test under alternating stress was performed using corner crack (CC) specimens [5-18][5-19].

After the test, the specimens were cracked under cooling with liquid nitrogen and the fracture surfaces were measured. The crack growth was calculated based on the potential signal recorded during the test and the crack length before and after the test, Fig. 5-12.

Probe KUP_C01

Kerb	1. Bruchhälfte M15_1354			2. Bruchhälfte M15_1355			Mittelwert
	10°	45°	80°	10°	45°	80°	
Erodierter Kerb	1,13	0,93	1,09	1,16	0,94	1,09	1,06
Ermüdungsriss	0,74	0,91	0,78	0,79	0,93	0,75	0,82
Versuchsriss	0,98	1,07	1,17	1,17	1,08	0,95	1,07

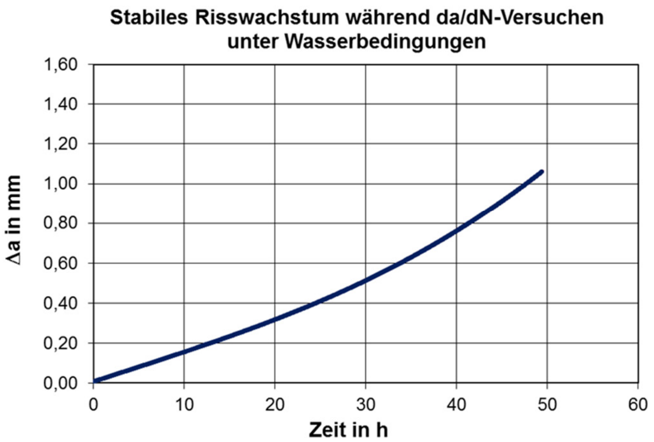

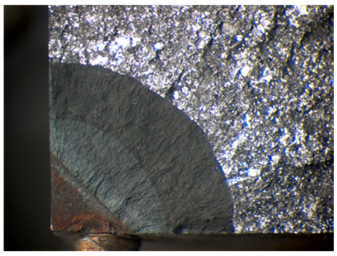

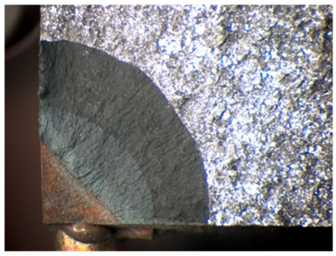

Fig. 5-12: Fracture surfaces of the CC specimens tested under water conditions; crack growth based on the potential measurement during the test

Translation	
German	**English**
Stabiles Risswachstum während der da/dN-Versuche unter Wasserbedingungen	Stable crack growth during da/dN tests under water conditions
Erodierter Kerb	Eroded notch
Ermüdungsriss	Fatigue crack
Versuchsriss	Experimental crack
Zeit	Time

To be able to compare the results of the tests with R = 0.1 and R = -1, the crack propagation velocity was plotted against ΔK_{eff} in Fig. 5-13 and Fig. 5-14.

The test results of the GS17CrMoV5-11 cast steel samples show a larger scatter band than the results for the forged steel WB 36 (15NiCuMoNb5).

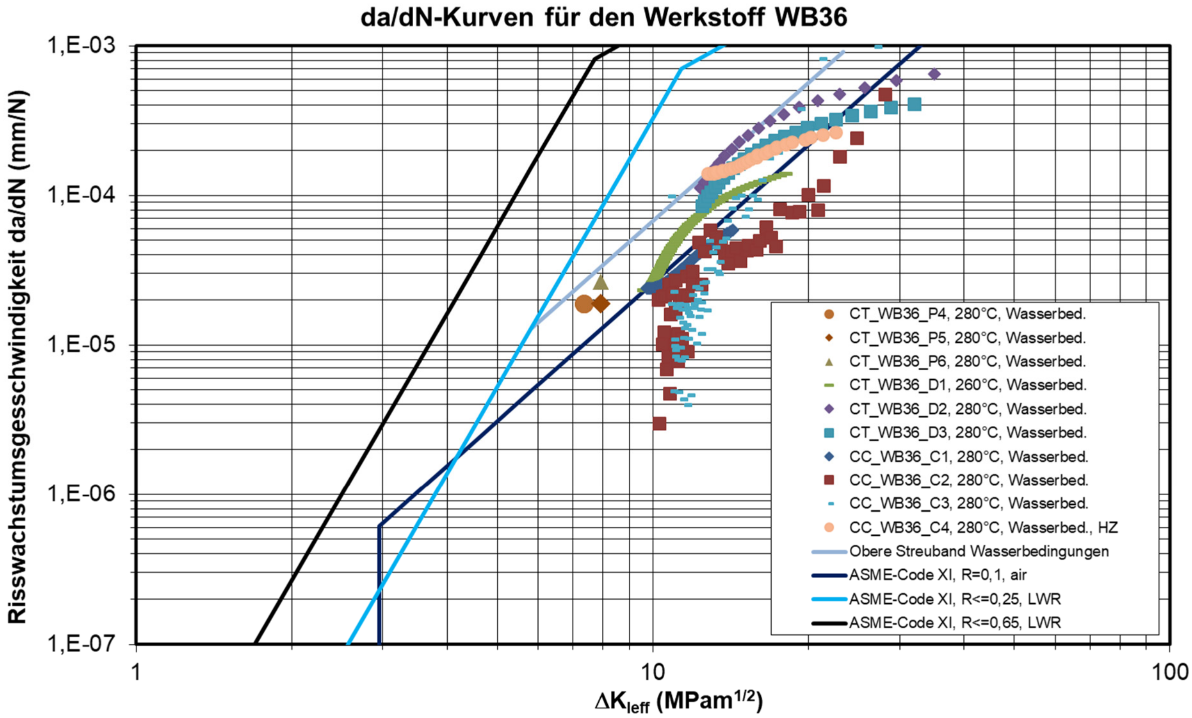

Fig. 5-13: da/dN curves for the material WB 36 (15NiCuMoNb5) [5-18]

Translation	
German	**English**
da/dN-Kurven für den Werkstoff WB 36	da/dN curves for the material WB 36
Risswachstumsgeschwindigkeit	Crack growth rate
Wasserbed.	Water conditions
Obere Streuband Wasserbedingungen	Upper scatter band water conditions

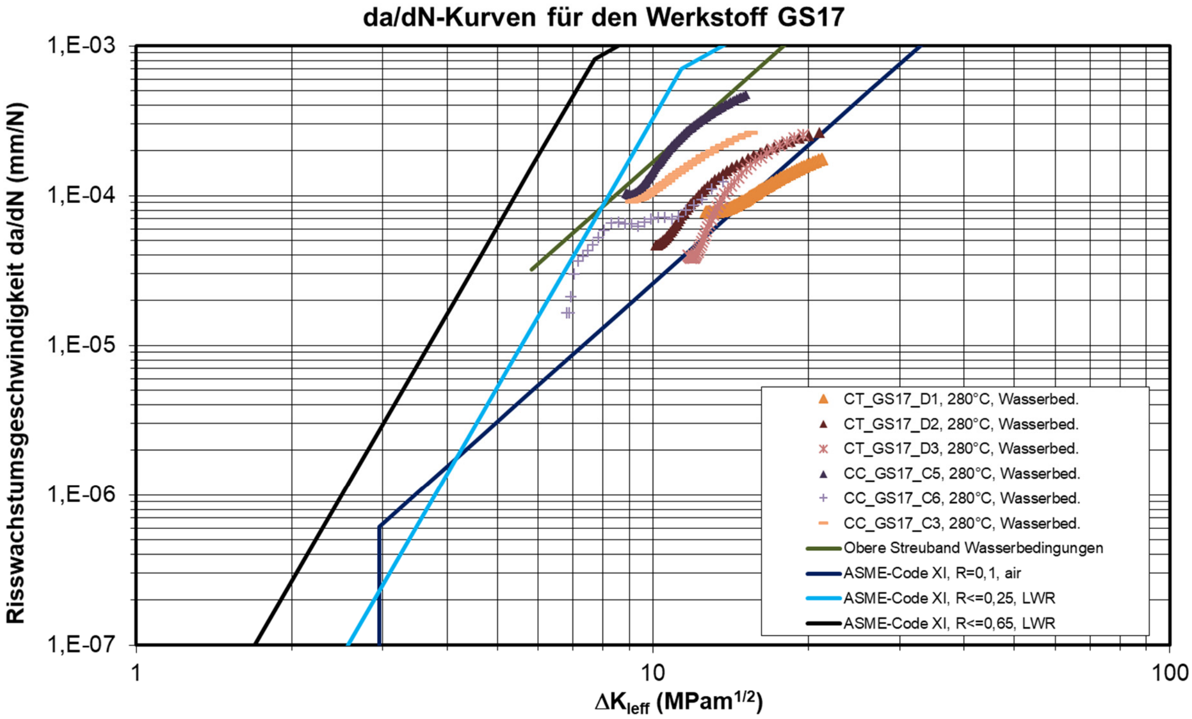

Fig. 5-14: da/dN curves for the material GS17CrMoV5-11 [5-19]

Translation	
German	**English**
da/dN-Kurven für den Werkstoff WB 36	da/dN curves for the material WB 36
Risswachstumsgeschwindigkeit	Crack growth rate
Wasserbed.	Water conditions
Obere Streuband Wasserbedingungen	Upper scatter band water conditions

As a result of the crack propagation tests, upper scatter band limits were defined for both materials, Tab. 5-2.

Tab. 5-2: Results of the da/dN tests [5-18][5-19]

Material	Sample Number	Sample form	m	C
				mm/LW
15NICuMoNb5 (WB36)	KUP_D1	CT sample	2.99	4.10E-08
	KUP_D2		1.65	2.89E-06
	KUP_D3		1.82	1.26E-06
	KUP_C1	Comer Crack	2.82	3.44E-08
	KUP_C2		2.48	5.28E-08
	KUP_C3		5.87	
	KUP_C4		1.34	
	Upper scatter band limit		**3,07**	**6.41E-09**
GS-17CrMoV5-11	WEI_D1	CT sample	2.00	4.19E-07
	WEI_D2		2.40	2.18E-07
	WEI_D3		3.68	6.72E-09
	WEI_C3	Comer Crack	2.36	4.70E-07
	WEI_C5		4.36	6.43E-09
	WEI_C6		5.91	1.78E-05
	Upper scatter band limit		**3.07**	**1.60E-08**

5.3 Calculation methods

As already mentioned at the beginning of Chapter 5, literature on fracture mechanics calculation methods as part of the methodology of fitness-for-service (FFS) analysis can be found in the FKM Guideline [5-1], in the ASME BPV Code Section XI for NPPs [5-2], in BS 7910:2013+A1:2015 [5-3], in API 579-1 2021 ed. [5-4] and in the VdTÜV data sheet MB DAMP 0468:2022-10-15 [5-5].

5.4 Requirements for the test report

The NDT test report, which serves as the basis for the fracture mechanics calculation, describes the geometry of the indications with quantitative variables with the associated inaccuracy variables.

<u>Proof of integrity:</u>

All input variables used are documented.

When preparing a fracture mechanics calculation, the steps must be documented in such detail according to the method used that subsequent reproducibility of the results and validation by the NDT after the next test interval are possible.

When using FEM, specific details of the model and, if applicable, the sub models and the calculation program must be documented to ensure subsequent reproducibility:

- Calculation software used with version number;
- Elements used, number per element type, size ratios (large to small);
- Mesh quality overall and in the critical evaluation range;
- Load applications (displacements, forces, temperature fields);
- Boundary conditions (special elements, such as special fixed-point constructions, restraints and degrees of freedom of cut surfaces);
- Images that support the above statements;
- The choice of special calculation options of the calculation software;
- The use of path evaluations; the paths must be described in a geometrically comprehensible manner.

5.5 Monitoring concept

The case-specific application of VGB Standard VGB-S-506-00-2019-02-EN “Condition monitoring and testing of components of steam boiler systems, pressure vessel systems and water or steam-carrying pipes in thermal power plants” (from 2019 edition) [5-21] is suitable for establishing an adequate monitoring concept with regard to the system areas potentially affected by strain induced corrosion cracking. Based on this, the next inspection interval can be quantified and defined as an effective means of monitoring. When monitoring the condition during a shutdown (see sections 4.5 and 4.6 in VGB-S-506-00-2019-02-EN), the evaluation of the results from periodic inspections, i.e. in particular the results of the non-destructive tests using endoscopy and ultrasound (from the outside), is of crucial importance. Any cracks that occur must be detected and tracked continuously. Tolerance-related inaccuracies must be considered conservatively when evaluating the results. The condition monitoring modules described in section 4 of VGB-S-506-00-2019-02-EN are applicable correspondingly. Details can be found directly in the reference. Explicit reference is made to the test procedures described in section 4.3 of this report. Further detailed specifications on these test methods for the testing of piping systems and their components can be found in VGB-S-509-00-2019-11-EN [5-22].

6 Summary

This technical-scientific report describes the state of knowledge at the time of publication on the damage mechanism of strain induced corrosion cracking in pressurized systems and components of conventional power plants.

In recent decades, but also in the recent past, SICC has repeatedly led to high downtime and replacement costs. In the course of the increasingly flexible operation of conventional power plants, damage caused by this mechanism has increased in recent years. As the cracks occur on the inside of the components and grow outwards, there is a risk of active damage not being detected until leakage or even catastrophic rupture.

This report therefore describes the damage mechanism and its triggering influencing factors, various representative examples of damage, useful avoidance strategies and suggestions for testing strategies through to proof of integrity for current test findings and the material characteristics required for this. The explanations and findings are partly detailed scientific and partly practice-oriented simplified descriptions.

This report raises the awareness of those technically responsible for the damage mechanism of strain induced corrosion cracking and supports them in mastering it based on the state of knowledge in 2024.

7 Literature, abbreviations, explanations

7.1 Literature and sources

[Chapter/Reference No.]

[1-1] VGB-TW 530 “Empfehlungen zum Betrieb und zur Überwachung von Kesselumwälzpumpen – Basierend auf den umfangreichen Nachuntersuchungen zum Schadensereignis 2014”, 11/2019

[2-1] a) Kußmaul, K., Blind, D., Läpple, V.:
New observations on the crack growth rate of low alloy nuclear grade ferritic steels under constant active load in oxygenated high-temperature water; Nuclear Engineering and Design 168 (1997) 53-75
b) Läpple, V., Blind, D., Deimel, P.:
Stand der Forschung zum korrosionsgestützten Rißwachstum niedriglegierter ferritischer Stähle in sauerstoffhaltigem Hochtemperaturwasser; VGB Kraftwerkstechnik 77 (1997), Heft 9, S. 754-761

[2-2] Seifert, H. P., Ritter, S., Hickling, J.:
Environmentally-Assisted Cracking of Low-Alloy RPV and Piping Steels under LWR Conditions;
Proc. 11th Int. Conf. on Environmental Degradation of Materials in Nuclear Power Systems – Water Reactors, 2003, Stevenson, WA (USA), American Nuclear Society, La Grange Park, IL (USA)

[2-3] ASM International Handbook Committee:
ASM Handbook, Vol. 13, “Corrosion”, ASM INTERNATIONAL, 1987

[2-4] Ford F. P., Andresen, P. L.:
Stress Corrosion Cracking of Low-Alloy Steels in 288 ° C Water, CORROSION '89, New Orleans, April 17-21, 1989, Paper No. 498

[2-5] Andresen P. L.:
Modeling of water and material chemistry effects on crack tip chemistry and resulting crack growth kinetics, 3rd Int. Symposium on Environmental Degradation on Materials in Nuclear Power Systems – Water Reactors, Traverse City, Michigan (USA), August 30 – September 3, 1988, G. J. Theus and J. R. Weeks (eds.), The Metallurgical Society, 1989, pp. 301-312

[2-6] Ford F. P., Horn R. M., Hickling J., Pathania R., Bruemmer G.:
Stress Corrosion Cracking of Low Alloy steels under BWR Conditions; Assessment of Crack Growth Rate Algorithms,
Proc. 9th Int. Symposium on Environmental Degradation on Materials in Nuclear Power Systems – Water Reactors, Newport Beach FL (USA), August 1-5, 1999, S. Bruemmer, P. Ford, G. Was (eds.), TMS 1999, pp. 855-863

[2-7] Ford, F. P.; Andresen, P. L.; Weinstein, D.; Ranganath, S.; Pathania, R.: Stress Corrosion Cracking of Low-Alloy Steels in High Temperature Water; Proc. 5th Int. Symposium on Environmental Degradation on Materials in Nuclear Power Systems – Water Reactors, Monterey, CA (USA), 25-29 August 1991, American Nuclear Society Inc., La Grange Park, IL (USA), 1992, pp. 561-569

[2-8] Lenz E., Wieling N.:
Strain-Induced Corrosion Cracking of Low-Alloy Steels in LWR-Systems – Interpretation of Susceptibility by Means of a Three-Dimensional (T, dε/dt, Dissolved Oxygen) Diagram,
Nuclear Engineering and Design, Vol. 91, 1986, pp. 331-344

[2-9] P.M. Scott, D.R. Tice: Stress corrosion in low alloy steels, Nucl. Eng. Des. 119 (1990): p. 399-413

[2-10] H. Hoffmeister, T. Böllinghaus, Modeling of Combined Anodic Dissolution/Hydrogen-Assisted Stress Corrosion Cracking of Low-Alloyed Power Plant Steels in High-Temperature Water Environments, Corrosion Science, Vol. 70, No. 6, p. 563-578

[2-11] D. M. Seeger, Wasserstoffaufnahme und -diffusion in Schweißnahtgefügen hochfester Stähle, Dissertation, 2004, S. 94

[2-12] E. Wendler-Kalsch • H. Gräfen Korrosionsschadenkunde, 1. Aufl. 1998, Nachdruck 2012, [Kapitel 4.2.2]

[2-13] Dayal, R.K., Parvathavarthini, N.:
Hydrogen embrittlement in power plant steels, Sadhana – Published by the Indian Academy of Sciences, Vol. 28, Parts 3 & 4, June/August 2003, pp. 431–451

[2-14] J. Woodtli, R. Kieselbach: Engineering Failure Analysis 7 (2000) 427 – 450

[2-15] H. P. Seifert:
Literature Survey on the Stress Corrosion Cracking of Low-Alloy Steels in High-Temperature Water;
PSI Bericht 02-06, February 2002, ISSN 1019-0643

[2-16] H.-P. Seifert, S. Ritter:
Research and Service Experience with Environmentally Assisted Cracking in Carbon and Low-Alloy Steels in High-Temperature Water;
SKI Report 2005:60, November 2005, ISSN 1104-1374

[2-17] F. P. Ford, P. M. Scott, P. Combrade
Environmentally Assisted Degradation of Structural Materials in Water Cooled Nuclear Reactors;
A.N.T. International, Skultuna S, 2006

[2-18] Friedrich, H.; Frank, J.; Gladen, H.; Stratmann, M.:
Stress corrosion cracking of low alloy steels under high pressure and high temperature conditions;
Corrosion 96, The NACE International Annual Conference and Exposition, 1996, Paper No. 98

[2-19] Rippstein K., Kaesche H.:
The stress corrosion cracking of a reactor pressure vessel steel in high temperature water at high flow rates,
Corrosion Science, Vol. 29, 1989, pp. 517-534

[2-20] Van der Sluys, W. A., Pathania, R.:
Studies of Stress Corrosion Cracking in Steels used for Reactor Pressure Vessels;
Proc. 5. Int. Symposium on Environmental Degradation on Materials in Nuclear Power Systems – Water Reactors, Monterey, CA (USA), 25-29 August 1991, American Nuclear Society Inc., La Grange Park, IL (USA), 1992, p. 571-578

[2-21] G.L. Wire:
Cessation of environmentally-assisted cracking in low-alloy steel: theoretical analysis, Nuclear Engineering & Design, Vol. 197, 2000, pp. 25 – 44

[2-22] Y. Yin Li,
Cessation of environmentally-assisted cracking in low-alloy steel: experimental results, Nuclear Engineering & Design, Vol. 197, 2000, pp. 45 – 60

[2-23] Hickling, J.:
Wasserstoffinduzierte Spannungsrißkorrosion in niedriglegierten Stählen;
4. MPA-Seminar 1978, Paper No. 7

[2-24] J.D. Atkinson, J. Yu:
The role of dynamic strain-ageing in the environment assisted cracking observed in pressure vessel steels, Fatigue Fract. Eng. Mater. Struct., Vol. 20, 1997, 1-12

[2-25] Hänninen, H.; Seifert, H.-P.; Yagodzinskyy, Y.; Ehrnstén, U.; Tarasenko, O.; Aaltonen, P.:
Effects of Dynamic Strain Aging on Environment-Assisted Cracking of Low Alloy Pressure Vessel and Piping Steels;
Proc. 10th Int. Conference on Environmental Degradation of Materials in Nuclear Power Systems – Water Reactors, August 5-9, 2001, Lake Tahoe, NV (USA), ANS, NACE, TMS, 2001

[2-26] A. Roth, H. Hänninen, G. Brümmer, O. Wachter, U. Ilg, M. Widera, H. Hoffmann:
Investigation of dynamic strain aging effects of low alloy steels and their possible relevance for environmentally-assisted cracking in oxygenated high-temperature water,
Proc. 11th Int. Conf. on Environmental Degradation of Materials in Nuclear Systems – Water Reactors, August 10-14, 2003, Stevenson WA (USA), Edited by G.S. Was, L. Nelson, P. King, Pergamon Press LTD., London, 2003, 317-329

[2-27] Devrient B., Roth A., Küster K., Ilg U., Widera M.:
Effect of dynamic strain aging on the environmentally assisted cracking of low-alloy steels in oxygenated high-temperature water,
Proc. 13th Int. Conf. on Environmental Degradation of Materials in Nuclear Power Systems – Water Reactors, August 19-23, 2007, Whistler, BC, Canada, TMS 2007

[2-28] Devrient, B.:
Untersuchungen zum Einfluss der dynamischen Reckalterung auf die mediumgestützte Risskorrosion von niedriglegierten Stählen in sauerstoffhaltigem Hochtemperaturwasser;
Dissertation, Universität Stuttgart, Fakultät Maschinenbau, Stuttgart 2007

[2-29] Choi, H.; Beck, F. H.; Szklarska-Smialowska, Z.; Macdonald, D. D.:
Stress Corrosion Cracking of ASTM A508 Cl 2 Steel in Oxygenated Water at Elevated Temperatures; Corrosion 38 (1982) 136-144

[2-30] V. Läpple, MPA Stuttgart:
Untersuchungen zum korrosionsgestützten Rißwachstum ferritischer Stähle in sauerstoffhaltigem Hochtemperaturwasser;
Techn.-wiss. Bericht der MPA Stuttgart (1996), Heft 96/02

[2-31] Congleton J., Shoji, T., Parkins, R. N.:
The stress corrosion cracking of reactor pressure vessel steel in high temperature water,
Corrosion Science, Vol. 25, No. 8/9, 1985, pp. 633-650

[2-32] Erve, M., Kleen U., Weber, J., Maußner G., Roth A., Schmidt G.:
“Schadensfalluntersuchungen an Rißbildungen in Rohrleitungen eines SWR-Speisewassersystems und daraus abgeleitete Vorsorge- und Abhilfemaßnahmen”,
21. MPA-Seminar, Stuttgart, 05./06. Oktober 1995, Paper No. 40

[3-1] M. Higuchi and K. Iida, “An Investigation of Fatigue Strength Correction Factor for Oxygenated High Temperature Water Environment”, 1988, Proceedings of 6th ICPVT, September 11-16, Beijing, China

[3-2] M. Higuchi and K. Iida, “Fatigue Strength Correction Factors for Carbon and Low-Alloy Steels in Oxygen-Containing High-Temperature Water”, 1991, Nuclear Engineering and Design Vol. 129, pp. 293-306

[3-3] Materials Reliability Program: Fatigue Management Handbook, Revision 1 (MRP-235 w/Corrections). EPRI, Palo Alto, CA: 2009. 1015010

[3-4] NUREG/CR–6909, Rev. 1. Effect of LWR Water Environments on the Fatigue Life of Reactor Materials. Final Report. U.S. NRC, May 2018

[3-5] Technische Regeln Dampfkessel (TRD) TRD 301 Anlage 1 Berechnung: Berechnung auf Wechselbeanspruchung durch schwellenden Innendruck bzw. durch kombinierte Innendruck- und Temperaturänderungen. Fassung August 1996. Carl Heimanns Verlag KG, Köln

[3-6] Gorsitzke, B.: Neuere Berechnungsvorschriften zum Ermüdungsfestigkeitsnachweis von Druckbehältern (Teil 2), TÜ-Z. 36 (1995), No. 7/8, pp. 301/310

[3-7] DIN EN 13445-3: Unbefeuerte Druckbehälter –Teil 3: Konstruktion; Deutsche Fassung EN 13445-12:2018. Beuth Verlag GmbH, Berlin

[3-8] DIN EN 12952-3: Wasserrohrkessel und Anlagenkomponenten – Teil 3: Konstruktion und Berechnung für drucktragende Kesselteile; Deutsche Fassung EN 12952-3:2011. Beuth Verlag GmbH, Berlin

[3-9] Reese, S.; Rudolph, J.: Environmentally Assisted Fatigue (EAF) Rules and Screening Options in the Context of Fatigue Design Rules within German Nuclear Safety Standards.
Proceedings of the ASME 2015 Pressure Vessels & Piping Conference, PVP2015,
July 19-23, 2015, Boston MA, USA. Paper No. 45022

[3-10] ASME Code Case N-792-1, Section III, Division 1, Fatigue Evaluation Including Environmental Effects

[3-11] ASME BPVC Code Case N-917, June 15th 2021 “Fatigue Crack Growth Rate Curves for Ferritic Steels in Boiling Water Reactor Environments, Section XI, Division 1”

[3-12] RCC-M, AFCEN, Design and Construction Rules for Mechanical Components of PWR Nuclear Islands, 2016 edition

[3-13] Métais T., Morley A., de Baglion L., Tice D., Stevens G. L. and Cuvilliez S., “Explicit Quantification of the Interaction Between the PWR Environment and Component Surface Finish in Environmental Fatigue Evaluation Methods for Austenitic Stainless Steels”. PVP2018-84240, ASME 2018 Pressure Vessels and Piping Conference, Prague, Czech Republic

[3-14] de Baglion L., Cuvilliez S., “An Extensive Fatigue Testing Campaign on 304L Austenitic Stainless Steel in Support of the Fen Integrated Approach: Explicit Quantification of the Interaction between Surface Finish and PWR Environment”. PVP2019-93080 (Technical Presentation), ASME 2019 Pressure Vessels and Piping Conference, San Antonio TX (USA)

[3-15] McLennan A., Morley A., Cuvilliez S., “Further Evidence of Margin for Environmental Effects, Termed Fen-Threshold, in the ASME Section III Design Fatigue Curve for Austenitic Stainless Steels Through the Interaction Between the PWR Environment and Surface Finish”. PVP2020-21262, ASME 2020 Pressure Vessels and Piping Conference, Virtual, Online

[3-16] Cuvilliez S., McLennan A., Mottershead K., Mann J. and Bruchhausen M., “INCEFA-PLUS Project: Lessons Learned from the Project Data and Impact on Existing Fatigue Assessment Procedures”. PVP2020-21106, ASME 2020 Pressure Vessels and Piping Conference, Virtual, Online

[3-17] Cuvilliez S., Li, J, Kong, Z., Rudolph, J., Billon, F., Xie, J. “AFCEN Fatigue Calculations Benchmark: Implementation of the RCC-M Rules in Probationary Phase for Environmentally Assisted Fatigue (EAF) Assessment on a Simple Test Case”. PVP2021- 61522, ASME 2021 Pressure Vessels and Piping Conference, Virtual, Online

[3-18] Y.S. Garud et al., “Corrosion Fatigue of Water-Touched Pressure Retaining Components in Power Plants”, EPRI Palo Alto CA USA, TR-106696, Final Report, November 1997 (historical report, not anymore available, at last listed 2006 at EPRI online in: http://mydocs.epri.com/docs/newsletter/1013673.htm)

[3-19] F.-J. Adamsky, B. Kempkes, J. Ernst, “Dehnungsinduzierte Risskorrosion in Rohrsystemen von konventionellen Kraftwerksanlagen”, VGB Kraftwerkstechnik, Oktober 2000, 128-138

[3-20] F.-J. Adamsky, H.D. Teichmann, “Betriebserfahrungen mit Speisewasserbehältern”, VGB KRAFTWERKSTECHNIK, Vol. 55, November 1977, 758-773

[3-21] P.-H. Efferz, P. Forchhammer, J. Hickling, “Spannungsrißkorrosionsschäden an Bauteilen in Kraftwerken – Mechanismen und Beispiele”, VGB KRAFTWERKSTECHNIK, Vol. 62, Mai 1982, 390-408

[3-22] “Betriebserfahrungen mit Speisewasserbehältern”, VGB Tätigkeitsbericht 1975/1976, VGB Essen 1976, 119-122, mit der „Empfehlung für die Behandlung von Speisewasserbehältern als Bestandteil von Dampfkesselanlagen”, ibid. 122-125

[3-23] NACE Standard Practice “Prevention, Detection and Correction of Deareator Cracking”, NACE Houston TX USA. NACE SP0590-2015

[3-24] “Deareator Tank Assessment Guideline, Current Industry Technology and Approaches”, EPRI Palo Alto CA USA, EPRI 1021199, 2010 https://www.epri.com/research/products/000000000001021199

[3-25] H. Spähn, H. Kaes, “Schäden an wasserberührten Kesselbauteilen im Spiegel des Schadensgeschehens und des Regelwerks, dargestellt am Beispiel der Kesseltrommeln”,
VGB KRAFTWERKSTECHNIK, Vol. 65 (1985) 42-56

[3-26] F.-J. Adamsky, H. Teichmann, E. Tolksdorf, “Betriebserfahrungen mit dem warmfesten Werkstoff 15 NiCuMoNb 5 in konventionellen KW-Anlagen“, VGB-Konferenz “Werkstoffe und Schweißtechnik im Kraftwerk 1996”, Vortrag 24, Tagungsband, VGB Essen

[3-27] F.-J. Adamsky, “Bericht über Untersuchungen an Speisewasserbehältern”, Prüf-Nr. W362/76, 923/630362/A/si, TÜV Rheinland e.V., Köln 19.01.1978 (not published, historical archive RWE / Historisches Konzernarchiv RWE)

[3-28] A. Roth, E. Nowak, M. Widera, U. Ilg, U. Wesseling, R. Zimmer “Recent In-Service Experience with Degradation of Low Alloy Steel Components Due to Localized Corrosion and Environmentally Assisted Cracking in German PWR Plants”, 12. Int. Conf. on Environmental Degradation of Materials in Nuclear Power Systems – Water Reactors, Snowbird UT, USA, 14.-18.08.2005, TMS, Warrendale PA USA, Paper 89

[3-29] R. Kilian, A. Roth, M. Widera, “Operational Experience of Siemens/KWU LWR Nuclear Power Plants”, Proc. 19. Int. Conf. on Environmental Degradation of Materials in Nuclear Power Systems – Water Reactors, Boston MA USA 18.-22.08.2019, ANS, Downers Grove IL USA, 485-493
https://www.ans.org/pubs/proceedings/article-47326/

[3-30] K. Kußmaul, D. Blind, J. Jansky, “Formation and Growth of Cracking in Feedwater Pipes and RPV Nozzles”, Nuclear Engineering and Design 91 (1986) 305-330

[3-31] M. Erve, U. Kleen, J. Weber, G. Maußner, A. Roth, G. Schmidt, “Schadensfalluntersuchungen an Rißbildungen in Rohrleitungen eines SWR-Speisewassersystems und daraus abgeleitete Vorsorge- und Abhilfemaßnahmen”, 21. MPA-Seminar, Stuttgart 05.-06.10.1995, Vortrag Nr. 40

[3-32] VGB-S-116-00-2016-04-DE: Konservierung von Kraftwerksanlagen/
VGB-S-116-00-2016-04-EN: Preservation of Power Plants

[4-1] Zander, A.; Nopper, H.; Roessner, R.: “COMSY – Das Software-Produkt für ein effizientes Lebensdauer- und Inspektionsmanagement”, VGB PowerTech 9 (2005); pp. 126/131

[4-2] Zander, A.; Söllner, A.; Glück, W.: “Heat recovery steam generators FAC mitigation by water chemistry control”, Chemie im Kraftwerk 2014, 29. -30. Oktober 2014; Linz, Österreich

[4-3] Zander, A.: “Degradation and Corrosion Assessment against the Backdrop of New Energy Policy Framework Conditions”, 3rd Meeting of the European HRSG Forum (EHF2016), May 09 – 12, 2016; Prague, Czech Republic

[4-4] Rudolph, J.; Zander, A.; Wildner, U.; Lafitte, S.: “Balance-of-plant BOP Based Expert System Screening for Corrosion Fatigue Sensitivity”, 10th International European HRSG Forum 2024 (EHF2024), Prato, Italy, May 13-15, 2024

[5-1] Berger, C., Blauel, J.G., Hodulak, L., Pyttel, B., Varfolomeyev, I., “Bruchmechanischer Festigkeitsnachweis für Maschinenbauteile, FKM Richtlinie“, VDMA-Verlag, Frankfurt am Main, 4. Auflage, 2018

[5-2] ASME BPV Code Section XI, Division 1, Article Y3000 “Ferritic Steels“, 2021

[5-3] BS 7910:2013+A1:2015, “Guide to methods for assessing the acceptability of flaws in metallic structures“, BSI Standards Publication, 2015

[5-4] API 579-1/ASME FFS-1, “Fitness-For-Service”, International Code of API and ASME, ed Dez. 2021API 579-1 2021 ed.

[5-5] TÜV-Verband, Merkblatt MB DAMP 0468:2022-10-15, “Richtlinie für die Anwendung der bruchmechanisch basierten Schadenstoleranzanalyse bei druckführenden Komponenten zur Integritätsbewertung und Festlegung von Prüfintervallen“, Berlin, Ausgabe 2022-20-15

[5-6] Schick, M., J. Wiedemann, D. Willer: Untersuchungen zur sicherheitstechnischen Bewertung von geschweißten Komponenten aus Werkstoff 15NiCuMoNb5 (WB 36) im Hinblick auf die die Zähigkeitsabnahme unter Betriebsbeanspruchung. Technischer Bericht zum BMU-Vorhaben SR 2239, MPA Stuttgart, März 1998

[5-7] Lenz, E. and W. Wieling: Strain-induced corrosion cracking of low-alloy steels in LWR-Systems-interpretation of susceptibility by means of a three-dimensional diagram (T, ε, dissolved oxygen). Nuclear Engineering and Design 91 (1986), S. 331-344

[5-8] Altpeter, I., G. Dobmann, K.-H. Katerbau, M. Schick, P. Binkele, P. Kizler, S. Schmauder: Kupferausscheidungen im Werkstoff 15NiCuMoNb5 (WB36): Werkstoffeigenschaften und Mikrostruktur, atomistische Simulation, ZfP mittels mikromagnetischer Prüfverfahren. 25. MPA-Seminar, Stuttgart, 7. und 8. Oktober 1999

[5-9] Uhlmann, D., S. Schmauder und G. Zies: Experimentelle und numerische Untersuchungen zu zwei Werkstoffzuständen des Werkstoffs 15NiCuMoNb5. 26. MPA-Seminar, Stuttgart, 5. und 6. Oktober 2000

[5-10] KTA 3206: Nachweis zum Bruchausschluss druckführender Komponenten in Kernkraftwerken. Fassung 2017-11

[5-11] Schüle, M.: Experimentelle und numerische Untersuchungen zum Verhalten von Stählen unter schlagartiger Beanspruchung. Dissertation 2001, MPA Universität Stuttgart

[5-12] ASME Boiler and Pressure Vessel Code, Section XI: Rules for Inservice Inspection of nuclear Power Plant Components, BPVC-XI-2021

[5-13] Kussmaul, K., J. Föhl und E. Roos: 12. MPA-Seminar 1986, Vortrag 25, Stuttgart

[5-14] Mikkola, T.P.J., H. Diem, D. Blind und H. Hunger: Versagensablauf eines Rohrleitungssystems mit Umfangsfehler unter zyklischer Belastung (Experimentelle und analytische Untersuchungen). 13. MPA-Seminar, 8. und 9. Oktober 1987, S. 152

[5-15] Blind, D.: Zur Korrosionsrissbildung in druckführenden Kraftwerkskomponenten infolge Einwirkung von Hochtemperaturwasser. Habilitationsschrift 1991, MPA Universität Stuttgart

[5-16] Kloos, K.H., Blind, D., Granacher, J. und K. Maile: Kriechrisseinleitung und Kriechrisswachstum warmfester Kraftwerksbaustähle unter Berücksichtigung des Größeneinflusses. AIF-Forschungsvorhaben 6038, 1988

[5-17] Abschlussbericht zum Forschungsvorhaben A202: Programmgestützte fortschrittliche Kriech- und Kriechermüdungsbeschreibung für typische langzeitbeanspruchte Kraftwerksbauteile, IfW Darmstadt und MPA Stuttgart, Juni 2005

[5-18] VGB Forschungsvorhaben 393: Auswirkungen flexibler Fahrweise auf Peripherkomponenten des Kesselkreislaufs am Beispiel Kesselumwälzpumpe. MPA Stuttgart, Februar 2016

[5-19] VGB Forschungsvorhaben 399: Auswirkungen flexibler Fahrweise und der Wasserbedingungen auf Peripherkomponenten des Kesselkreislaufs. MPA Stuttgart, März 2017

[5-20] ASTM E647-2015: Standard Test Method for Measurement of Fatigue Crack Growth Rates. 2015

[5-21] VGB-S-506-00-2019-02-DE: Zustandsüberwachung und Prüfung der Komponenten von Dampfkesselanlagen, Druckbehälteranlagen und Wasser oder Dampf führenden Rohrleitungen in Wärmekraftwerken (Dritte Ausgabe 2019)/ VGB-S-506-00-2019-02-EN: Condition Monitoring and Inspection of Components of Steam Boiler Plants, Pressure Vessel Installations and Water- or Steam-Pipes in Thermal Power Plants

[5-22] VGB-S-509-00-2019-11-DE “Inhalte wiederkehrender Prüfungen an Rohrleitungen und deren Komponenten in Wärmekraftwerken”
(vormals VGB R-509, Neuausgabe 2019)

7.2 Abbreviations

BWR	Boiling Water Reactor
CERT	Constant Extension Rate Tensile Test
CF	Corrosion Fatigue
CUF	Cumulative Usage Factor
DO	Dissolved Oxygen
EAC	Environmentally Assisted Cracking
EAF	Environmentally Assisted Fatigue, equivalent to CF
EC	Erosion corrosion, cf. FAC
EPRI	Electric Power Research Institute (USA)
ET	Eddy Current Testing
FAC	Flow Assisted Corrosion cf. EC
FFS	Fitness-For-Service
H-SCC	Hydrogen-induced Stress Corrosion Cracking
H-SICC	Hydrogen-assisted strain Induced Corrosion Cracking
HT	High Temperature
KTA	Kerntechnischer Ausschuss (German NPP code)
KUP	Kesselumwälzpumpe (Boiler circulation pump)
LCF, vLCF	Low Cycle Fatigue, very Low Cycle Fatigue
LWR	Light Water Reactor
mPAUT	Mechanized Phased Array Ultrasonic Testing
MT	Magnetic Particle Testing

NDT	Non-Destructive Testing (equivalent to NDE)
NDE	Non-Destructive Examination (equivalent to NDT)
NPP	Nuclear Power Plant
PA-UT	Phased Array Ultrasonic Testing
PT	Penetrant Testing
PWR	Pressurized Water Reactor
RT	Radiographic Testing
SCC	Stress corrosion cracking
SCI	Surface Crack Inspection
SICC	Strain Induced Corrosion Cracking
SSRT	Slow Strain Rate Test
TR	Transmitter-Receiver (ultrasonic probes)
UT	Ultrasonic Testing
VT	Visual Testing
WKP	Wiederkehrende Prüfung (Periodic inspection)

7.3 Formula symbols

da/dN	Crack growth rate: crack extension per cycle
da/dt	Crack growth rate: crack extension per time
dε /dt	Strain rate
K	Stress intensity factor

ENERGY IS US

Editor:
vgbe energy e. V.
Deilbachtal 173
45257 Essen
Germany

Publishing house:
vgbe energy service GmbH
Deilbachtal 173
45257 Essen
Germany

t +49 201 8128-0
e sales-media@vgbe.energy

be informed

www.vgbe.energy
www.vgbe.services

ISBN 978-3-96284-366-3 (print, English)
ISBN 978-3-96284-367-0 (e-book, English)

ISBN 978-3-96284-364-9 (print, German)
ISBN 978-3-96284-365-6 (e-book, German)